BALTEX
Baltic Sea Experiment

Parameterization of surface fluxes, atmospheric planetary boundary layer and ocean mixed layer turbulence for BRIDGE -

What can we learn from field experiments?

Proceedings from a workshop arranged by
The BALTEX Working Group on Numerical Experimentation and
The BALTEX Working Group on Process Studies

Abisco, Lapland
Sweden
20-21 June 1999

edited by
Nils Gustafsson

International BALTEX Secretariat
GKSS Research Center
Max Planck Straße
D-21502 Geesthacht
Germany
Phone: +49 4162 87 1536
Fax: +49 4152 87 2020
e-mail: baltex@gkss.de

Parameterization of surface fluxes, atmospheric planetary boundary layer and ocean mixed layer turbulence for BRIDGE –

What can we learn from field experiments?

Proceedings from a workshop arranged by

The BALTEX Working Group on Numerical Experimentation and

The BALTEX Working Group on Process studies

Abisko, Lapland, Sweden, 20-21 June 1999

CONTENTS

Introduction

Participants in BALTEX working groups on Process Studies and Numerical Experimentation have realized the lack of communication between experimentalists and modelers with regard to the parameterization of surface fluxes as well as the parameterization of turbulence in the atmospheric planetary boundary layer and in the ocean mixed layer. With the urgent needs to improve atmospheric, ocean and hydrological models to prepare for the BALTEX main experiment (BRIDGE), a Workshop on surface fluxes was arranged in Abisko, Sweden 20 – 21 June 1999. The workshop included presentations by invited speakers during the first day and group discussions during the second day. All presentations are included in this volume as well as summaries of the group discussions.

The main general recommendations for the future are

- For improved physical parameterization in atmospheric, ocean and hydrological models we need measurements representative of the model scales. Thus area means of observed fluxes and long continuos measurements are important for model verifications.

- Climate mode simulations are important for detection of accumulative errors in the parameterizations.

- Further workshops with participation of scientists from the other GEWEX continental scale experiments should follow to learn from their experiences.

In summary this means that both field campaigns and model experiments should be set up in agreement between experimentalists and modelers.

It was a general impression among the participants that the workshop was a very successful one and that such a forum for experimentalists and modelers to meet is highly needed. We would therefor like to thank all participants for their contributions.

On behalf of the BALTEX Working Groups for Process studies and Numerical Experimentation

Eberhard Ruprecht and Nils Gustafsson

Reports and recommendations from working group discussions.

WG 1   *Working Group on Marine Processes*

Participants: Ann-Sofi Smedman, Chairwoman
Renate Hagedorn, Rapporteur
Andreas Lehmann
Martin Schmidt
Ute Karstens
Anna Rutgersson
Felix Hamelbeck
Eberhard Ruprecht
Xiaohua Yang
Markus Meier

The marine group discussed the five topics given by the chairmen of the BALTEX working groups on numerical experimentation and process studies, respectively.

1. Comparison of model and field data

The participants are aware of various difficulties related to this topic (see presentations during the workshop). Main problems seem to be that comparisons are often performed without consideration of the following problems:

- the variability of the two data sets has to be comparable
- representativeness of the measurements
- existence of different scales (spatial, temporal) in both data sets

Recommendation: Point measurements should be temporally averaged over the time period, which represents the spatial average over the grid box of the model data. Under this assumption of ergodicity, comparable variability of the observed data and model data can be achieved.

2. Tests of new parameterizations

The participants discussed advantages and disadvantages of the different methods to test new parameterizations and concluded that a clear effect of a new parameterization is often not discernible because other effects overlap.

Recommendation: A mixed strategy is suggested with process oriented tests as first step, followed by longer simulations to address interactions with other effects. These longer runs should first be performed in climate mode, to avoid that the effects of the new parameterizations are superimposed by initialization or assimilation effects. After that, the new parameterizations should be used in forecast mode and/or runs with data assimilation.

3. What have we learned from BALTEX field experiments so far?

Meteorologists:

- Most models overestimate fluxes at sea surface in comparison to observations
- Precipitation seems to be too high in models
- Vertical distribution of humidity seems to be not correct represented in models
- COADS is a good data set for model validation, but only for longer time scales
- Measurements on short time scales are needed. For precipitation radar measurements could fill this gap, although there are still problems with the application of this data.
- The PIDCAP period is too short to cover the whole range of different situations.

Oceanographers:

The results of the oceanographic field experiment DIAMIX, which was concentrated on measurements of vertical mixing and advection in the Gotland basin, are not yet included in the general model activities.

Recommendation: More oceanographic fieldwork is required, and the Main BALTEX Experiment (BRIDGE) is urgently needed to investigate the full range of synoptic systems and accompanying processes.

4. Improvements for simulations of the BRIDGE period? (data assimilation)

The participants agreed that in special situations SSTs and sea ice distribution can have a non negligible influence on the development of atmospheric fields.

Recommendation: Special effort should be made to use the best possible SST fields (what is not always done up to now). To get consistent simulations of the BRIDGE period the runs should be performed without changes in the model during the simulation.

5. Objects for future studies

Future studies should try to fill the gap between the scales of models and observations.

Recommendation: Implementation of a mesoscale, higher resolution model (e.g. GESIMA), 2-way nesting of GESIMA and a lower resolution model in regions with existing measurements (e.g. Östergarnsholm). The representation of turbulent mixing in the ocean should be improved, e.g. by implementation of a mixed layer model based on the k-epsilon closure.

Another discussion point was the question whether the coupling to a wave model is necessary to improve fluxes at sea surface. It seems to be that the information from a wave model could be very useful for the correct calculation of fluxes via bulk formulae. The coupling effects of a wave model are seen in the ocean, whereas the response of the atmospheric model seems to be only at a lower level. It is recommended to review the existing literature about the effects of a wave model, and to perform experiments, to test the cost/effectiveness relation of a coupling.

3

WG 2   Working Group on Land Surface Processes

Participants: Bart van den Hurk, Chairman
Frank Beyrich, Rapporteur
Sten Bergström
Stefan Gollvik
Phil Graham
Sven-Erik Gryning
Michael Hantel
Piotr Kowalczak
Burkhardt Rockel
Michael Tjernström
Werner Wergen
Niels Woetman-Nielsen

1. Field experiments

Field experiments in BRIDGE are separated into two different types of campaigns:

a) Intensive Observation Periods (IOPs) in a certain region using special measurement systems (aircraft, tethered balloons, frequent radiosoundings, special turbulence measurements) and devoted to process studies (like NOPEX-CFE 94 / 95, WINTEX-97, LITFASS-98)

b) Monitoring activities realizing a comprehensive long-term measurement programme of land surface and atmospheric parameters exceeding that of standard networks from the national weather and hydrological services / agencies (NOPEX Central facilities at Norunda / Marsta, LITFASS project).

While IOPs aim to yield a better understanding of special processes at the land-air interface and thus contribute to improve the physical parameterization in numerical models, the long-term monitoring activities are of special relevance with regard to the evaluation of model performance on a seasonal timescale. In particular, modelers need comprehensive long-term datasets of land-, vegetation- and atmospheric parameters from different parts of the BALTEX area, since model validation must be performed for a broad spectrum of weather situations in different climate regions covering even a variety of extreme events.

2. Land use data and tiling

In order to account for the heterogeneity of the land surface, an increasing number of models uses different surface types within one grid cell, and solves the energy budget equation separately for each of these types (tiling approach). The characteristic values of land surface parameters and fluxes for each grid cell are then obtained from a fractional weighting of the relevant landuse classes. At primary level, landuse types in the BALTEX area should be distinguished between forest, open agricultural land, water, snow / ice, and wetlands. Landuse data for the BALTEX region are available through the CORINE database with sufficiently high resolution and containing more details than we have the means of evaluating its impact. To distinguish between different types of vegetation or crops within the agricultural area (e.g.,

grass, rye, barley, maize, rape, sunflowers, potatoes etc.) is of secondary importance, at least for climatological studies. It might be of some relevance for short range weather prediction. However, representative sensitivity studies on this question are lacking.

3. Area averaging of surface fluxes

Basic model output to characterize surface-atmosphere interaction are area-averaged values of the fluxes of momentum, energy, and water. To verify the results of the "tile method", measurements of the energy budget components over different surface types are needed. Ideally these measurements should be done with micrometeorological / flux stations over typical surfaces within one model grid cell. In addition to the energy budget components, measurements of soil moisture (and merely its dynamics) are essential for model validation purposes since soil moistrure effectively controls the exchange of energy and water between the land surface and the atmosphere. BRIDGE should concentrate on the realization of such measurements in a few different climate regions of the BALTEX area rather than setting up a large number of measurements distributed through the whole study area. NOPEX is such a succesfully realized measurement programme in the 90ies, continuation of these measurements during BRIDGE is highly desirable. The strategy of the LITFASS project currently set into operation by DWD at Lindenberg perfectly meets these requirements.

4. Aircraft measurements

Aircraft measurements are the only means available at present to directly measure area-averaged values of the turbulent fluxes. Airborne flux measurements should therefore be planned during the IOPs of BRIDGE in those regions where extensive flux measurements are performed at the ground. Access to research aircraft might be possible on a European level through the EU funding of access to large research facilities (TMR programme, STAAARTE project or its successor). Coordinated activities between the different field sites in the BALTEX area are recommended.

5. Closure of the surface energy budget

A presently unsolved problem in most experimental programmes is the non-closure of the surface energy budget. The disbalance seems to depend, inter alia, on the heterogeneity of the land surface. On the other side, models always close the energy budget. Comparison between model results and measurements is thus faced with an additional problem. Therefore, it is recommended not only to compare absolute values of the fluxes but also relative values or flux ratios, like the Bowen ratio. Flux profile measurements at towers up to 100-200 m might contribute to understand the flux averaging over a heterogeneous surface since the footprint area becomes less uniform with increasing height.

6. Snow and ice

Large parts of the BALTEX area are covered with snow and ice over considerable times of the year. To characterize the properties of the snow, quite a number of parameters needs to be considered in the models and should be determined experimentally (snow cover, snow depth, snow density / snow water equivalent, albedo of snow). Datasets on these parameters from the BALTEX region are still rare. Valuable data sources on snow characteristics have been produced in North America during BOREAS and should be made available for BALTEX. Finnland runs an extensive monitoring programme on snow regularly in winter, this should be

used for BALTEX as well. NOPEX plans to perform special field activities on winter conditions during the winter 2000 / 2001 in order to obtain a high-quality dataset.

7. Orography

Orography plays an important role in the interaction between the atmosphere and the surface. Mountain drag and gravity wave drag are phenomena which influence the momentum budget and which have not yet been fully understood. However, experimental investigation of these phenomena would require a specially designed field experiment. This seems to be outside the scope of BRIDGE.

8. Field data and modelling

A barrier still seems to exist between experimentalists and modellers concerning the availability of field data for use in numerical modelling. Some typical problems preventing the fast and comprehensive use of experimental data by the modelling community are

- lack or poor quality of the meta-data necessary to characterize the measurements
- time delay between experiments and the free data access for non-participants
- considerable differences in data quality, data formats etc. between different providers of the same type of data.

Experimentalists have realized these deficits and take steps in order to improve the situation towards a better exploitation of existing (and new) datasets for BRIDGE and the BALTEX modelling community, e.g.,

- data from the NOPEX CFE-1/CFE-2 will be published on a CD-ROM along with a special issue of Agricultural & Forest Meteorol. by the end of 1999
- organizations running field monitoring programmes of surface-atmosphere exchange (MIUU, DWD, KNMI, FMI, Risø) have prepared an EU application within the actual call of the 5th Framework Programme aiming at the harmonization of measurement programmes, data formats, data descriptions, data quality etc. across the BALTEX community during BRIDGE.

It would be valuable to have land surface data availabale for near real-time flux validation, i.e., with a time delay of only a couple of days.

9. Communication

Meetings like the Abisko workshop are extremely useful in order to improve communication between the experimental and modelling communities. BALTEX should try to provide a frame for continuation of this discussion. Taking the central question of the workshop, this could be easily turned around providing stimulus for new discussions under the topic: "What can experimentalists learn from numerical modelling of air-surface interaction processes ?". It should be also considered that BALTEX is just one of the continental scale experiments within GEWEX. Communication needs be set up (improved) with representatives from the other experiments of WCRP - GEWEX in the future.

WG 3   *Working Group on Snow and Ice*

Participants: Jouko Launiainen, Chairman
                        Hannu Savijärvi, Rapporteur
                        Toni Amnell,
                        Carl Fortelius
                        Nils Gustafsson
                        Ulf Andrae

1. Problem areas

The group first discussed about the processes to be studied in the snow/ice-surfaced boundary layer typical in the boreal winter of Scandinavia over forest-field-lake patches or over frozen sea, especially in cases of drift ice and broken ice fields with cracks and leads.

In determination and modelling of radiation processes, problem areas were defined as:

1) Multireflexions of short-wave radiation at low solar angles over ice and snow surfaces,
2) Effects of snow between and within trees,
3) Penetration and absorption of solar radiation in snow/ice,
4) Melting and water pool formation (albedo) in snow/ice,
5) Long-wave flux profiles very near above the snowy and cold ground.

In turbulence and surface interactions, problem areas were listed as:

1) Determination of detailed roughness lengths over snow and ice (packs, ridging, drifting),
2) Temperatures and heat fluxes within snow and ice,
3) Heat fluxes from below (from soil or ocean),
4) Subgrid scale patchiness and parametrization in large-scale models.

Further research and parameterization is encouraged in these key areas.

The group noted that snow state (ageing) is important and recommended for BRIDGE it be included and updated in NWP and climate models, e.g. by introducing snow density as a model variable, or via expressing it as a snow-type classes.

2. Comparisons of model results against observations

The group discussed about the comparison of model results against observations. In process validation, it was felt that if flux data e.g. from observation masts are available, column model (1-D) comparisons of fluxes directly would be relevant. For climate and NWP models, long time series would be good as these cover various weather types, and reveal systematic errors. For horizontal small-scale variability associated with the patchiness, aircraft observations are considered useful (as in WINTEX and BASIS). Also, radar winds were suggested as a one new possibility.

The group recommended that the extra BRIDGE stations should be available as long as possible, and extra field campaigns with aircraft would be very useful. Also, BRIDGE data assimilation increments and their statistics should be utilized to discover possible systematic errors in the model processes (wether they are of dynamical or physical, or both).

3. What we have learned

The group discussed what has been learned from the field experiments (apart from measuring techniques etc. in cold conditions) so far. It was agreed that aircraft measurements over patchy areas (forests/ice cracks; WINTEX/BASIS) had revealed strong horizontal differences in the sensible and latent heat fluxes, but not so much in the radiative fluxes. The vertical and temporal structure of H and LE in a wintertime boreal forest was quite variable according to mast measurements, and presumably dependent on the forest structure. Coupled high-resolution atmosphere-ground/ice column models seem to work well over ice, and they are expected to work properly over boreal forest as well.

The group recognized that the question of strong horizontal inhomogeneity needs extra work and further field campaigns would be needed. Radiation measurements would be needed, too.

3. BRIDGE data assimilation

The group discussed BRIDGE data assimilation schemes, and recommended a concept of snow ageing should be included in the assimilating models. Real-time satellite observation derived albedos(of clear weather) could be utilized as well. For a long-time goal, fully interactively coupled 3-D high-resolution atmosphere-ice-ocean limited area models were considered necessary.

4. Workshops

Workshops (as the current one) were considered as a very useful link between modelers and experimentalists. They were strongly recommended and perhaps having those every second year. Specialists might be invited from other international measurement campaigns (e.g. from the U.S. and Canada). Finally, the group encouraged to proceed and carry out the BRIDGE field campaigns, in frames of the resources allow, even in a case if the planned new projects (WINCON) would not get the funding applied from the EC.

List of participants

Name	Adress	E-mail
Amnell, Toni	Department of Meteorology P.O. Box 4 (Yliopistonkatu 3) FIN-00014 University of Helsinki Finland	toni.amnell@helsinki.fi
Andræ, Ulf	SMHI SE-601 76 Norrköping Sweden	ulf.andrae@smhi.se
Bergström, Sten	SMHI SE-601 76 Norrköping Sweden	sten.bergstrom@smhi.se
Beyrich, Frank	DWD Lindenberg Meteorologisches Observ. Postfach 60 05 52 D-15864 Lindenberg Germany	frank.beyrich@dwd.de
Bringfelt, Björn	SMHI SE-601 76 Norrköping Sweden	björn.bringfelt@smhi.se
Fortelius, Carl	Finnish Meteorological Inst. P.O. Box 903 FIN-00101 Helsinki Finland	carl.fortelius@fmi.fi
Gollvik, Stefan	SMHI SE-601 76 Norrköping Sweden	stefan.gollvik@smhi.se
Graham, Phil	SMHI Rossby Centre SE-601 76 Norrköping Sweden	phil.graham@smhi.se

Gryning, Lars-Erik	Risø National Laboratory P.O. Box 125, Building 125 DK-4000 Roskilde Denmark	Sven-Erik.Gryning@Risoe.dk
Gustafsson, Nils	SMHI SE-601 76 Norrköping Sweden	nils.gustafsson@smhi.se
Hagedorn, Renate	Inst. für Meereskunde Universität Kiel Düsternbrooker Weg 20 D-24105 Kiel Germany	rhagedorn@ifm.uni-kiel.de
Hamelbeck, Felix	University of Vienna Inst. for Meteorology and Geophysics (IMG) Hohe Warte 38 A-1190 Vienna Austria	felix.hamelbeck@univie.ac.at
Hantel, Michael	University of Vienna Inst. for Meteorology and Geophysics (IMG) Hohe Warte 38 A-1190 Vienna Austria	michael.hantel@univie.ac.at
Karstens, Ute	GKSS Postfach 1160 D-21494 Geesthacht Germany	karstens@gkss.de
Launiainen, Jouko	Finnish Inst. of Marine Research Box 33 FIN-00931 Helsinki Finland	jouko@fimr.fin

Lehmann, Andreas	IfM – Kiel Düsternbroker Weg 20 D-24105 Kiel Germany	alehmann@ifm.uni-kiel.de
Meier, Markus	SMHI Rossby Centre SE-601 76 Norrköping Sweden	markus.meier@smhi.se
Piotr Kowalczak	Inst. of Meteorology and Water Management Bransch of Poznan ul. Dabrowskiego 174/176 Pl-60-594 Poznan Poland	dyr.imgo@rose.man.poznan.pl
Rockel, Burkhardt	GKSS Postfach 1160 D-21494 Geesthacht Germany	rockel@gkss.de
Ruprecht, Eberhard	Institut für Meereskunde Düsternbrooker Weg 20 24105 Kiel Germany	eruprecht@ifm.uni-kiel.de
Rutgersson, Anna	SMHI SE-601 76 Norrköping Sweden	anna.rutgersson@smhi.se
Savijärvi, Hannu	Department of Meteorology P.O. Box 4 (Yliopistonkatu 3) FIN-00014 University of Helsinki Finland	hannu.savijärvi@helsinki.fi

Schmidt, Martin	Institute of Baltic Sea Research Rostock-Warnemünde Postfach 30 10 38 D-18111 Rostock Germany	martin.schmidt@io-warnemuende.de
Smedman, Ann-Sofi	Dept. of Earth Sciences, Meteorology Villavägen 16 Uppsala Sweden	annsofie@big.met.uu.se
Tjernström, Michael	Dep. of Meteorology Stockholms University SE-106 91 Stockholm Sweden	michaelt@misu.se
van der Hurk, Bart	KNMI P.O. Box 201 NL-3730 AE de Bilt Netherlands	hurkvd@knmi.nl
Wergen, Werner	DWD Postfach 100465 D-63004 Offenbach Germany	werner.wergen@dwd.de
Woertman Nielsen, Niels	DMI Lyngbyvej 100 DK-2100 Copenhagen Ø Denmark	nwn@dmi.dk
Xiaohua, Yang	Danish Meteorological Inst. Lyngbyvej 100 DK-2100 Copenhagen Denmark	xiaohua@dmi.dk

What have we learnt from the field experiments?

Ann-Sofi Smedman and Ulf Högström,
Department of Earth Sciences, Meteorology, University of Uppsala

1 Introduction

The vertical fluxes of momentum, sensible heat and water vapor at the surface of the Earth are parameterized in numerical atmospheric models through relations that include estimates of wind speed, temperature and water vapor at some low height (of order 10 m) and corresponding estimates of these variables at the ground surface. This form of parameterization is, in principle, a two-layer approach, which includes: (i) processes taking place at or very close to the surface and (ii) bulk atmospheric transfer up to the lowest point of the atmospheric model. The *surface processes* depend very strongly on the character of the surface. *Over land*, surface friction is largely determined by the bluff body effect, which is parameterized in terms of a roughness length z_0, and a zero plane displacement d; sensible heat flux, on the other hand, is accomplished by molecular conduction at the surface, which results in an effective 'roughness length for temperature' z_T which may be very different from z_0; evaporation is strongly controlled by stomatal aperture. *Over the sea*, a very complicated interaction takes place between near-surface fluctuating wind field and surface waves. This results in roughness length variation with wind speed and possibly with other factors related to the state of the sea.

The *bulk transfer* between the ground surface and the atmosphere is accomplished by turbulent fluctuations. The effectiveness of this process depends very strongly on the stability of the surface layer. This effect is currently parameterized with the aid of mathematical expressions obtained from Monin - Obukhov similarity theory (MO-theory).

This note will concentrate on bulk transfer relations. But for the case of oceanic conditions, effects of the sea state will also be discussed. In Sec. 2 basic mathematical relations are given. Sec. 3 is an overview of state-of-the-art mean formulations for the various expressions. In Sec. 4 recent results from experiments in the Nordic area will be discussed. They include results from the following

field studies:

- NOPEX, Marsta (land)

- PEP in BALTEX, Östergarnsholm (sea)

- Nässkär and Utlängan (sea).

2 Basic mathematical relations

MO-theory has been the basic tool for expressing mathematical relations between turbulent fluxes and mean gradients in the atmospheric surface layer for about 50 years. The theory essentially predicts that statistical quantities in the surface layer are properly normalized by the velocity scale $u_* = \sqrt{(-\overline{u'w'})_0}$, where $(-\overline{u'w'})_0$ is the kinematic momentum flux at the surface, the temperature scale $T_* = -Q_0/u_*$, where Q_0 is the temperature flux at the surface and the height above the ground z, and that the quantities normalized with these parameters are unique functions of the dimensionless height z/L, where

$$L = -\frac{u_*^3 T_0}{kgQ_0} \qquad (1)$$

is the Monin - Obukhov length. In this form the theory is strictly valid for dry air (k = von Karman constant = 0.4 and g = acceleration of gravity). For moist air, the flux of virtual temperature replaces the 'ordinary' temperature flux. For the wind gradient $\frac{\partial U}{\partial z}$, we then have:

$$\frac{kz}{u_*}\frac{\partial U}{\partial z} = \phi_m(z/L) \qquad (2)$$

and for the potential temperature gradient $\frac{\partial \Theta}{\partial z}$:

$$\frac{kz}{T_*}\frac{\partial \Theta}{\partial z} = \phi_h(z/L) \qquad (3)$$

Integrating Eq. (2) from $z = z_0$ to the lower model level z (order 10 m):

$$u_* = [k/(\ln z/z_0 - \Psi_m)] \cdot U \qquad (4)$$

where Ψ_m is the integral of the function $\phi_m(z/L)$. The corresponding expression for $T_* = -Q_0/u_*$ is:

$$T_* = [k/(\ln z/z_T - \Psi_H)] \cdot (T - T_0) \qquad (5)$$

where Ψ_H is the integral of the function $\phi_h(z/L)$. For air-sea interaction parameterizations, it is customary to introduce bulk coefficients:

$$C_D = (u_*/U)^2 = [k/(\ln z/z_0 - \Psi_m)]^2 \qquad (6)$$

$$C_H = \overline{w'\theta'}/U \cdot (T - T_0) = [k/(\ln z/z_0 - \Psi_m)] \cdot [k/(\ln z/z_T - \Psi_H)] \quad (7)$$

where T_0 is the temperature of the ocean surface. Equivalently for the flux of water vapor, $\overline{w'q'}$:

$$C_E = \overline{w'q'}/U \cdot (q - q_0) = [k/(\ln z/z_0 - \Psi_m)] \cdot [k/(\ln z/z_{0q} - \Psi_q)] \quad (8)$$

where q_0 is the water vapor pressure at the surface of the ocean, which is assumed to equal the saturation vapor pressure at temperature T_0, z_{0q} is the roughness length for water vapor and Ψ_q is the integral of the ϕ-function of vapor pressure ϕ_q (formally similar relation as Eq. 3).

From Eq. (4) - (8) it is clear that the vertical fluxes of momentum, sensible heat and water vapor can be obtained when U, Θ and q are given at a height z (of order 10 m) and at the surface, provided that, in addition, the following parameters are known: z_0, z_T and z_{0q} and that the functions $\phi_m(z/L)$, $\phi_h(z/L)$ and $\phi_q(z/L)$ are specified functions of z/L. Note, that specifying C_D is equivalent to specifying z_0, specifying C_H is equivalent to specifying z_T and specifying C_E is equivalent to specifying z_{0q}.

3 State-of-the-art ϕ-functions and bulk functions

A. Conditions over land

Högström (1996) reviewed the available literature for the ϕ-functions and recommended the following expressions:

$$\phi_m = (1 - 19z/L)^{-1/4}, -2 \leq z/L \leq 0 \quad (9a)$$
$$= 1 + 5.3z/L, 0 \leq z/L \leq 0.5 \quad (9b)$$

For $z/L > 0.5$, ϕ_m levels out and becomes constant but with great scatter in the data.

$$\phi_h = \phi_q = 0.95(1 - 11.6z/L)^{-1/2},$$
$$-2 \leq z/L \leq 0 \quad (10a)$$
$$= 0.95 + 8.0z/L,$$
$$0 \leq z/L \leq 0.5 \quad (10b)$$

Also ϕ_h levels out and becomes constant (with great scatter) for $z/L > 0.5$.

As traditionally done since the advent of MO-theory around 1950, it was taken for granted by Högström (1996) that ϕ_m, ϕ_h and ϕ_q are functions of z/L only and that the scatter found in all experimental data is due solely to sampling inadequacy, instrumental errors and terrain inhomogeneity. As discussed in Sec. 4, it has now been shown that, for unstable conditions, ϕ_m has an additional dependence on the height of the convective boundary layer z_i, or more precisely on z_i/L.

B. Conditions over the sea

a. ϕ-functions

By analyzing data from oceanic expeditions, it has recently been demonstrated by Edson and Fairall (1998) that the ϕ-functions found over land are valid over the ocean as well. This is true at least in an *average* sense, but scatter in the data is much larger than in corresponding data sets over land, and it is very likely that this scatter conceals several important effects which are due to the state of the surface waves, see Sect.4.

b. Bulk functions

The situation concerning bulk functions is still controversial and the subject of intensive measurement programs. This is particularly the case for C_D. For open ocean conditions the following expression appears to be acceptable for mean conditions (Yelland and Taylor, 1996):

$$C_{DN} = [0.6 + 0.070 \cdot U_{10}] \cdot 10^{-3},$$
$$6 \leq U_{10} \leq 26 ms^{-1} \quad (11a)$$

Note that C_{DN} is bulk coefficient for neutral conditions, so that we obtain with Eq. (6):

$$C_D = C_{DN}(\ln z/z_0)^2/[\ln z/z_0 - \Psi_m)]^2 \quad (12)$$

Eq. (11a) is supported by results from several recent oceanic expeditions. The corresponding relation for winds below 6 ms^{-1} is less clear. There seems, however, to be consensus that C_{DN} increases with decreasing wind speed below 6 ms^{-1}, although different studies give widely different variation with U_{10}. The expression given by Yelland and Taylor (1996) is:

$$C_{DN} = [0.29 + 3.1/U_{10} + 7.7/U_{10}^2] \cdot 10^{-3},$$
$$3 \le U_{10} \le 6 \, ms^{-1} \quad (11b)$$

For C_{DN} it is equally valid what is said in Sec 3a: Scatter in the data is very large, and it is very likely that this scatter conceals several important effects which are due to the state of the surface waves, see Sect. 4.

Concerning bulk functions for sensible heat and water vapor, there seems to be consensus that the corresponding 'neutral' coefficients are virtually constant over a wide wind speed range. Thus e.g. DeCosomo et al. (1996) found as a result of the HEXOS experiment in the North Sea:

$$C_{HN} \approx C_{EN} \approx 1.1 \cdot 10^{-3}, \quad (13)$$

They found this relation valid for C_{EN} up to at least 18 ms^{-1} and up to at least 23 ms^{-1} for C_{HN}. To obtain C_H and C_E, Eq. (13) must be multiplied by expressions obtained from Eq. (7) and (8) respectively, i.e.

$$C_H = C_{HN}(\ln z/z_T)^2/[\ln z/z_T - \Psi_H)]^2 \quad (14)$$

and similarly for C_{EN}.

4 Some new results

A. ϕ-functions

Khanna and Brasseur (1997) employed large-eddy-simulation technique (LES) to study the influence of boundary-layer size eddies on surface-layer characteristics during convective conditions. Their results were tested against field data by Johansson et al. (1999) with the aid of a combination of turbulence data from 10 m, profile data of wind and temperature and aircraft data and radiosoundings from CFE1 and CFE2 (CFE = Concentrated Field Effort) of the NOPEX project, which were carried out during the summers of 1994 and 1995 in the NOPEX area (the mast measurements were made at the agricultural site Marsta). Figure 1 shows ϕ_m as a function of z/L. The various symbols represent groups of data with different values of z_i/L (z_i = the height of the convective boundary layer), see Figure legend. The thin full line is Högström's expression (9a). The thick full line, the dashed line and the dotted line are results from the LES of Khanna and Brasseur. Their results represent a much more limited range of z_i/L than the measurements (see Figure legend). Considering this, it is clear that there is indeed an ordering of the data with z_i/L. The effect is quite large, but as the scatter is also large, it is useless at this stage to formulate any explicit mathematical expressions.

Corresponding analysis of ϕ_h in Johansson et al. (1999) demonstrates a similar effect from z_i/L, but the effect is much less, and consequently the deviations from Högström's Eq. (10a) are much less.

B. Validity of ϕ-functions over the sea

a. Effect of low level jets

Figure 2a and 2b show ϕ_m and ϕ_h over the sea during stable stratification for cases without a low-level jet present near the surface. The dashed lines are Högströms expressions (9b) and (10b) respectively. The agreement between model and measurements is very good. Figure 2c shows the corresponding plot for ϕ_m from the same experiment (at Nässkär, Bergström and Smedman 1995) during stable situations with a low level jet present (at or below 100 m). The ϕ-values are seen to be much larger than predicted by Eq. (9b). The reasons for this 'anomaly' are discussed in Bergström and Smedman (1995).

b. Effects of sea state

Donelan (1990) discusses in detail the effect of wave development or 'wave age' on the exchange processes at the surface of the ocean. His results have been partly corroborated by recent experiments, but in some experiments the authors fail to see effects. Here we will illustrate with some recent results from our ongoing measurements at Östergarnsholm.

Figure 3 shows the mean wind gradient at 10 m plotted as a function of wind speed during the period 14 - 19 September, 1995. The figure has different symbols for different days (see Figure legend)

and it is possible to follow the development with time of the wind gradient. Thus, wind speed first increases during 14 to 16 September to a maximum of about 16 ms^{-1} and then decreases to values between 2 and 6 ms^{-1} during 18 and 19 September. Two features are notable: (i) The curve shows an hysteresis effect: e.g. a mean wind speed of 8 ms^{-1} during 14 September gave $\partial U/\partial z \approx 0.05s^{-1}$, but the same wind speed during 17 September gave $\partial U/\partial z \approx 0.02s^{-1}$ only. (ii) During the last two days, the wind gradient was negative. Note, that stratification was very close to neutral during the entire period studied, so stability effects can be ruled out as cause for the observed features.

It is thus clear that Eq. (6) with Eq. (11) is not valid during this entire period. The general explanation for this must be that the exchange process is governed by still another factor, the sea state. It can be quantified in terms of the 'wave age', c_0/U_{10}, where c_0 is the speed of the dominant waves. During the last two days of the measuring period c_0/U_{10} was found to be > 1.2, which characterizes swell.

This swell situation has been extensively studied in Smedman et al. (1999). One result is seen immediately from Figure 3: the negative wind gradient at 10 m. This is interpreted as a 'wave-driven wind', which is due to momentum being transported upwards by the swell. That this is not an exceptional state is seen from Figure 4, which shows the distribution of $(U_{14} - U_8)$ evaluated for the period 1995 - 1998 at Östergarnsholm. During 12% of the time, the wind gradient is negative.

The study of swell has received intensive interest during the last few years with several publications in international journals. The exchange of momentum is strongly reduced during swell and sometimes it is even negative (directed upwards), but parameterization of the phenomenon still needs to be done.

REFERENCES

Bergström, H. and Smedman, A., 1995: Stably stratified flow in a marine atmospheric surface layer. *Boundary-Layer Meteorol.*, **72**, 239 - 265.

Bergström, H. and Smedman, A., 1999, Wind climatology for a well-exposed site in the Baltic Sea. Submitted to *Wind Engineering*.

DeCosomo, J., K.B. Katsaros, S.D. Smith, R.J. Anderson, W.A. Oost, K. Bumke and H. Chadwick, 1996, Air-sea exchange of water vapor and sensible heat: The Humidity Exchange Over the Sea (HEXOS) results, *J. Geophys. Res.*, **101**, 12001 - 12016.

Donelan, M., Air-sea interaction. In: *The Sea*, 9, Ocean engineering science; Wiley, New York, 239 - 292, 1990.

Edson, J.B. and C.W. Fairall, 1998: Similarity relationships in the marine atmospheric surface layer for terms in the TKE and scalar variance budgets. *J. Atm. Sci.*, **55**, 2311 - 2328.

Högström, U., 1996, Review of some basic characteristics of the atmospheric surface layer. *Boundary-Layer Meteor.*, **78**, 215 - 246.

Johansson, C., A. Smedman, U. Högström, J.G. Brasseur and S. Khanna, Critical test of Monin - Obukhov similarity during convective conditions. Submitted to *J. Atm. Sci.*

Khanna, S. and J.G. Brasseur, 1997, Analysis of Monin-Obukhov similarity from large-eddy simulation. *J. Fluid Mech.*, **345**, 251-286.

Smedman, A., U. Högström, H. Bergström, A. Rutgersson, K.K. Kahma and H. Pettersson, 1999, A case-study of air-sea interaction during swell conditions, Accepted for publ. in *J. Geophys.Res.*

Yelland, M. and P. Taylor, 1996, Wind stress measurements from the open ocean, *J. Phys. Ocean.*
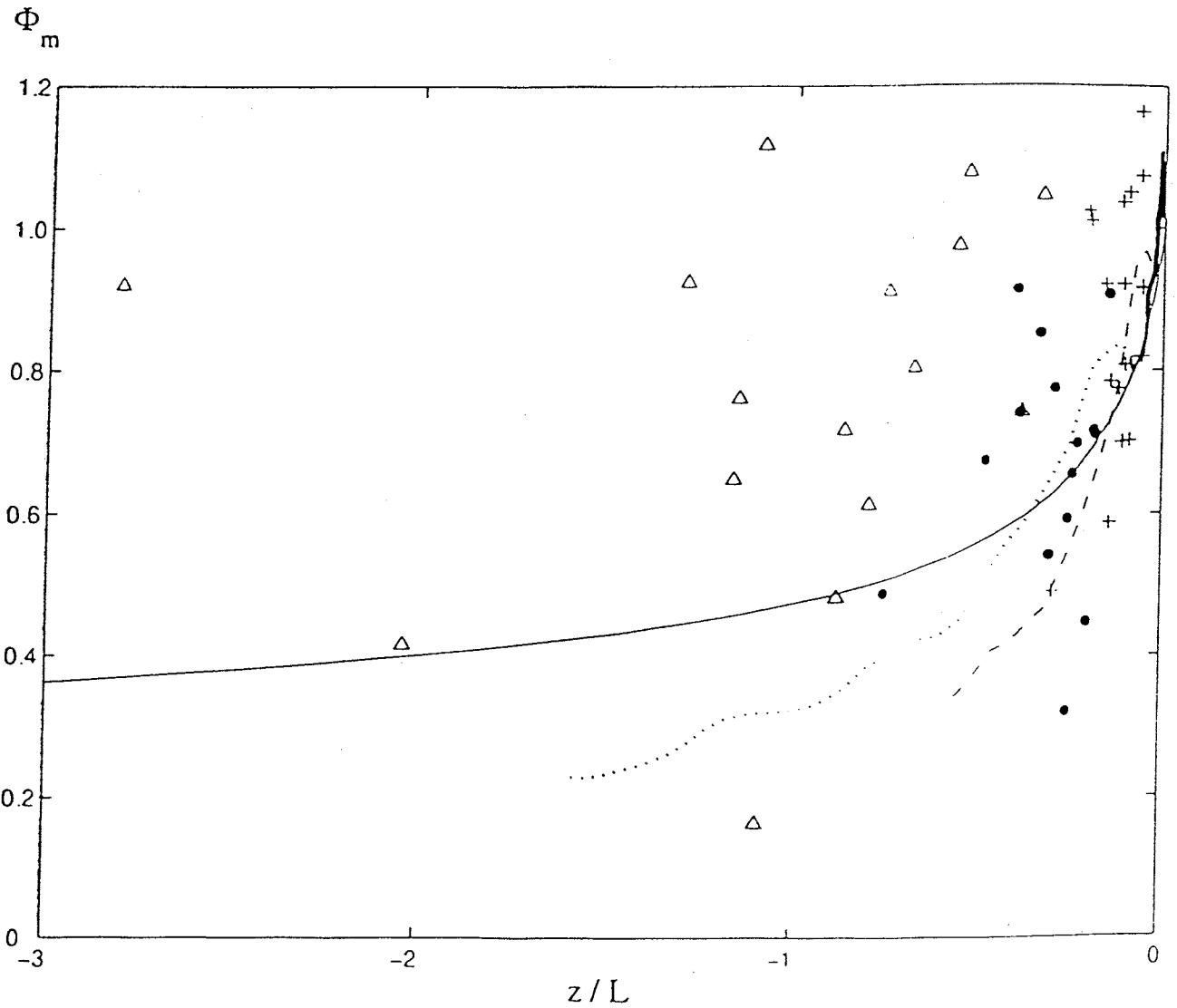
Figure 1. Plot of ϕ_m against z/L for measurements at Marsta in three z_i/L ranges: pluses, - 0.5 > z_i/L > - 5, filled circles, - 25 > z_i/L > - 35, and triangles, z_i/L < - 60. The thin line from Högström (1996). The other three lines are from the LES of KB97: full line, z_i/L = - 0.44; dashed line, z_i/L = - 3; dotted line, z_i/L = -8. - From Johansson et al (1999).
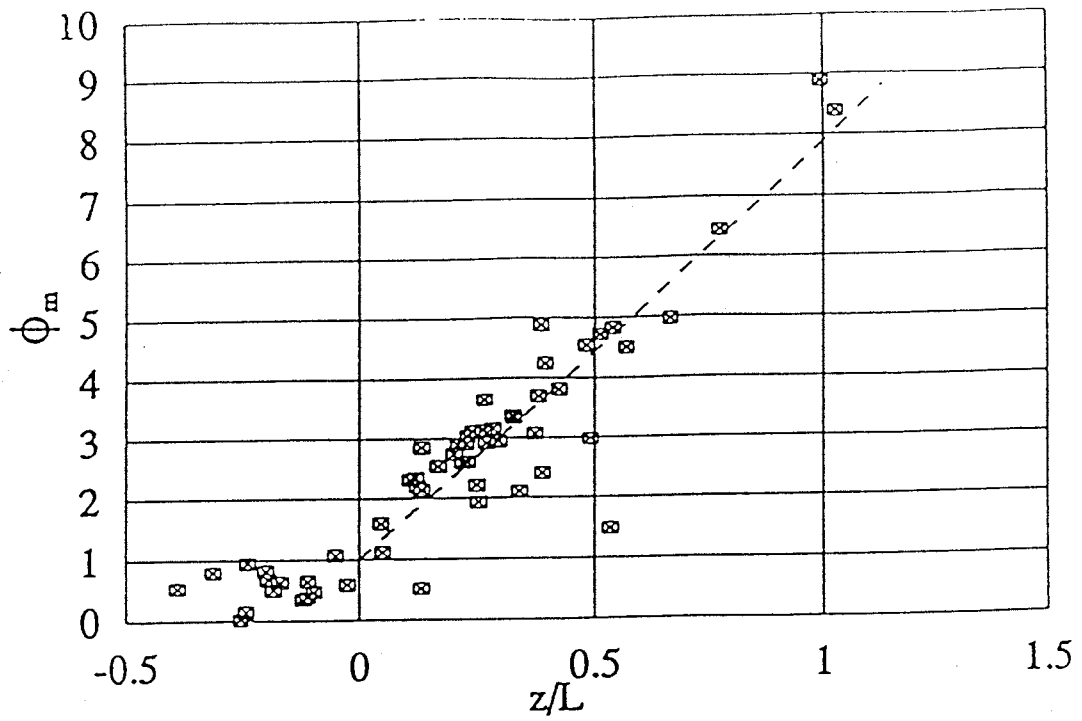
Figure 2.*a*. Non-dimensional wind gradient at 8 m at Nässkär as a function of z/L, no low-level jet. The dashed line is Eq. (9b). - From Bergström and Smedman (1995).
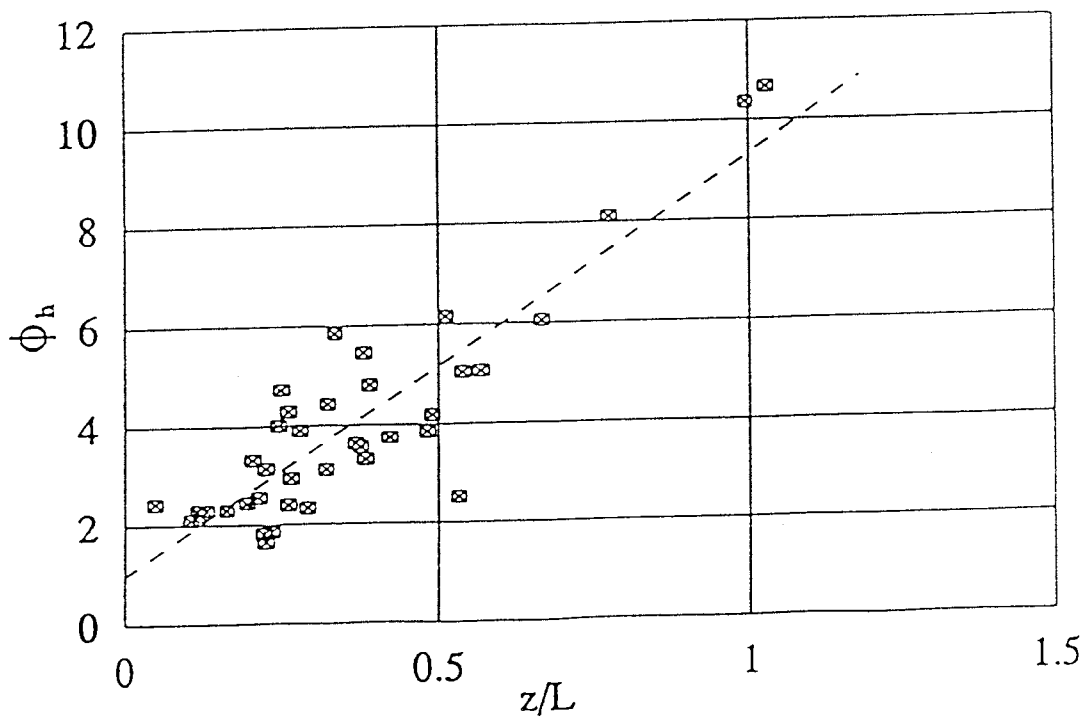
Figure 2*b*. Same as 2*a*, but for ϕ_h. The line is Eq. (10b). - From Bergström and Smedman (1995).
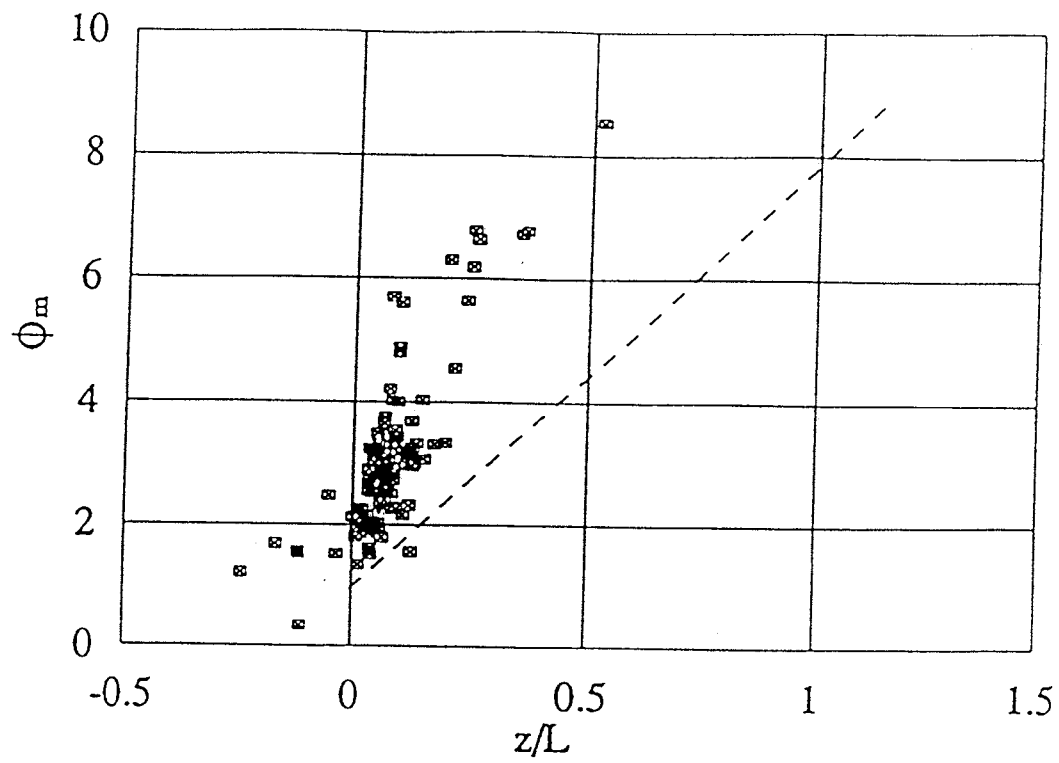
Figur 2c. Same as 2a but for cases with a low level jet. The dashed line is Eq. (9b). - From Bergström and Smedman (1995).
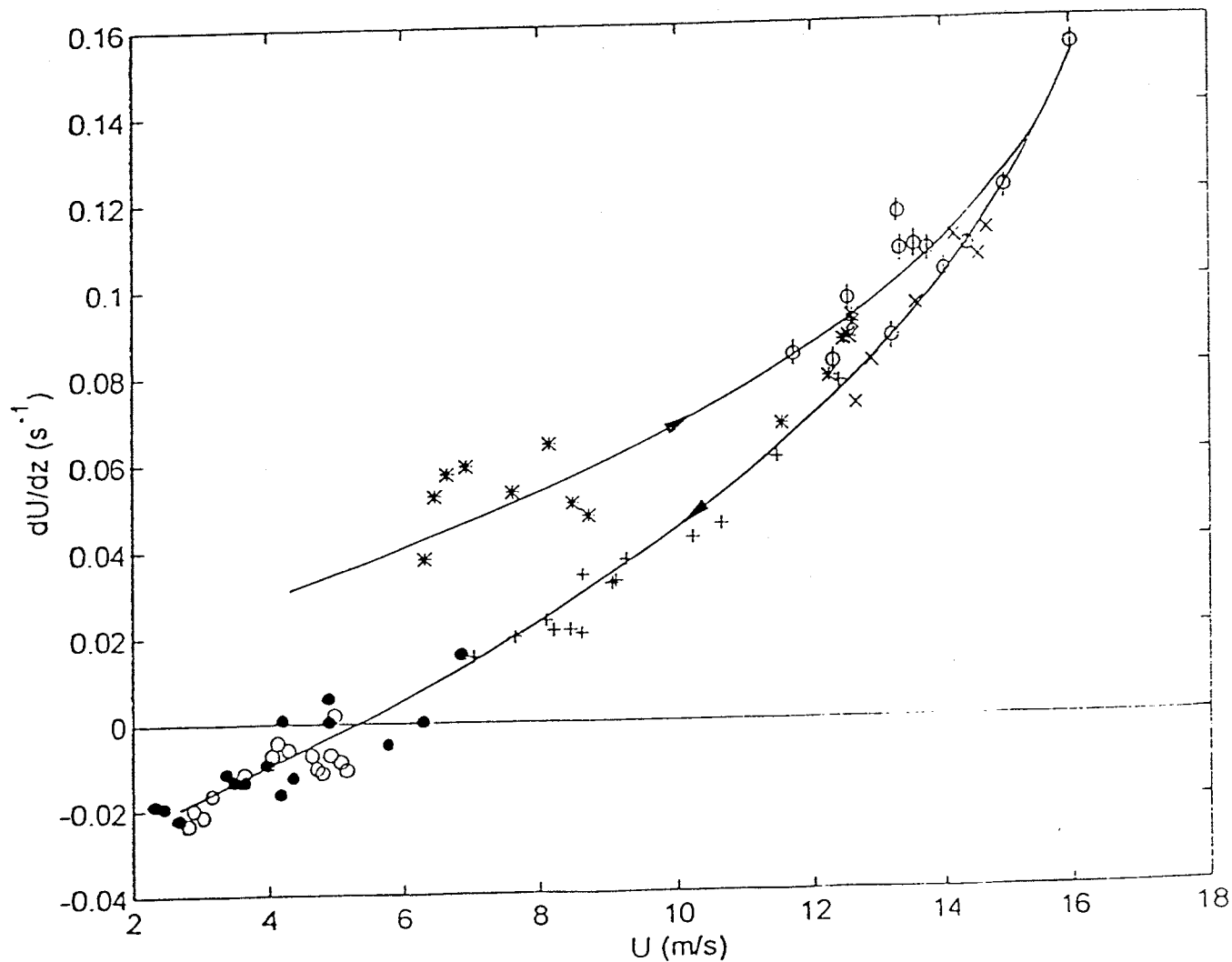
Figure 3. Estimated values of hourly mean wind speed gradient at 10 m (determined from cup anemometer measurements at 5 levels) at Östergarnsholm for the entire time period 14 - 19 September, 1995 plotted as a time sequence in the direction of the arrows indicated and as a function of wind speed at 10 m. Symbols: '*' 14 September; 'φ' 15 September; 'x' 16 September; '+' 17 September; ' •' 18 September;'o' 19 September. - From Smedman et al. (1999).
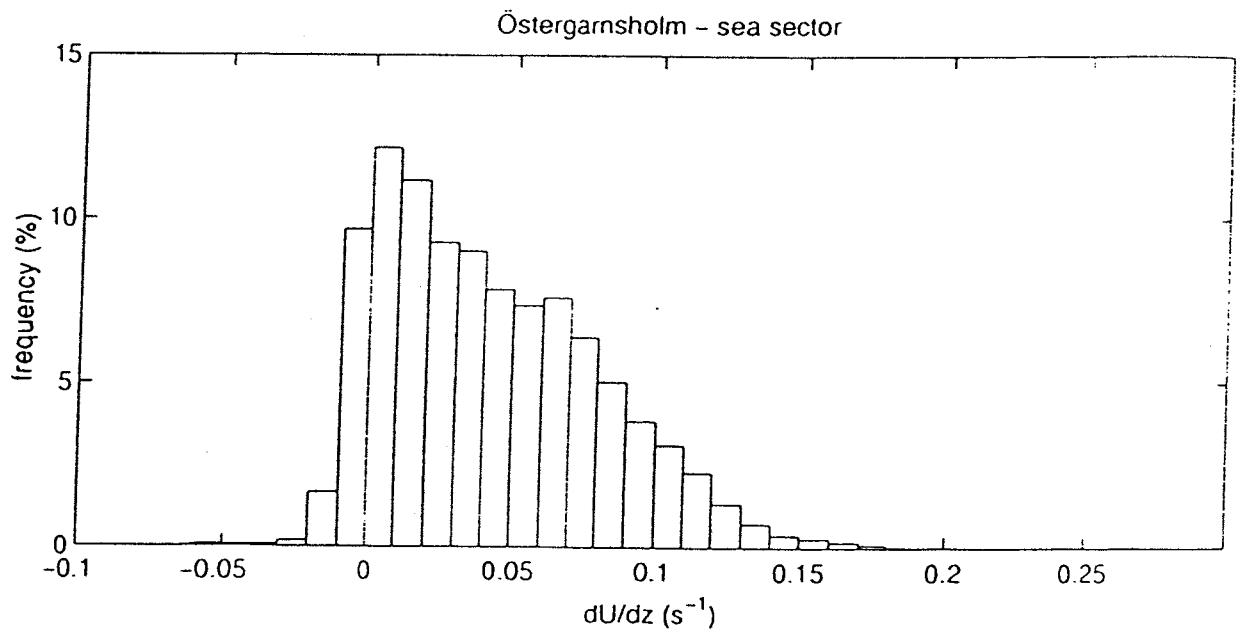
Figure 4. Observed frequency distribution of the wind gradient between 7 m and 14 m for the sea sector at Östergarnsholm wind from (60° - 220°). - From Bergström and Smedman (1999).

Modelling activities and model intercomparisons within BALTEX

Daniela Jacob

Max-Planck-Institute for Meteorology, Hamburg, Germany

1 Introduction

The major objective of BALTEX (the BALtic Sea Experiment) is to explore and quantify the energy and water cycles of the Baltic region (Bengtsson, 1995). One way to contribute to this objective is to reduce uncertainties in our understanding through modelling aiming for the quantification of the variety of processes which determine the space and time variability of the water and energy cycles. During the last years, within the EU-founded projects NEWBALTIC I and II (Numerical Studies of the Energy and Water Cycle of the Baltic Region) effort has been made to simulate atmospheric phenomena on time scales from days to decades and to validate the results against observations. In this paper some examples of the work within NEWBALTIC are presented, including simulations of one month, a model intercomparison effort for three months, sensitivity tests of almost two years and long climate simulations of 10 years. All groups participating in NEWBALTIC I and II (see final (1998) and annual reports (1999)) contributed to this work either through modelling activities or in the context of validation.

2 Model development

As an example for the development of parameterization schemes, a comparison of the total cloud cover derived from ISCCP (International Satellite Cloud Climatology Project) data and two simulations using REMO-DWD (physical parameterization schemes similar to the Europa Modell from the German Weather Service, DWD) for March 1994 is shown in Fig. 1.

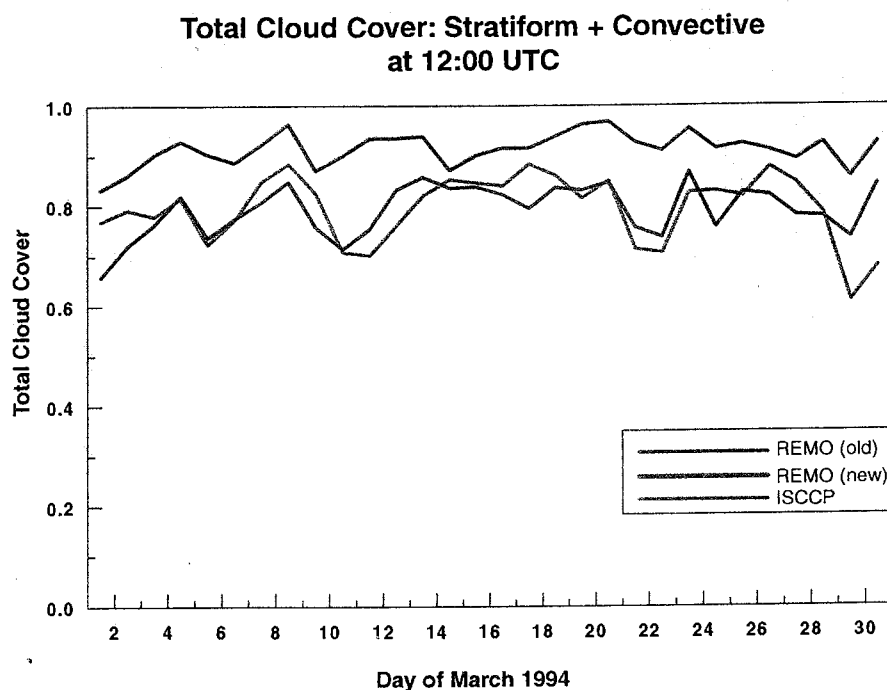**Total Cloud Cover: Stratiform + Convective
at 12:00 UTC**

Figure 1: Total cloud cover during March 1994, ISCCP (blue), REMO new (red) and REMO old parameterization (green)

It can clearly be seen that the old cloud ice parameterization led to an overestimation of total cloud cover compared to ISCCP. The new parameterization includes changes in the nucleation rate and takes into account that the supersaturation over ice is higher than over water. Both simulations have been started with no cloud ice; they were driven by DWD-analyses and performed at the GKSS research centre. For further detail see also Zhang et al, 2000.

3 Model Intercomparisons

Within NEWBALTIC all project partners agreed to carry out a model intercomparison, which will point to differences in numerical modelling of the atmospheric water and energy cycles. Observational data do not cover all components of the hydrological and energetic cycles, therefore the model intercomparison will discover uncertainties in model generated values. Together with a careful validation against observations the deficiencies of the models and the accuracy of model results can be determined.

Initial studies were performed with the different models taken as they were used within the groups. It turned out that the results became incomparable due to large differencs in resolutions and boundary conditions. Therefore a unique effort has been

made: all participating groups (the Britsh (UK met office), Danish (DMI), Dutch (KNMI), German (DWD) and Swedish (SMHI) weather services, and the German research centers: GKSS and Max-Planck-Institute for Meteorology (MPI)) agreed on a common vertical and horizontal grid spacing, identical initial and boundary conditions and a validation strategy which has been followed in the project.

The simulations have been performed on an area covering well the Baltic Sea catchment, on a horizontal resolution of 1/6°. Boundaries have been provided by DMI for the period 1st of August 1995 to 31st of October 1995, the PIDCAP period (Pilot study of Intense Data Collection and Analyses of Precipitation). During this time the data coverage over the Baltic Sea catchment was enhanced. All models were initialized in the same way, but run either in forecast mode (30 hour forecasts including 6 h spin-up time, model: REMO-GKSS), in assimilation mode (30 hours forecasts including 6 h spin-up time and data assimilation, models: DWD using the Baltex Model and DMI using HIRLAM) or in climate mode (initialized once and continuously forced at the lateral boundaries, models: HIRLAM at SMHI, RACMO at KNMI, UKMO at UK met office and REMO at MPI: using either DWD physical parameterizations (REMO-DWD) or the physical schemes from the global climate model ECHAM4 (REMO-EC4)).
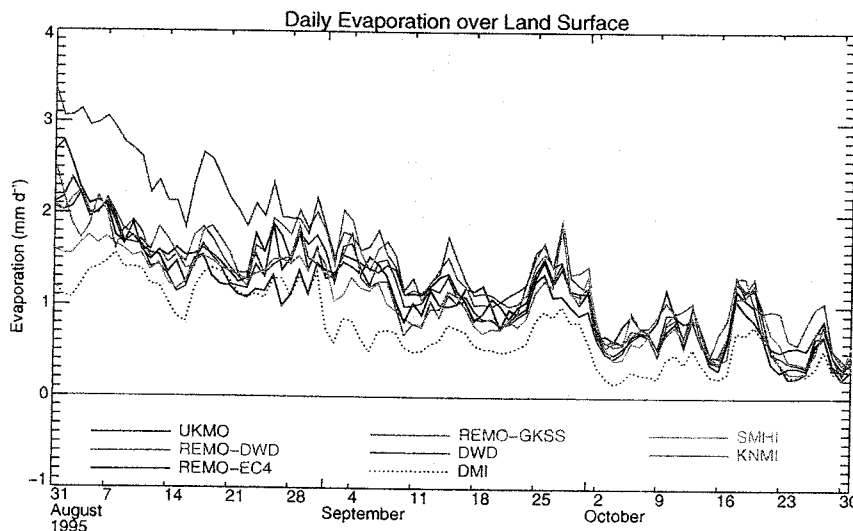

Figure 2: Daily evaporation over land surfaces within the Baltic Sea drainage basin during August to October 1995

Results

Different variables important for the water and energy cycles have been compared against each other and against observations. All models captured the development of synoptic events quite well, which is reflected in a good agreement between observations of precipitation and vertically intergrated specific humidity (derived from GPS-data) compared to model results (not shown here). Large inconsistencies have been found in the comparisons of evaporation over land and runoff into the Baltic Sea due to different but related reasons. Fig. 2 shows the time series of evaporation derived from seven model runs.

Large differences occur during the first three weeks. This points to deficiencies in the initializations. Although all models started from the same soil moisture field, the method of interpolating the amount of moisture on to the different soil parameterization variables was slightly different and led to differences in the percentage of saturation. Differences were as large as 2 mm/day (REMO-DWD, DMI). A comparison of the time series of REMO-GKSS and REMO-DWD, which are using the identical surface parameterizations but started from different filling percentages of the soil, show clearly the importance of the soil moisture initialization. During the rest of the simulation period differences in evaporation were strongly influenced by the treatment of soil and vegetation. For example all HIRLAM realizations show less evaporation than the other models. This can probably be referred to the parametrization of vegetation, which is missing in HIRLAM.

The comparison of total runoff (Fig. 3) to the Baltic Sea is another very useful study, because it gives an integrated view of the simulated hydrological components in the atmospheric models. The observation of runoff has been substituted by a control run of the hydrological HBV-model at SMHI (Bergström, 1995). This model is well tested and can be seen as close to reality.

There are large differences in the runoff simulations: one model produces no runoff (UKMO), most of the other models over-estimate the runoff during precipitation events. A clear correlation between runoff generation and precipitation can be seen, which is not so strong in reality. Again deficiencies in the soil moisture initialization together

with the formulation of runoff generation within the soil can be detected, see for example REMO-EC4. In this simulation most of the precipitation is stored in the soil and used to fill up the soil with water until saturation is reached. It takes almost one month before a sufficient amount of runoff is produced. A similar behaviour can be seen in RACMO results, which is reasonable since the parameterization schemes of REMO-EC4 and RACMO are very similar.

Conclusions

The large differences between the model results can clearly be related to differences in the parameterization of physical processes, especially for models using identical numerics and dynamics (REMO-DWD, REMO-EC4, REMO-GKSS). Most surprising is the substantial influence of the handling and initialization of soil moisture and soil hydrology. Other aspects are related to cloud processes.

The model intercomparison effort was not only successful in describing differences between the models and observations, it gave a first impression on the uncertainties involved in the modelling of the water and energy cycles and it led also to further model developments. For example, a systematic underestimation of total cloud cover using REMO-EC4 has been detected. Changes in the treatment of clouds in REMO-EC4 cured the problem.

4 Intercomparison of horizontal resolution and physical parameterizations

A detailed investigation was carried out for the period January 1992 to September 1993 to study the influence of horizontal resolution and again physical parameterizations. Four simulations have been performed using REMO-EC4 and REMO-DWD on 0.5° and 0.16° horizontal resolutions. Both parameterization schemes are implemented in one model code, therefore it is guaranteed that differences occur due to the above mentioned changes. All runs were carried out using DWD-analyses at the lateral boundaries. As an example, the time series of total precipitation over land (for the Baltic Sea catchment) as well as the corrected observations (provided by SHMI) are shown in Fig. 4.
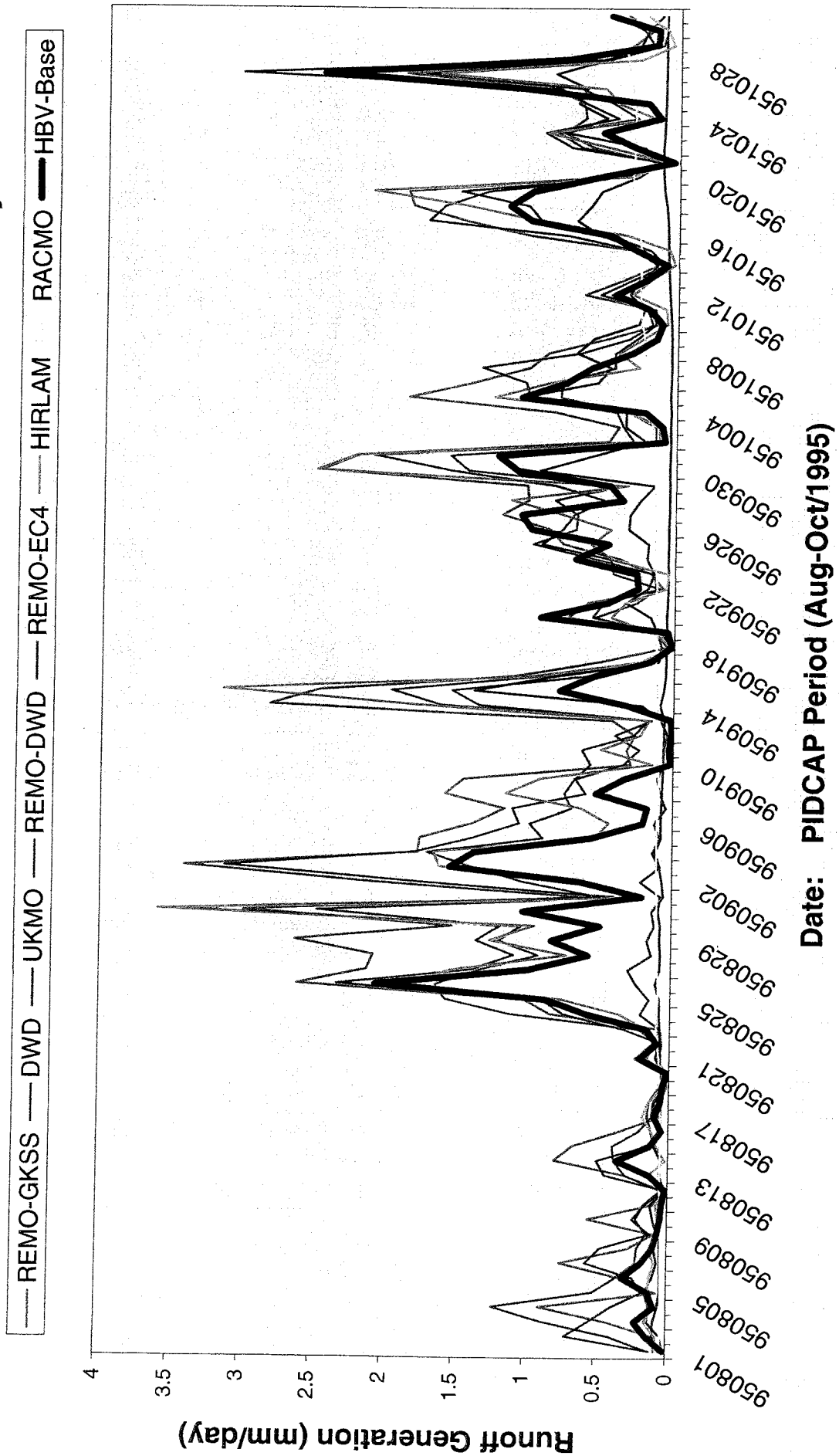
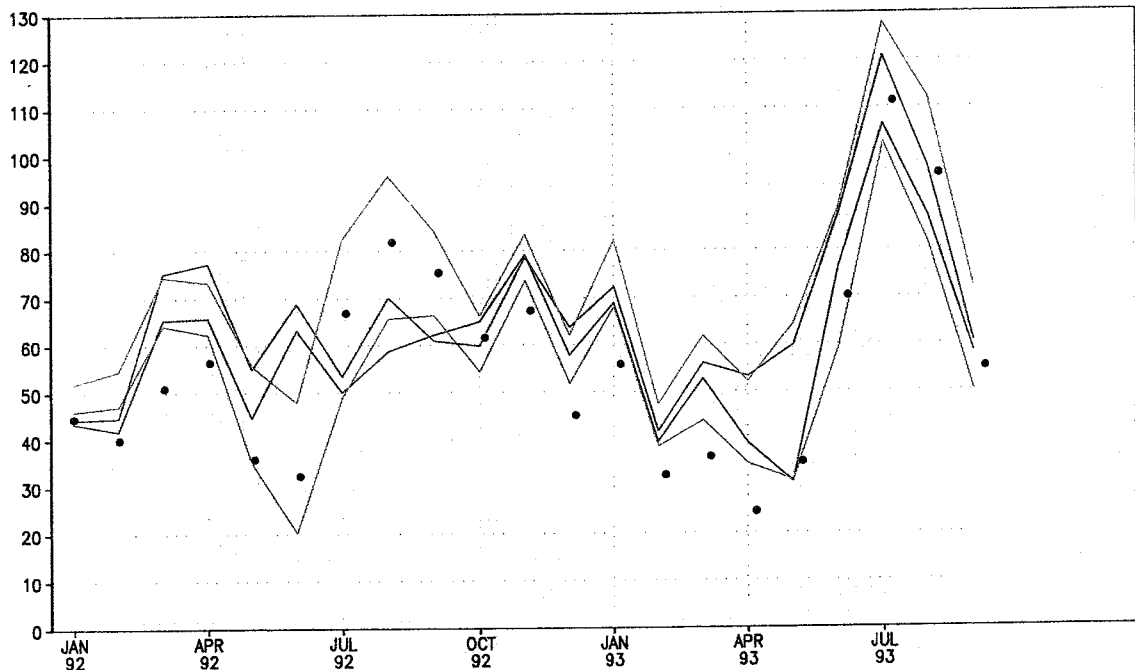Figure 3: Total runoff into the Baltic Sea during August to October 1995

Figure 4: Total precipitation over land surfaces within the Baltic Sea drainge basin. Horizontal resolution 0.5°: REMO-DWD (red) and REMO-EC4 (green), horizontal resolution 0.16°: REMO-DWD (blue) and REMO-EC4 (orange). Observations are corrected values for precipitation (dots). Unit is mm.

It is obvious, that the general structure of the annual cycle is well captured by all realizations. Especially during winter, there is a good agreement between observations and all simulations, however the amount of precipitation is generally slightly overestimated from Nov. 92 until April 93. REMO-EC4 has a strong overestimation of precipitation in spring on both resolutions, which seems to be related to an intense convection over saturated soils. This leads to an enhanced vertical moisture transport triggering preci-pitation. The simulation of precipitation in spring using REMO-DWD is in much better agreement with observations, however the peak in July 1993 is under-estimated. Using REMO-EC4 only the extreme value in July seems to be well captured. Both 0.5° runs are very similar, but during the first summer both deviate from observations. Both show no annual cycle in 1992. The detailed structure of the observed time series is much better represented using REMO on 0.16° resolution. However during the first spring and summer the runs using different physical packages differ strongly. It can not be decided from this study which simulation is closest to reality. Further work is in progress.

5 Annual and interannual variability

To investigate the annual and interannual variability of the water budget for todays climate, several experiments with REMO-EC4 have been performed on a time scale of 10 years (Jacob and Podzun, 2000).

For validation, REMO-EC4 on 0.5° resolution was driven by ECMWF re-analyses for the period 1979 to 1988. The time series of uncorrected observed and calculated total precipitation over the Baltic Sea drainage basin (land only) are shown in Fig. 5.

The good agreement demonstrates that REMO-EC4 driven by *perfect boundaries* is able to simulate an annual cycle close to observations. It also shows that there is no systematic bias in the long term climate simulation. However there are still deviations in spring and early summer resulting in an overestimation of precipitation, which might be due to deficiencies in the soil parameterization as mentioned earlier. Comparing the means, REMO-EC4 overestimates the long term mean by roughly 10 %, assuming the correction of precipitation for undercatch is about 5 %.
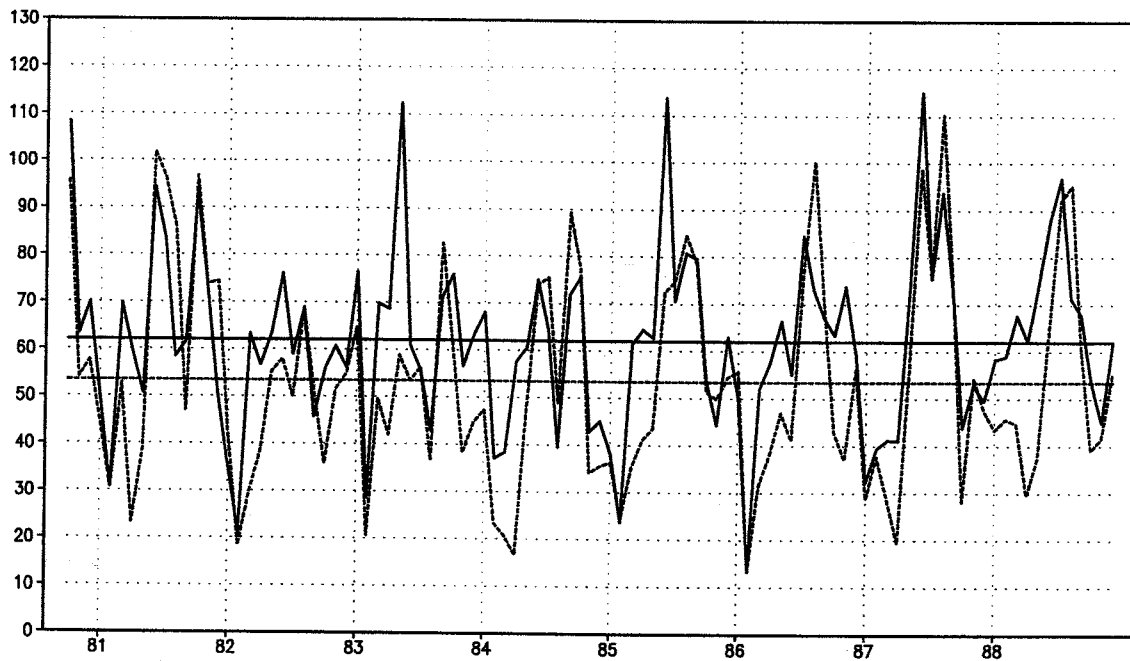
26

Figure 5: Time series of observed (uncorrected, dashed) and simulated (solid) mean and monthly total precipitation for 1980 to 1988 over land surfaces within the Baltic Sea drainge basin. Unit is mm.

To investigate the influence of horizontal resolution REMO-EC4 has been driven by ECHAM4-T106 data (horizontal resolution about 1°) from a ten years long AMIP-simulation using observed sea surface temperatures for the period 1979 to 1988. Both runs have been analysed.

Fig. 6 shows the mean annual cycles over ten years of the total precipitation within the Baltic Sea drainage basin compared to uncorrected observations (bullets) for the ECHAM4-T106 (red curve), REMO-EC4 driven by ECHAM4-T106 (blue) and REMO-EC4 driven by ECMWF re-analyses (green). It is evident that REMO-EC4 driven by so-called perfect boundaries is closest to observations. In fall and winter a very good agreement can be seen, but the above mentioned over-estimation of precipitation in spring can still be detected. Furthermore the calculated total precipitation in the global model shows no annual cycle for this period, while the results of REMO-EC4 driven by ECHAM4 output provide an annual cycle. In the last experiment again an overestimation of precipitation in winter and spring is visible, which seems to be a result of the too moist boundary conditions and the deficiencies in the soil parameterization. A detailed investigation of the long runs is in progress.

6 Conclusions

Major progress has been made in exploring and quantifying the water and energy cycles of the Baltic region with numerical models. It could be demonstrated that all models simulate atmospheric phenomena without any systematic biases after proper initialization. This could partly be achieved through the strict model intercomparison study, which gave insight into the uncertainties involved in modelling the water and energy cycles. The careful validation against observations led to a good progress in model development. However the water and energy cycles for the Baltic region are not quantified until now.

7 References

Bengtsson, L. (1995): Baltic Sea experiment BAL-TEX: Initial Implementation Plan. Intern. BAL-TEX Secr., Publ. No.2, 84pp.

Bergström, S. (1995): The HBV model. In: Singh VP (ed) Computer Models of Watershed Hydrology. Water Resources Publications, Highland Ranch, Colorado, p.443-476
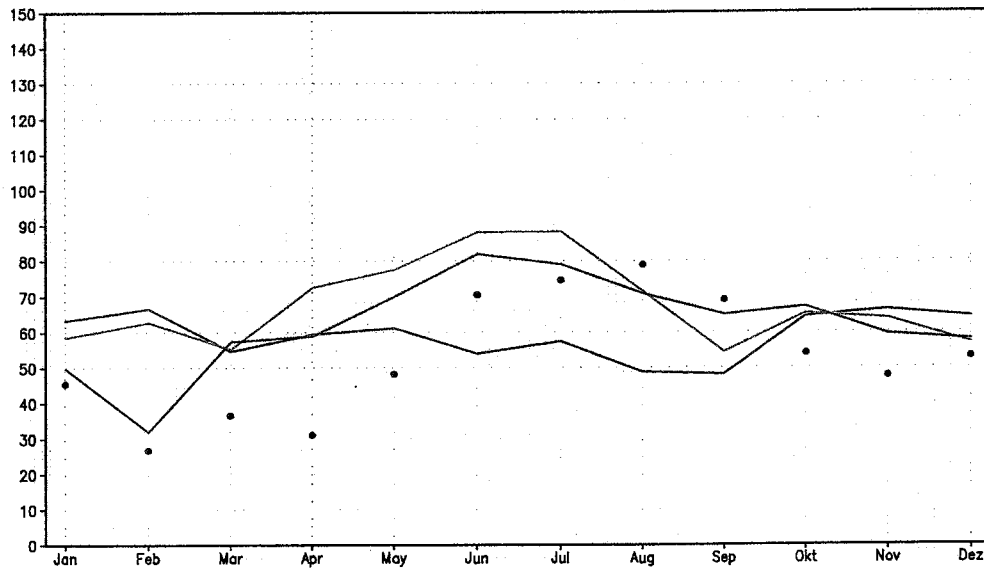
Figure 6: Ten years monthly mean observed (uncorrected, dots) and simulated total precipitation over land surfaces within the Baltic Sea drainge basin. ECHAM4-T106 (red), REMO-EC4 driven by ECHAM4-T106 (blue) and REMO-EC4 driven by ECMWF re-analyses (green). Unit mm/month.

Jacob, D., Podzun, R. (2000): Investigation of the annual and interannual variability of the water budget over the Baltic Sea drainage basin using the regional climate model REMO. WMO/ JCSU/IOC report 1999, in print.

NEWBALTIC I final (1998) and II annual (1999)

reports available at Max-Planck-Institute, Hamburg; Germany

Zhang, Y., B. Rockel, R. Stuhlmann, R. Hollmann and U. Karstens (2000): REMO Cloud Modeling: Improvements and Validation with ISCCP DX Data, accepted by Journal of Applied Meteorology

A comparison of three different turbulence parameterization schemes for HIRLAM

Niels Woetmann Nielsen, DMI, Copenhagen

1. INTRODUCTION

Turbulent transport of moisture, sensible heat and momentum plays an important role in the atmosphere. The parameterization of turbulence in numerical models of the atmosphere is therefore of great concern. Until recently the turbulence parameterization in HIRLAM has been a variant of the Louis scheme (Louis et al., 1981). Three alternative turbulence parameterization schemes have now been developed for HIRLAM. The purpose here is briefly to account for the most significant difference between the schemes.

The schemes in concern are a 1.order nonlocal scheme (T1), a 1.5 order local turbulent kinetic energy (TKE) scheme (T2) and a 1.5 order nonlocal TKE scheme (T3). In HIRLAM terminology T1, T2 and T3 are known as the Holtslag scheme, the CBR scheme and the Perov scheme, respectively. Basic references to these schemes are respectively, Holtslag and Boville, 1993; Cuxart et al., 1995, and Perov and Gollvik, 1996.

2. BASIC EQUATIONS

The effect of turbulence on the mean flow is approximated by

$$\partial \overline{u}/\partial t = -\partial \overline{u'w'}/\partial z, \tag{1}$$

$$\partial \overline{v}/\partial t = -\partial \overline{v'w'}/\partial z, \tag{2}$$

$$\partial \overline{\theta}_v/\partial t = -\partial \overline{\theta_v'w'}/\partial z, \tag{3}$$

$$\partial \overline{q}/\partial t = -\partial \overline{q'w'}/\partial z, \tag{4}$$

$$\partial \overline{q}_c/\partial t = -\partial \overline{q_c'w'}/\partial z, \tag{5}$$

i.e. the horizontal derivatives of the second order covariance (Reynold) terms are assumed to be much smaller than the vertical derivatives. Note that specific cloud water (q_c) is included as a prognostic variable. To the same level of approximation the TKE equation takes the form

$$\frac{\partial \overline{E}}{\partial t} + \overline{u_j} \cdot \frac{\partial \overline{E}}{\partial x_j} = - \left[\overline{u'w'} \cdot \frac{\partial \overline{u}}{\partial z} + \overline{v'w'} \cdot \frac{\partial \overline{v}}{\partial z} + \overline{w'w'} \cdot \frac{\partial \overline{w}}{\partial z} \right]$$
$$+ \left[\frac{g}{\overline{\theta_v}} \overline{w'\theta_v'} \right] - \left[\frac{1}{\rho} \frac{\partial \overline{p'w'}}{\partial z} \right] - \left[\frac{\partial \overline{E'w'}}{\partial z} \right] - \epsilon \tag{6}$$

In (6) $\overline{E} = \frac{1}{2}\left(\overline{u'^2 + v'^2 + w'^2} \right)$ is the TKE and ϵ is the dissipation of TKE. Other symbols have their usual meaning. T2 and T3 use simplified forms of (6). In T2 the last term in the first square bracket (SB) is neglected together with the pressure-vertical velocity covariance (third SB term) and the divergence of the vertical TKE transport (fourth SB term). In T3 only the pressure-vertical velocity covariance term is neglected.

The parameterization relates the second order moments to mean variables by assuming relations of the form

$$-\overline{\zeta'w'} = K_\zeta \cdot \left(\frac{\partial \overline{\zeta}}{\partial z} - \gamma_\zeta \right); \tag{7}$$

$$\zeta = u, v, \theta, q, q_c.$$

In (7) K_ζ is an eddy exchange coefficient analogous to the molecular viscosity and diffusivity coefficients and γ_ζ is a countergradient term accounting for upgradient turbulent transport of for example sensible heat in the convective boundary layer. The only exception from this rule is the parameterization of $-\overline{w'w'}$, which only appears in T3. This term is instead parameterized by assuming (Rodi, 1980; Perov and Gollvik, 1996)

$$\overline{w'w'} = \frac{2}{3}\overline{E} - 2K_u\frac{\partial \overline{w}}{\partial z}. \tag{8}$$

K_u is defined in the next section.

3. EDDY EXCHANGE COEFFICIENTS

In T1 the eddy exchange coefficient is specified differently in and above the planetary boundary layer (PBL).

In the PBL ($z \leq h$, where h is the PBL height) K_ζ is given by

$$K_\zeta = k \cdot w_\zeta \left(z/L \right) \cdot z \cdot \left(1 - z/h \right)^2, \qquad (9)$$

and above the PBL ($z > h$)

$$K_\zeta = l^2 \cdot \left| \frac{\partial \overline{V}}{\partial z} \right| \cdot f_\zeta \left(Ri \right). \qquad (10)$$

In (9) k is the Von Karman constant and w_ζ is a vertical velocity scale depending on the Monin-Obukhov stability parameter z/L and on the variable ζ in concern, i.e. u, v, θ, q or q_c. For more details, see Holtslag and Boville, 1993 and Nielsen, 1998. In (10) l is a mixing length (see section 5) and $f_\zeta \left(Ri \right)$ a stability function depending on the Richardson number Ri following Louis et al., 1981 for $Ri > 0$ and Holtslag and Boville, 1993 for $Ri \leq 0$.

The two TKE schemes are more advanced in the sense that the eddy exchange coefficients depend on TKE. In T2 K_ζ is specified as

$$K_\zeta = c_\zeta \cdot K_u \cdot \phi_3 \left(Rs \right), \qquad (11)$$

where c_ζ is a nondimensional constant and $K_u = l \cdot \sqrt{\overline{E}}$ is the eddy exchange coefficient for momentum. ϕ_3 is a function of the dry Redelsperger number Rs

$$Rs = \frac{g}{\overline{\theta_v}} \cdot \frac{l^2}{\overline{E}} \left(1 + 0.61 \overline{q} \frac{\partial \overline{\theta}}{\partial z} + 0.61 \overline{\theta} \frac{\partial \overline{q}}{\partial z} \right). \qquad (12)$$

ϕ_3 takes the form (Cuxart et al. 1995)

$$\phi_3 = \left(1 + 0.139 \cdot Rs \right)^{-1}, \qquad (13)$$

where Rs is controlled by the condition $Rs = max\{-3.924, min\{Rs, 71935.252\}\}$. The scheme is prepared for a change from the "dry" variables θ, q and q_c to the "moist" variables θ_l (liquid water potential temperature) and $q_t = q + q_c$ (total specific humidity). The Redelsperger number should for example be replaced by its moist version, i.e. the vertical gradients of $\overline{\theta}$ and $\overline{q}$ in (12) should be replaced by corresponding gradients of $\overline{\theta_l}$ and $\overline{q_t}$.

Finally, in T3 the eddy exchange coefficient is specified as

$$K_\zeta = \alpha_\zeta \cdot K_u, \qquad (14)$$

where $K_u = c_\epsilon \cdot \overline{E}^2 / \epsilon = l\sqrt{\overline{E}}$. c_ϵ is a nondimensional constant and α_ζ is the inverse turbulent Prandtl number for variable ζ (Bougeault and Lacarrére, 1989). Like T2 the scheme is prepared for a change from "dry" to "moist" variables. Note that the covariance $\overline{E'w'}$ is retained in the TKE equation (6). Accordingly, the list of variables in (7) is expanded with $\zeta = \overline{E}$. T3 also contains a prognostic equation for the dissipation of TKE (see section 6), which requires a further expansion of the variable list in (7) with $\zeta = \epsilon$.

4. COUNTERGRADIENTS

In all schemes the countergradient γ_ζ is set to zero if the surface layer is stably stratified ($z/L > 0$). It is assumed in T1 that only the countergradient for sensible heat is nonzero. Following Holtslag and Moeng, 1991 and Nielsen and Sass, 1995

$$\gamma_\theta = d_0 \left(\frac{z}{h} \right)^{1/3} \frac{w_*}{w_m{}^2 \cdot h} \left(\overline{iw'\theta'_v} \right)_s, \qquad (15)$$

where w_* is the convective velocity scale (Deardorf, 1972), $\left(\overline{w'\theta'_v} \right)_s$ is the kinematic vertical virtual sensible heat flux at the surface, d_0 a nondimensional constant and w_m given by

$$w_m = w_* \left(\left(\frac{u_*}{w_*} \right)^3 + 15 \cdot k \frac{z}{h} \right)^{1/3}. \qquad (16)$$

The T2 scheme has no countergradient terms.

In T3 γ_θ is calculated as in T1. T3 also contains a countergradient term for TKE given by (Perov and Gollvik, 1996)

$$\gamma_E = \frac{k_{1E}}{\alpha_E \cdot K_u} \cdot \frac{g}{\theta_v} \left(\overline{w'\theta'_v} \right)_s \cdot w_* \cdot \frac{\overline{E}}{\epsilon}. \qquad (17)$$

Here k_{1E} is a nondomensional constant and α_E is the inverse turbulent Prandtl number for TKE.

5. MIXING LENGTH

An expression for the mixing length l is needed to close the system of equations in T1 and T2. In T3 the system is closed by adding a prognostic equation for ϵ and close this equation by a number of assumptions (for details, see Perov and Gollvik, 1996).

In T1 the term $k \cdot z \cdot \left(1 - z/h \right)^2$ in (9) can be interpreted as a diagnostic mixing length within the PBL and the velocity scale w_ζ can be considered as a crude measure of $\sqrt{\overline{E}}$. Above the PBL a Blackadar formula (Blackadar, 1962) is used with an assymptotic mixing length of 30 metre.

In T2 l is calculated diagnostically from

$$l = \sqrt{l_u \cdot l_d}, \qquad (18)$$

where l_u and l_d are the distances an air parcel must be displaced upward or downward before its TKE has been consumed by buoyancy (Bougeault and Lacarrére, 1989).

In T3 l is given by

$$l = c_\epsilon \frac{\overline{E}^{3/2}}{\epsilon}, \qquad (19)$$

i.e. l is determined by the two prognostic variables $\overline{E}$ and ϵ.

6. TKE DISSIPATION

$\overline{E}$ and ϵ are not available for T1.
In T2 ϵ is determined by

$$\epsilon = c_l \cdot \frac{\overline{E}^{3/2}}{l}, \qquad (20)$$

where c_l is a nondimensional constant. Note here a basic difference between T2 and T3. ϵ is determined by $\overline{E}$ and a diagnostic l in T2, while ϵ in T3 is a prognostic variable and l subsequently determined from (19).

The prognostic equation for ϵ in T3 reads (Perov and Gollvik, 1996)

$$\frac{\partial \epsilon}{\partial t} = \frac{\epsilon}{\overline{E}} \left[C_1 \epsilon \left(-\overline{u'w'}\frac{\partial \overline{u}}{\partial z} - \overline{v'w'}\frac{\partial \overline{v}}{\partial z} - \overline{w'w'}\frac{\partial \overline{w}}{\partial z} + \frac{g}{\theta_v}\overline{\theta_v'w'} \right) \right]$$
$$-C_{2\epsilon}\frac{\epsilon^2}{\overline{E}} - \overline{w}\frac{\partial \epsilon}{\partial z} + \frac{\partial}{\partial z}K_\epsilon\frac{\partial \epsilon}{\partial z}, \qquad (21)$$

where the coefficients $C_{1\epsilon}$ and $C_{2\epsilon}$ are functions of the turbulent Reynolds number $Re = 4\overline{E}^2/9\nu\epsilon$ (Aupoix et al., 1989 ; Lykossov, 1993). In the latter formula ν is the molecular kinematic viscosity of air.

7. BOUNDARY LAYER HEIGHT

The PBL height is calculated in all the schemes, but it is only an important parameter in the turbulence parameterization in the nonlocal schemes T1 and T3. In T2 it only has a rather weak impact through the convective velocity scale in the lower boundary condition for TKE (see section 8).

Following Troen and Mahrt, 1986, h is in T1 and T3 determined as the height where the bulk Richardson number Ri_b

$$Ri_b = \frac{z \cdot g \cdot (\theta_v(z) - \theta_{vs})}{\theta_{vs} \cdot \left|\overrightarrow{V}(z)\right|^2}, \qquad (22)$$

first time exceeds a critical bulk Richardson number (in the range from 0.25 to 0.5) when increasing z from zero (i.e. when moving upward from the surface). In the convective PBL an excess temperature is added to θ_{vs} (Troen and Marht, 1986; Holtslag and Boville, 1993). In T1 the denominator in (22) has been replaced by $\theta_{vs} \cdot \left(\left|\overrightarrow{V}(z) - \overrightarrow{V}(z_b)\right|^2 + 100 \cdot u_*^2 \right)$, where z_b is the height of the lowest model level (Vogelezang and Holtslag, 1996).

In T2 h is simply estimated as the height above the ground where the TKE first time becomes less than $0.01\,m^2s^{-2}$.

8. LOWER BOUNDARY CONDITION FOR $\overline{E}$ AND ϵ

It is necessary to specify a lower boundary condition for $\overline{E}$ in T2 and for both $\overline{E}$ and ϵ in T3.

In T2 the TKE at the bottom level (index b) is specified as

$$\overline{E_b} = 3.75 \cdot u_*^2 + \delta_u \cdot \left[u_*^2 \cdot \left(-\frac{z_b}{L} \right)^{2/3} + 0.2w_*^2 \right], \qquad (23)$$

with $\delta_u = 1$ or 0 if the surface layer is unstably or stably stratified, respectively.

The corresponding equation in T3 is identical with (23) except that the term $(-z_b/L)^{2/3}$ is replaced by $(-Ri)^{3/2}$.

The lower boundary condition for the TKE dissipation in T3 is specified as

$$\epsilon_b = \frac{u_*^3}{k \cdot z_b} \left(\phi_m\left(\frac{z_b}{L}\right) - \frac{z_b}{L} \right), \qquad (24)$$

where ϕ_m is the nondimensional wind profile function (Businger et al., 1971).

9. PARALLEL EXPERIMENTS

The schemes have been verified in parallel data assimilation-forecast runs in a period from 27th January to 12th February within the Fastex experiment period in 1997. The HIRLAM 4.3.4 reference data assimilation-forecast system was utilized. The selected integration area , $110 \cdot 100$ gridpoints, covered the North-East Atlantic, Europe and Greenland with a resolution of $0.5° \cdot 0.5°$ and with 31 hybrid levels. +48 hour forecasts were run from the analyses at 00 UTC and 12 UTC (making a total of 29 two-day forecasts).

The forecasts were verified against observations. The verification results are presented in Kållberg and Ivarsson, 1999. Here the bias and root mean square error (rms) of surface parameters (mean sea level pressure, temperature and dewpoint at 2 metre height, total cloud cover in octas and wind speed at 10 metre height) are reproduced in Table 1 and 2. The differences in the verification scores are rather small.

The quality of precipitation forecasts (12 hour accumulation from + 18h to + 30h and from +30h to +42h) is summarized in Table 3. This table shows that the differences in precipitation forecast quality between the schemes also are small. More specifically: For the limit of 2.0 mm in 12 hours, T2 has the best probability of detection, 70.3%, with 67.6% and 67.3% for T1 and T3, respectively. The false alarm rate is 44.7% in both T2 and T3, while it is 46.9% in T1.

Somewhat larger differences were found in the vertical profiles of bias and rms of temperature, wind and humidity, mostly in favor of the T2 scheme (figures are presented in Kållberg and Ivarsson,1999). These results has lead to a replacement of T1 (Holtslag scheme) with T2 (CBR scheme) in the HIRLAM reference system.

After the experiment was done in January 1999 a few modifications and error corrections have been made in both T2 and T3, which further has improved the performance of these schemes. The documentation of T2 and T3 presented in the previous sections is for the updated versions of the schemes. A thorough parallel test with the updated schemes in data assimilation-forecast mode remains to be done.

TABLE I: **Bias against Synop/Ship for all +30/+42/+48 hour forecasts**

experiment	P_{msl} hPa	T_{2m} K	Td_{2m} K	$Octas$	$Wind_{10m}$ m/s
T1	+0.2	-0.8	+0.7	+0.6	+0.1
T2	+0.2	-0.4	+1.0	+0.6	+0.2
T3	+0.2	-0.5	+0.8	+0.0	+0.1

TABLE II: **RMS against Synop/Ship for all +30/+42/+48 hour forecasts**

experiment	P_{msl} hPa	T_{2m} K	Td_{2m} K	$Octas$	$Wind_{10m}$ m/s
T1	1.2	3.0	3.1	3.2	2.5
T2	1.3	3.0	3.3	3.2	2.5
T3	1.2	2.9	3.1	3.2	2.5

TABLE III: **+12h precipitation > / < 2.0 mm**

$forecasts$:	$observed < 2.0$ mm/12h	$observed > 2.0$ mm/12h	$cases$
$T1 < 2.0$	3678	202	3880
$T1 > 2.0$	372	421	795
$T2 < 2.0$	3696	185	3881
$T2 > 2.0$	354	438	792
$T3 < 2.0$	3711	204	3915
$T3 > 2.0$	339	419	758
$obser-$ vations	4050	623	4673

REFERENCES

[1] . Aupoix, B., J. Cousteix, and J. Liandrat (1989) MIS, a way to derive the dissipation equation. In: "Turbulent shear flows 6", Springer Verlag, 6–17.

[2] Blackadar, A. K. (1962). The vertical distribution of wind and turbulent exchange in a neutral atmosphere. J. Geophys. Res.**67**, 3095–3102.

[3] Bougealt, P., and P. Lacarrére (1989). Parameterization of orography-induced turbulence in a mesobeta scale model. Mon. Wea. Rev.**117**, 1872–1890.

[4] Businger, J. A., J. C. Wyngaard, Y. Izumi, and E. F. Bradley (1971). Flux-profile relationships in the atmospheric surface layer. J. Atmos. Sci.**26**, 181–189.

[5] Cuxart, J., P. Bougault and J.-L. Redelsperger (1995) Turbulence clousure for a non-hydrostatic model. 12th AMS symp. on Boundary Layer Turbulence, pp 409–412.

[6] Deardorf, J. W. (1972). Theoretical expression for the countergradient vertical heat flux. J. Geophys. Res.**77**, 5900–5904.

[7] Holtslag, A. A. M. and Boville, B. A. (1993). Local versus nonlocal boundary layer diffusion in a global climate model. J. Climate **6**, 1825–1842.

[8] Holtslag, A. M. M., and C.-M. Moeng (1991). Eddy diffusivity and countergradient transport in the convective atmospheric boundary layer. J. Atmos. Sci.bf 48, 1690–1698.

[9] Kållberg, P., and K.-I. Ivarsson (1999). Verification of an analysis-forecast test of three different turbulence closure schemes. Hirlam 4 Workshop on Physical Parameterization, Madrid, 125–133.

[10] Louis, J. F., Tiedtke, M., and Geleyn, J. F. (1981). A short history of the PBL parameterization at ECMWF. In ECMWF Workshop on Boundary-Layer Parameterization, pages 59–79, ECMWF.

[11] Lykossov, V. N. (1993). The parameterization of the atmospheric boundary layer in the global circulation models. Numerical Processes and Systems, 65–95.

[12] Nielsen, N. W. (1998a). The first order nonlocal diffusion scheme in HIRLAM 4.1. Hirlam Newsletter **31**, 12–13.

[13] Nielsen, N. W. and Sass, B. H. (1995). Recent work at DMI on vertical diffusion. *Hirlam Newsletter* **22**, 17–28.

[14] Perov, V. and S. Gollvik (1996). A 1-D Test of a Nonlocal E-ε Boundary Layer Scheme for a NWP Model Resolution. *HIRLAM Technical Report* **25**.

[15] Rodi, W., (1980). Turbulence models and their applications in hydraulics. *IAHR, Delft, The Netherlands.*

[16] Troen, I., and Mahrt, L. (1986). A simple model of the atmospheric boundary layer: Sensitivity to surface evaporation. *Boundary-Layer Meteorol.* **37**, 129–148.

[17] Vogelezang, D. H. P., and Holtslag, A. M. (1996). Evaluation of model impacts of alternative boundary-layer height formulations. *Boundary-Layer Meteorol.* **81**, 245–269.

WINTEX and modelling of winter conditions: What can we learn from field experiments?

Hannu Savijärvi
Department of Meteorology, P.O.Box 4
00014 University of Helsinki (UH), Finland

Extended abstract

Many WINTEX extra measurements at the Sodankylä site were available on the 14-15 March 1997, so this short review of the WINTEX activities most relevant for atmospheric modelling concentrates around these. For more details and results of the WINTEX experiment, consult Halldin (1999). Also the British Meteorological Office (BMO) research flights took place on the 15th of March 1997, which was a cool but sunny day with NW 8-10 m/s upper winds, after a very cold night with weak surface winds. The nighttime 2m and snow surface temperatures went down to -28°C and -36°C, respectively, and the operational FMI HIRLAM 24h forecast was up to 13°C too warm that night. In the extra low-level wind sounding 15.3.1997 at 07 local time (Figure 1), one can see a strong wind shear near the surface associated with a strong surface inversion, a low level jet structure, and some oscillation in the stable boundary layer wind, which may be of internal gravity wave origin. A typical high-resolution BL model (the UH 1-D model) can roughly reproduce most of these features but the small and possibly intermittent nighttime turbulence with strong shears is a problem in larger-scale models, where large parts of the gridsquares may be turbulence-free in nature. Figure 1 also displays the small levels of turbulence (drag coefficient of 1% from its neutral value), which are needed for a fair simulation of the near-surface local winds in extremely stable conditions. Most models do not allow for such small values.

The BL processes of interest in WINTEX were radiation, turbulence, and surface interactions in the boreal landscape during winter. The landscape around Sodankylä was a fairly flat but strongly heterogeneous black-and-white checkerboard pattern of pine forest patches and snowy non-forest patches of fields, lakes and mires.
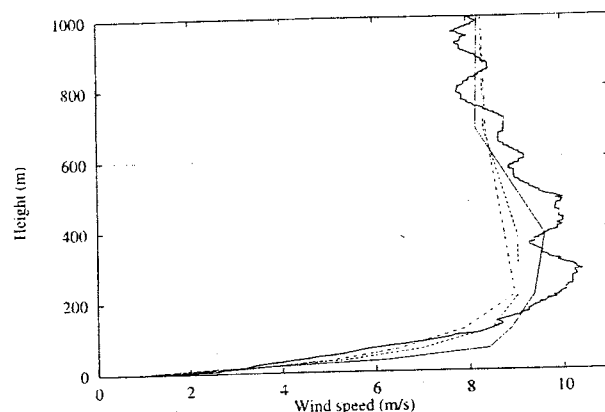

Figure 1. Observed and simulated (UH model) wind speed profile at Sodankylä on 15 March 1997 07 local time. The background turbulence level is varied in the model, 10% (dash-dotted), 5% (dotted) and 1% (thin line) from neutral value.

Radiation

was observed during the BMO horizontal flight tracks with SW and LW fluxes up and down, measured with 1 Hz (about 100 m spatial) resolution at 4 altitudes along three 25-30 km long tracks centered downstream around Sodankylä at 13-14 LT, 15 March 1997. This vast data reveals surprisingly little spatial variation along the tracks, except that the reflected SW radiation varies strongly with surface albedo and the upward LW flux correlates well with the remotely sensed ground temperature below the aircraft, dark forest patches being warmer than bright snowy patches. The measured albedos for forest patches are about 40%, snowy patches reach up to 70%,

and track average (valid for a larger-scale model's single grid square) is around 47%. A GCM-type radiation scheme (the UH model code with 4 SW and 6 LW bands) reproduces the observed fluxes fairly well with prescribed albedos based on land use maps. It seems that the horizontal subgridscale variation is not a big problem for radiation.

There is one point, however. Near the surface, at 0-30 m, we do not know the flux profiles well enough, and measurements were made in WINTEX only at one level near the surface. Advanced radiation schemes can produce quite different net flux profiles with the same "weather" input, depending on their boundary conditions and what kind of temperature and moisture profiles near the surface they assume. In calm and stable conditions turbulence is low or nil. Then, radiation can drive the BL evolution and hence surface temperature evolution as well. Thus we need, in future field experiments, radiative flux profile measurements from masts, preferably within typical forest canopies and aloft, as well as in the snow-covered areas free of trees.

Turbulence

was continuosusly observed in WINTEX at Sodankylä by 18 m mast measurements within a typical low pine forest patch, and during the BMO flight. Latent heat fluxes (LE) were small in general. The mast-observed sensible heat flux (H) was small and negative during the cold, stable nights, but turned positive up to 100 Wm^{-2} during sunny days. It often indicated maxima at about 2 hours before and after local noon. This feature is not predicted by models, as seen in Figure 2, which shows the 18 m observed and MIUU model fluxes of H and LE during 15.3.1997. The feature may be due to morning and afternoon low sunbeams hitting the dark pine-tree canopies only, heating up these, while near local noon sunbeams penetrate to the more reflective snowy surfaces between the trees. If so, this effect can be parameterized knowing the typical canopy heights, canopy albedos ($\approx$ 12-15%) and tree densities. Low albedos and high sensible heat fluxes over springtime boreal forests were also found out during BOREAS (e.g. Harding and Pomeroy 1996). They can lead to mesoscale "snow breezes" near forest patch boundaries in sunny spring and winter days.

H typically increased toward and above the canopy top ($\approx$ 12 m) during the daytime mast measurements as yet another indication of the darkness of the Lappish pine canopy, which quickly sheds off snow. - In the BMO flight measurements there was a lot of spatial variation with small eddy scales in the lowest level H and LE. The track average ($\pm$ std) of H at the lowest flight level, at about 80 m, was 16 $\pm$ 15 Wm^{-2}, at 180 m H was generally negative, -2 $\pm$ 5 Wm^{-2}, and H was small higher up. A typical first order closure scheme (the UH 1-D mixing length scheme) could roughly imitate these mean H and LE profiles along the 25 km track, given the track mean u, v, T, q values as input. Larger-scale eddies could be detected in the 400 and 1100 m observations of H and LE, but the amplitudes were small. They may be indications of convection and snow breezes above the dark pine forest bathing in spring sunshine, like in BOREAS.
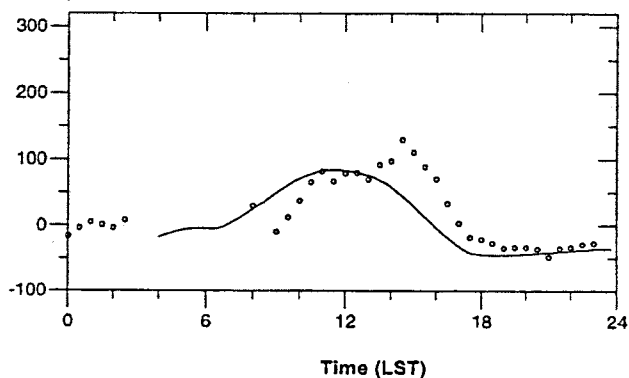

Figure 2. Diurnal variation of the sensible heat flux (Wm^{-2}) 15 March 1997 at the Sodankylä site. Dots: Mast observations (eddy correlation method); Solid line: Simulation (MIUU model).

Snow surface

Snow surface and within-snowpack observations were also made. These gave temperatures as low as -36°C during the cold night of 15 March 1997, due to weak surface winds (1-2 m/s), new snow at the top, and a clear dry night; resulting in little turbulence and mixing, well-insulating topsnow layer, and

strong net outradiation. The HIRLAM forecast was probably too warm because 1) it tended to make fog, 2) it used average and thereby less insulating snow properties, and 3) it produced presumably too much mixing in the extremely stable conditions. Figure 3 shows the Sodankylä surface temperature as observed and as from the UH model forecast with different values of snow properties, starting from 14 March 1997, 12 UTC, pointing out the importance of local up-to-date snow properties.
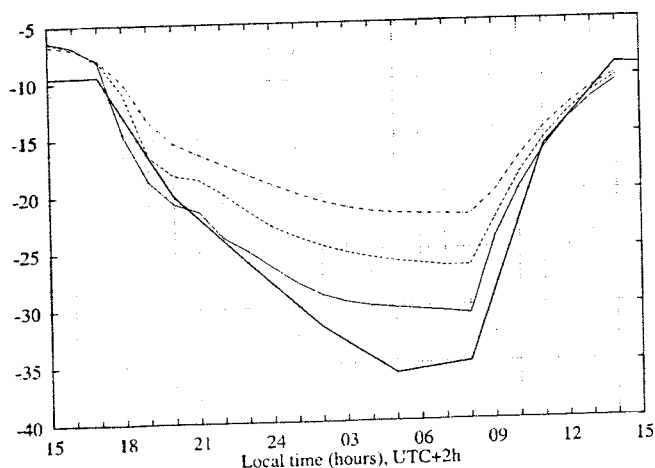

Figure 3. Observed (thick line) and simulated (UH model) snow surface temperatures (°C) at Sodankylä from 14 March 1997 12 UTC onward. Snow heat capacity is varied in the model; the top model curve is for old "typical" snow, the lowest (thin line) for fresh new snow.

flows. Their net effect on the larger-scale flow appears to be insignificant, though.

Sometimes instabilities were noticed in the UH model experiments with the most extreme parameter settings, although the numerical methods used were known to be absolutely stable. These "crashing" problems were recently noticed and named by Derbyshire (1999), who showed that they are a real physical instability of the very stable surface layer. He gave examples from the BMO observation site at Cardington, where the associated decoupling of the surface from air (no turbulence at all, hence rapid cooling of the nighttime surface) could be seen in observations but was not predicted by the BMO mesoscale model. It appears that a lot can still be learned from present and future field experiments!

References:

Halldin, Sven (ed.), 1999: Final report for WINTEX. NOPEX Technical Report No. 29, ISSN 1404-0492. [Available from NOPEX Central Office, Uppsala University]. 70 pp.

Harding, R.J., and J.W. Pomeroy, 1996: The energy balance of the winter boreal landscape. J.Clim., 9, 2778-2787.

Derbyshire, S.H., 1999: Boundary-layer decoupling over cold surfaces as a physical boundary-instability. Boundary-Layer Meteor., 90, 297-325.

Modelling

The UH 1-D and 2-D mesoscale models were used in WINTEX for various sensitivity studies as indicated above. The 3-D Uppsala University (MIUU) mesoscale model was used likewise. It simulated the near-surface winds and fluxes H and LE quite well in the 14-15 March 1997 mast intercomparison (c.f. Fig. 2). It also indicated significant topographic effects on near-surface winds during nighttime, i.e. local shallow katabatic flows leading to "cool pools" well known to the locals in Lapland. A meso-net of anemometers could be utilized in future experiments to observe these weak mesoscale

Pre-processing of Heat Flux and Incoming Solar Radiation at a Northern Site during Winter Conditions

Sven-Erik Gryning and *Ekaterina Batchvarova*[*†]

[*]Risø National Laboratory, DK-4000 Roskilde, Denmark
[†]National Institute of Meteorology and Hydrology,
Bulgarian Academy of Sciences, Tzarigradsko Chaussee 66, Sofia, Bulgaria

Abstract. Measurements from Northern Finland on radiation and turbulent fluxes over a sparse boreal forest with snow covered ground were analysed. The measurements represent harsh winter conditions characterized by low sun angles. The absorption of incoming solar radiation (turbidity) was found to be a strong function of the solar elevation. Commonly used expressions for the absorption did not fit the measurements well at these low solar elevation angles. A simple energy balance type met-processor was found to perform well during daytime, but the performance during nighttime was not satisfactory. The simplifications in the energy balance model and possible improvements are discussed.

Introduction

As a part of WINTEX, meteorological measurements were carried out at Sodankylä in Finnish Lapland March 1997 in order to study the feasibility of applying sonic anemometers for turbulence measurements during harsh winter conditions, and to investigate the fluxes of heat and humidity over a sparse boreal forest typical for the Northern hemisphere. The measurements were started on March 12, 15:30 Finnish winter time and ended on 16:00 March 24, 1997. The sonic anemometer measurements were carried out in co-operation between the Swedish National Defense Research Establishment and Risø National Laboratory. The Finnish Meteorological Institute performed 3 hourly radiosoundings during the experimental period, and routine measurements of global radiation. Data on global radiation used for this analysis cover the period March 6 to May 31, 1997.

Site and instrumentation

The measurements were carried out at the Sodankylä Meteorological Observatory (67° 29' N, 26° 39' E) at Tähtelä. The observatory is located in a sparse forest of typically 6-8 meter tall pine trees. The area is typical for the subarctic Northern Finland with coniferous forests and large open mires dominating the landscape. The river Kitinen flows a few hundred meters west of the Observatory. The town Sodankylä is located 6 km north of the Observatory. The area is rather flat both on small and large scales, with hills reaching 500 meters height within 20 km.

During the experimental period, March 12 to 24, 1997 the ground was covered with snow, river and lakes frozen, and the trees most of the time bare without snow cover. Day and night were approximately equally long.

The instrumentation of the site was rather comprehensive. Turbulence was measured by the use of sonic anemometers in and above the sparse forest, mounted on a mast at heights of 2, 6, 12 and 18 meters. Measurements of humidity fluctuations were performed at 18 meters height by use of an OPHIR optical hygrometer. Wind speed and temperature were measured at 8 and 16, and wind direction at 16 meters height. The Finnish Meteorological Institute measured the global radiation routinely at a height of 16 meters, well above the forest, and profiles of atmospheric properties were measured by radiosondes released regularly every 3 hours during the entire experimental period. As a part of the STAAARTE initiative the English Hercules research air-plane performed measurements on two occasions during the

experiment. In addition to the routine meteorological observations snow properties were measured.

In this study we will concentrate on the radiation and turbulence measurements. The wind and temperature fluctuations were measured with 4 sonic anemometer (Solent Research 3D ultrasonic anemometers). This instrument is well suited for measuring low wind speeds, because it contains no moving parts. The probe is designed for omnidirectional winds, and is good for use in areas with varying winds. The measuring principle of the sonic anemometer is based on the flight time of sound pulses transmitted back and forth between pair of transducers. The three dimensional wind vector can be constructed by using three pairs of acoustic transducers. As the sound velocity is dependent on air temperate the sonic system can also be used for measuring air temperature fluctuations. Measurements of humidity fluctuations were performed with an OPHIR optical hygrometer (measuring height 18m). The measuring technique is based on absorption at two different infrared wavebands. Sampling frequency was 20 Hz.

Hourly averaged radiation measurements were performed with a pyranometer, mounted at 16 meters height to obtain a free horizon, as part of the regular observations at Sodankylä. A 3-month period (March-May 1997) is analysed here. Cloud observations were performed every three hours.

Meteorological pre-processor of incoming solar radiation

The radiation measurements provide the opportunity to test simple models of the incoming solar radiation, based on solar elevation and cloud cover. The measurements are unique because the solar elevation is very low (typically 20 deg during mid day) at the site. A number of models were tested with poor result, because the modeling of the turbidity, which describe the attenuation of incoming solar radiation by the atmosphere, was too crude. The following models for incoming solar radiation were tested:

- Holtslag and van Ulden (1983):

$$K_O^+ = -1041 \sin\phi + 69$$

- Karpinen et al. (1996):

$$K_O^+ = -1372 \left(0.987 - 0.909(\sin\phi + 0.118)\sin\right.$$

- Stull (1988):

$$K_O^+ = -1370(0.6 + 0.2\sin\phi)\sin\phi$$

- and a proposed new model:

$$K_O^+ = -1370 \sin\phi \exp(-0.1/\sin\phi)$$

where K_O^+ is the incoming global radiation (note upward is positive) for a cloud free sky and $\sin\phi$ is sinus to the solar elevation angle, abbreviated sin_sea on Fig 1.

Defining the atmospheric turbidity (atmospheric absorption) as $K_O^+/\sin\phi$ Fig 1 shows the turbidity plotted against sinus of the solar elevation angle. The crosses shown measurements for cloud free days in March, April and May 1997. The dashed line shows the function suggested by Holtslag and van Ulden (1983), the dashed-dotted line the suggestion by Stull (1988), and the dashed-dot-dot line the function of Karpinen et al. (1996). It is clearly seen that none of the functions is a fair approximation at small solar elevation angles. The full line shows a turbidity function suggested by Haurwitz (1945), but with the empirical constant adapted to the measurements at Sodankylä, which resulted in the rather nice agreement between measurements and model.

The effect of clouds are empirically modeled as (Kasten and Czeplak, 1980)

$$K^+ = K_0^+ (1 - 0.75C^{3.4})$$

which was found to be slightly superior to the other commonly suggested relationship

$$K^+ = K_O^+ (1 - 0.6C)$$

where C is decimal cloud cover (N is cloud cover in Oktas: C=N/8). Fig 2 shows the modelled and measured incoming radiation including the effects of clouds. Overall the agreeemnt is good but with some spread.
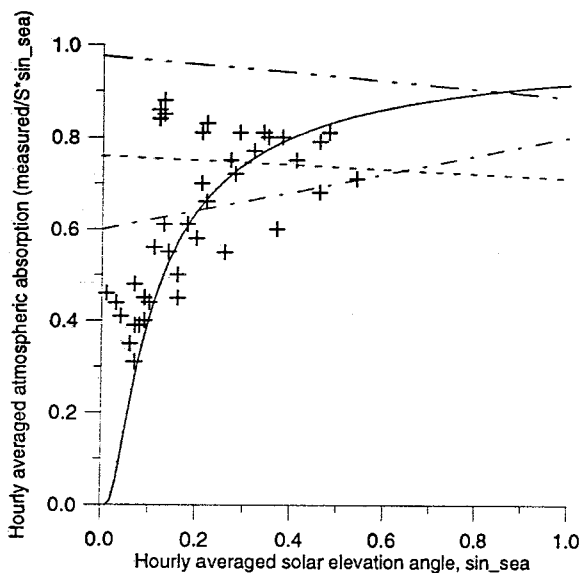
Fig 1. Turbidity or atmospheric absorption of the short wave radiation as function of sinus to the sun elevation angle for cloud free days. Crosses show measurements, the full line is the suggested model for turbidity, the dashed line represents the model suggested by Holtslag and van Ulden (1983), the dashed-dotted line the model of Stull (1988), and the dashed-dot-dot line is Karpinen et al.(1996).
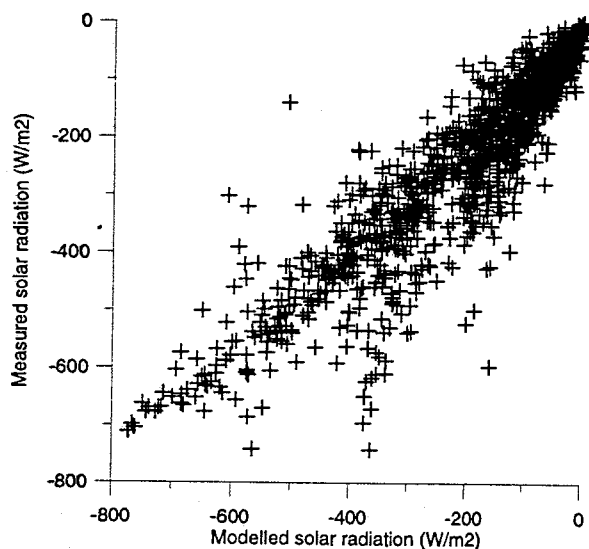
Fig 2. Modeled and measured incoming solar radiation including the effect of clouds.

To investigate the spread in more detail modelled and incoming radiation for cloud cover $N \geq 7$, $N \leq 6$ and $N \leq 4$ are shown in Fig 3.
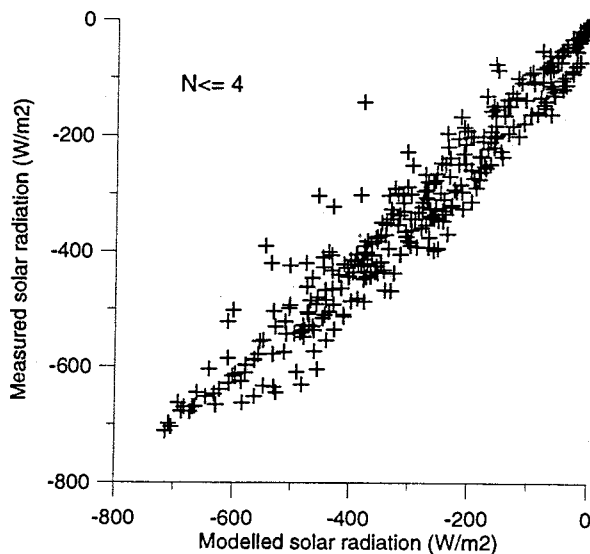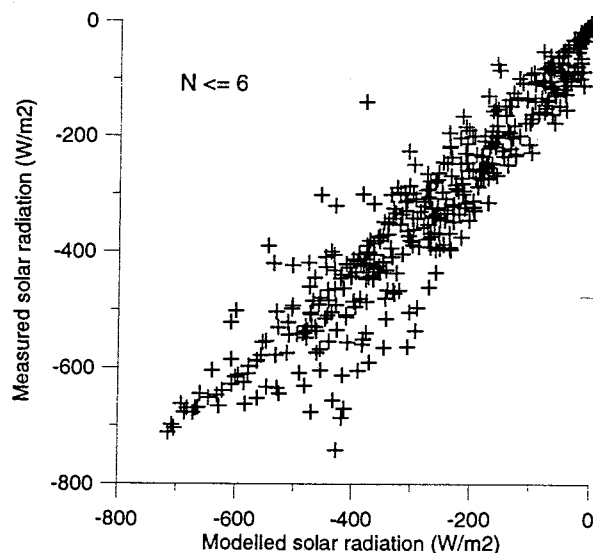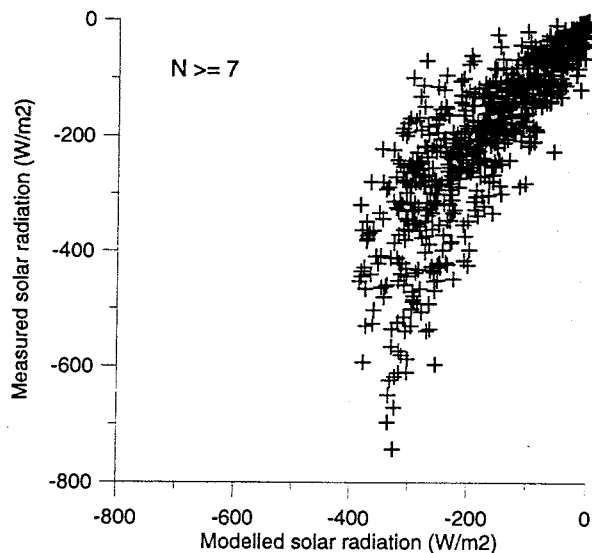
Fig 3. Modeled and measured incoming solar radiation, for 1) cloud cover $N \geq 7$ Oktas, 2) cloud cover $N \leq 6$ Oktas and 3) cloud cover ≤ 4 Oktas. Note that upward is positive, thus incoming radiation is negative.

The agreement is indeed good when N≤4 and only slightly degraded for N≤6, , whereas the agreement for $7 \leq N \leq 8$, clearly indicate that the major part of the spread originates mainly for conditions with cloud cover 7 or 8. It is clear that the many different types of clouds and cloud characterists cannot be modelled in this simplistic way and therefore leads to uncertainty in the modelled turbidity, but it is a promising result that even up to cloudcover N=6 the agreement is fair despite the crude parameterization of the effect of the clouds.

The formula for the global radiation suggested here reads:

$$K^+ = -1370\sin(\phi)\exp(\frac{-0.1}{\sin(\phi)})(1-0.75C^{3.4})$$

where K^+ is the global solar radiation near the ground, - 1370 the Solar constant (Wm^{-2}), ϕ the solar elevation.

Fluxes in and above the forest

It is a very characteristic feature of the measurements that a pronounced gradient in the sensible heat flux and temperature can be observed between the lowest level of measurements inside the forest and the measurements above the forest. Fig 4 shows the sensible heat flux at 2 and 18 meters height, representing the conditions inside the forest just above the snowpack and above the forest. The amplitude of the sensible heat flux is pronounced bigger for the measurements at 18 meters compared to the measurements at 2 meters. It is clearly seen that during daytime, the sensible heat flux above the forest is noticeable bigger than inside the forest, which is caused by warming of the trees by the incoming radiation. During night-time the sensible heat flux above the forest is smaller than inside the forest.

The latent heat flux, shown in Fig 5, is measured at 18 meters height only. By comparing with Fig 4 it is seen to be much smaller than the sensible heat flux, typically only 10 Wm^{-2} during both day and night time.
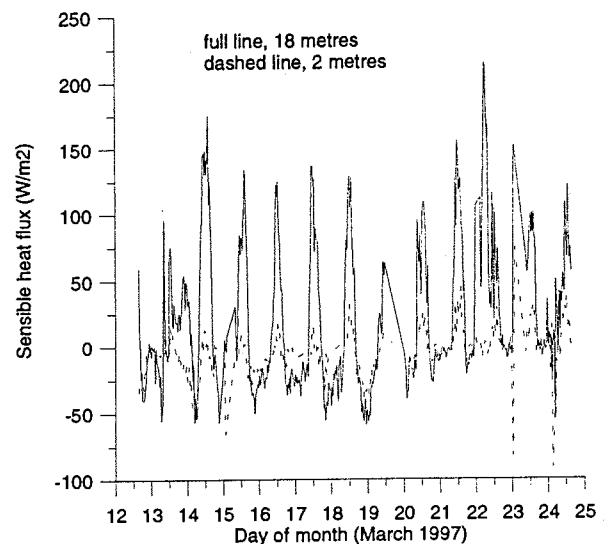

Fig 4. Sensible heat flux at 2 and 18 meters height as function of time.
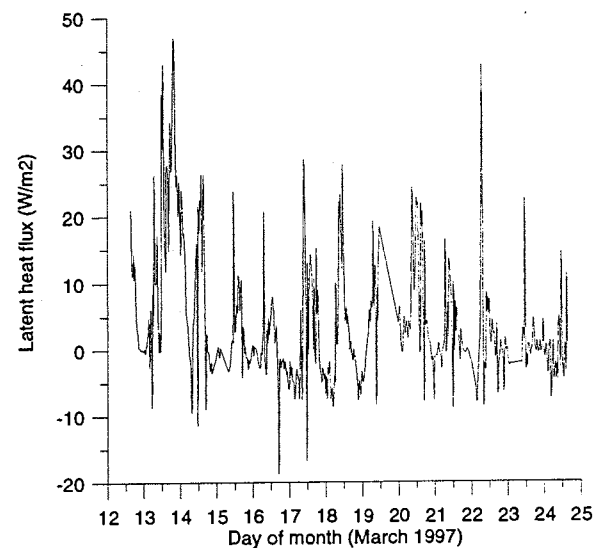

Fig 5. Latent heat flux at 18 meters as function of time.

The temperature at 2 and 18 meters is shown at Fig 6 for the experimental period. The amplitude of the temperature at 2 meters is bigger than at 18 meters. It is characteristic that during daytime the temperature decreases with height, which is characteristic for an unstable atmosphere and associated generally with positive heat flux. During night the temperature increases with height, typical for a stable atmosphere.
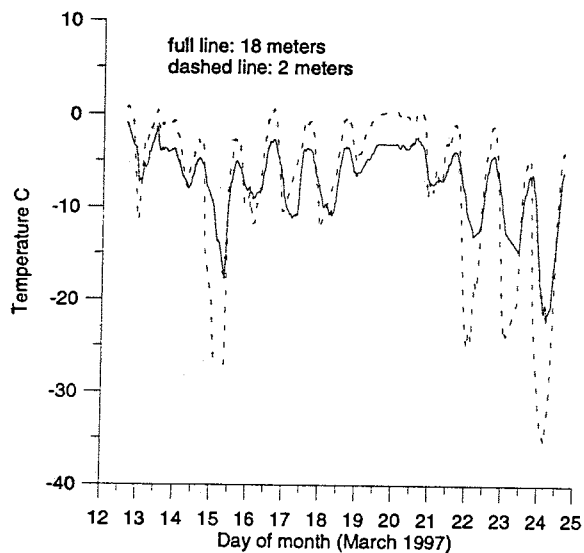
Fig 6. Temperature at 2 and 18 meters height as function of time.

Met-processor of the sensible heat flux above the forest

Using the above formula for the global incoming radiation the sensible heat flux over the forest was determined by a conventional simplified energy balance:

$$Q = -K^+(1-r) + c_1 T^6 + c_2 N - \sigma T^4 \qquad (1)$$

where Q is the upward directed sensible heat flux, r is albedo, $c_1 T^6$ accounts for longwave incoming radiation from the air in absence of clouds (Swinbank, 1963), $c_2 N$ the incoming longwave radiation from the clouds (Paltridge and Platt, 1976), and σT^4 the outgoing longwave radiation from the surface according to Stefan-Bolzmans law. The empirical value of the constants are:

$c_1 = 5.31 \; 10^{-13} \; W \, m^{-2} \, K^{-6}$
$c_2 = 60 \; W \, m^{-2}$
$\sigma = 5.67 \; W \, m^{-2} \, K^{-4}$

The temperature measured at 18 meters height, T, is used to represent both forest and surface conditions. The ability of the simplified model to predict the sensible heat flux is illustrated in Fig 7. The agreement between measured and modelled sensible heat flux during day-time is generally good. The agreement for the nighttime heat fluxes is not

satisfactory. The met-processor grossly underestimate the heat fluxes, indicating that the energy exchange inside the snow plays an important role for the fluxes above the forest. It should be noted that in Equation (1) the effect of latent heat fluxes and the sensible ground/snow heat flux are neglected, as well as storage of heat due to warming or cooling of the trunks of the trees. The good performance of the model during daytime shows that these assumptions are fair during daytime, where the flux is controlled by the forest. However it is not permissible to neglect these terms during nighttime. Especially the use of the temperature at 18 meters height to represent the radiation temperature of the snow during nighttime is a very poor approximation. It is known that the temparature of the air can be 10 to 20 degrees C warmer than the snow surface temperature. This effect has to be accounted for in modelling of the nighttime fluxes, which can only be done by applying detailed modelling of the energy balance within the snowpack, thus taking into account the detailed characteristics of the snow cover.
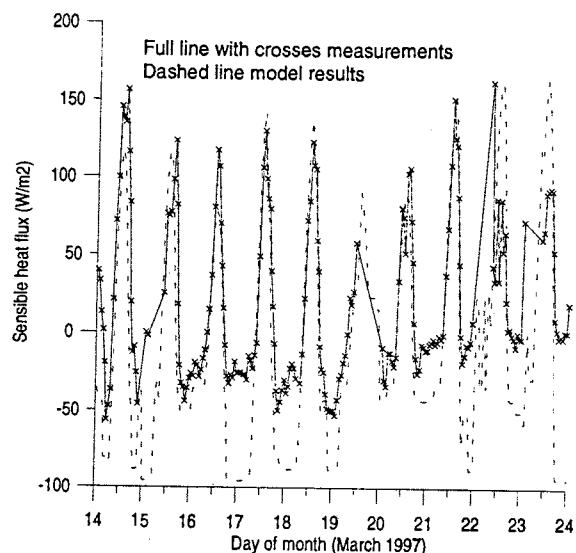

Fig 7. Measurements of sensible heat flux above the forest at 18 meters height (full line, the crosses represent the individual measurements) and modeled sensible heat flux using Equation (1) (dashed line).

Discussion

The meteorological conditions with rather long days, a snow covered ground surface and bare pine or spruce trees is rather typical for the

41

Northern boreal forest during the last part of the winter, but hardly characteristic for the whole winter period. The measurements shows that the forest has a pronounced effect on the local meteorology. The forest induced convective heat flux is comparable to heat fluxes found in middle Europe, and is able to form a convective mixing layer that can reach depths of typically 1000 meters in the late afternoon. The convection is caused by warming of the trees by solar radiation. The trees are bare (not snow covered) with low albedo and thus an efficient absorber of short-wave radiation. The forest floor is covered with snow which reflects short wave radiation. The upward directed heat flux above the forest originates mainly from the warming of the trees, while the heat flux from the forest floor remains small.

The foregoing discussion has been focused on the heat flux at one point in a forest. The area around the measuring point contains also mires and lakes, which have very different thermal and radiation characteristics compared to the forest. Based on the radiosoundings it is possible to estimate the area averaged sensible heat flux. Application of the method is based on the evolution of the boundary layer, and is restricted to cloud free days. The analysis will be reported elsewhere, but main results will be summarized here. The regional heat flux determined on the basis of the growth of the mixed layer was found to be significantly smaller than at the forest sites. The regional heat flux represents a zone of approximately 20 to 200 times the height of the mixed layer depending on atmospheric stability, and thus integrates the heat flux over 20 to 200 km upwind of the Observatory. The surrounding area consists of mires and lakes, which were snow covered during the experiment and thus expected to have a relatively high albedo and consequently small heat flux. The area averaged heat flux suggest that the aggregated heat flux is approximately 50% of the heat flux measured over the forest.

Acknowledgements

References

Holtslag A. and van Ulden A. (1983), A simple scheme for daytime estimates of the surface fluxes from routine weather data. *Journal of Climate and Applied Meteorology*, Vol 22, p 517-529

Haurwitz, B. (1945), Insolation in relation to cloudiness and cloud density. *J. Meteor.*, Vol 2, p 154-166.

Karpinen A., Joffre S. & Vaajama P. (1996) Boundary layer parameterization for Finnish regulatory dispersion models. *Proceedings form the 4th Workshop on harmonization within Atmospheric Dispersion Modelling for Regulatory purposes*. Oostende 6-9 May, 1996.

Kasten F. & Czeplak G. (1980), Solar and terrestrial radiation dependent on the amount and type of cloud. *Solar Energy*, Vol 24, p 177-189.

Paltridge G.W. & Platt C.M.R. (1976), *Radiative Processes in Meteorology and Climatology*. Elsevier, p 318.

Stull R.B. (1988) *An Introduction to Boundary Layer Meteorology*. Kluwer Academic Publishers, p 666.

Swinbank W.C. (1963) Longwave radiation from clear skies. *Quart. J. Roy. Meteor. Soc.*, Vol 89, p 339-348.

VALIDATION OF HIRLAM WITH NOPEX DATA

B. Bringfelt

Swedish Meteorological and Hydrological Institute, Norrköping, Sweden

To improve the accuracy of forecasting near-surface atmospheric variables over a heterogeneous landscape, a framework of subgrid surface types and the ISBA parameterisation scheme for land surfaces have been tested in the operational weather forecast model HIRLAM, using a 5.5 km grid resolution. Surface energy fluxes measured during a single summer day at six fixed sites in the NOPEX area, representing agricultural fields, boreal forests and lakes, were used for verification.

HIRLAM (HIgh Resolution Limited Area Model, Källen 1996) is a complete weather forecasting system in operational use and under development in the international HIRLAM project participated in by Denmark, Finland, Iceland, Ireland, The Netherlands, Norway, Spain and Sweden. Cooperation also takes part with France.

The task of a land-surface scheme is to predict the surface variables (e g temperature and moisture) from the energy and water balances of the surface. See e.g. Viterbo (1996) for a review. In the present operational HIRLAM surface scheme, soil-vegetation-atmosphere processes such as movement of water in the soil, evapotranspiration and heat exchange, are treated in a simplified manner. To improve model performance, there is a need to take more realistic account of the various biogeophysical properties of the vegetation and soil and to let these properties vary spatially. In order to improve forecasts of surface fluxes as well as the near-surface variables, a new surface scheme with a framework for land classification was implemented and tested for HIRLAM.

The aggregation of subgrid features to the whole model grid can be done using various techniques. The main approaches to subgrid averaging are parameter aggregation (e.g. Collins and Avissar 1994), where important surface parameters are averaged to represent the whole grid area, and flux aggregation, where the surface fluxes are averaged, as in Ducoudre et al. (1993). Aggregation approaches were recently evaluated for the NOPEX area by Frech and Jochum (2000) using aircraft measurements. They found that the effective, grid-averaged, exchange coefficient for momentum transfer was independent of the averaging scale, whereas this was not the case for the sensible heat transfer. This implied that the sensible heat flux, and possibly all other scalar fluxes as well, should be calculated for each subgrid element separately to obtain the correct grid-averaged flux. Another potential advantage of the flux averaging approach, adopted for the present

experiments with HIRLAM, is better performance on terrain borders, such as those between ice sheets and open sea or on coasts, where there are drastic differences horizontally in physical properties between the contrasting surface types.

Validation of a surface scheme can be made against standard network observations or special measurements of physical processes. The NOPEX field campaign (Halldin et al. 1995 and Halldin et al. 2000) provides a unique opportunity to perform model validation by using the process validation approach. During the field campaign in 1994 and 1995, surface flux measurements at fixed sites and from low-level aircraft traverses, mostly using the direct eddy-correlation technique, were carried out over the typical surface types of the boreal landscape. In addition the programme included vertical soundings of air pressure, temperature, humidity and wind.

In this study, a version of HIRLAM with a high spatial grid resolution (5.5 km), using the ISBA surface scheme (ISBA = Interaction Soil-Biosphere-Atmosphere, Noilhan and Planton 1989) and a classification system for subgrid surface types (Bringfelt 1996), were applied in the context of the NOPEX field programme. This HIRLAM system was applied to an area covering part of southern Scandinavia and Finland and part of the Baltic Sea. The necessary lateral boundary data were extracted from the relevant routine HIRLAM forecast using a 22 km grid resolution and an area covering northern Europe and part of the Atlantic.

The main objective was to test the adequacy of the surface classification and parameterisation for resolving the variation of surface fluxes between the major surface types. Experiments with this HIRLAM version were compared, for 13 June 1994, with local point measurements over a lake, over open agricultural land and over forest and along an aircraft flight traverse. The measurements used in this study were carried out at six fixed sites, three of which were located on agricultural fields, two in and above a coniferous forest and one over a lake, see Figure 1. The NOPEX area, located in Sweden N to W of Uppsala, is flat, with forest dominating in the north-western part, while there is more open agricultural land in the south-east. Figure 1 shows the spatial variation of forest cover within the 5.5 km x 5.5 km grid squares as deduced from the physiographic database prepared for this experiment. The geographical location of the NOPEX area is indicated.

During the day, magnitudes of surface heat fluxes could be produced that were comparable with measurements, and the relative differences in fluxes from the surface types could be well resolved. Results indicated that explicit parameterisation of the reflective, aerodynamic and plant physiological properties inherent to the major boreal land surface types is of particular importance for correct simulation of the surface heat fluxes.

Both in-situ field measurements and the HIRLAM simulation indicated that the Bowen ratio (=H/LE where H is sensible heat flux, LE is latent heat
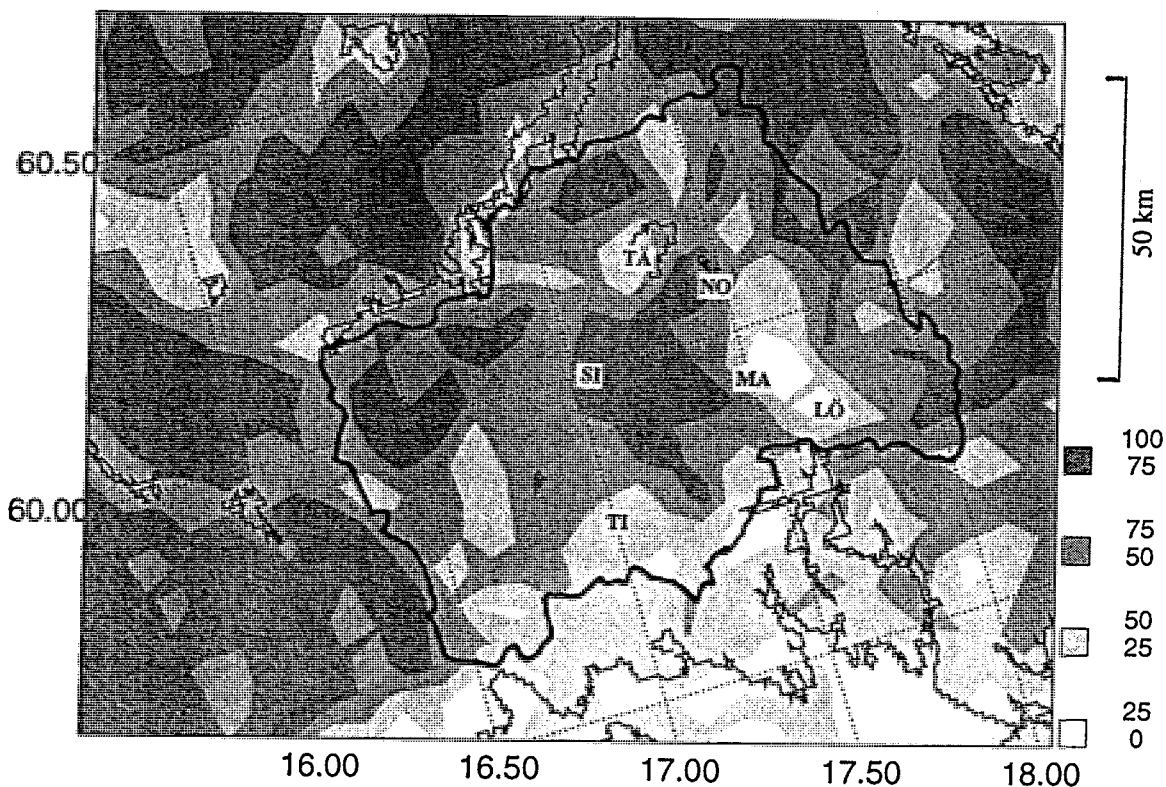
Figure 1. Coverage of forest according to the present physiographic data used in HIRLAM. Forest coverages are expressed as areal fractions within each 5.5 km x 5.5 km grid area and shown here with different degrees of shading. The locations of the field sites in the NOPEX experiment area (framed) are marked as: NO: Norunda (forest), SI: Siggefora (forest), TI: Tisby (field), LÖ: Lövsta (field), MA: Marsta (field), TÄ: Tämnaren (lake). Lake Mälaren is in the south.

flux, E is water vapour flux and L is the latent heat of vaporization) over forests was about twice as large as that of adjacent agricultural fields, see Figure 2. This difference could be explained by the more effective turbulent mixing and larger surface resistance associated with the forest, thus making the sensible heat flux relatively large there.

The differences in heat fluxes between the various surface types were also demonstrated by airborne flux measurements flown along a track at a height of about 100 m above the terrain, see Figure 3. The sensible and latent heat fluxes for the aircraft flights show variations which are in corrorrelatin with the major type of underlying land surface (low vegetation, forest, lake): i.e. where forests dominate, the sensible heat flux is larger than over the smooth agricultural land surfaces. For the latent heat flux there is no detectable contrast between agricultural and forest surfaces. Over the lake the aircraft measurements indicate realistically a significant drop in both sensible and latent heat fluxes. The HIRLAM-based latent heat fluxes were on average of the same order of magnitude along the track as the fluxes based on aircraft measurements, whereas the forecast sensible heat flux was larger. This difference is due to the larger amount of total energy available in HIRLAM because HIRLAM predicted too much clear skies whereas the measurements were more influenced by cloudiness.

45

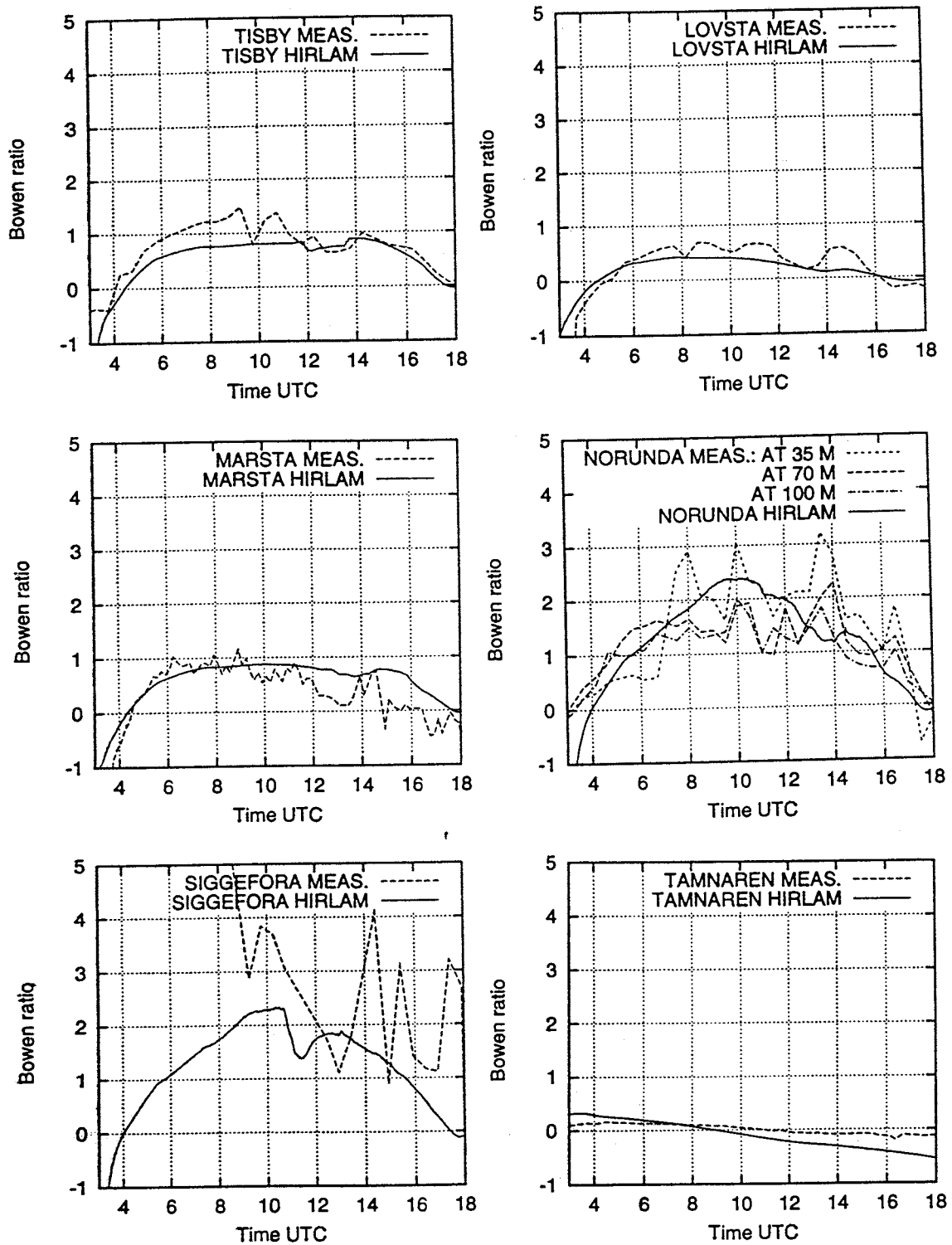Figure 2. Diurnal variation of the Bowen ratio (β=H/LE) during 13 June 1994 as derived from the measured (dashed lines) and modelled fluxes (solid lines; HIRLAM) at the six NOPEX field sites. For the Norunda site, results of flux measurements from three heights are shown.
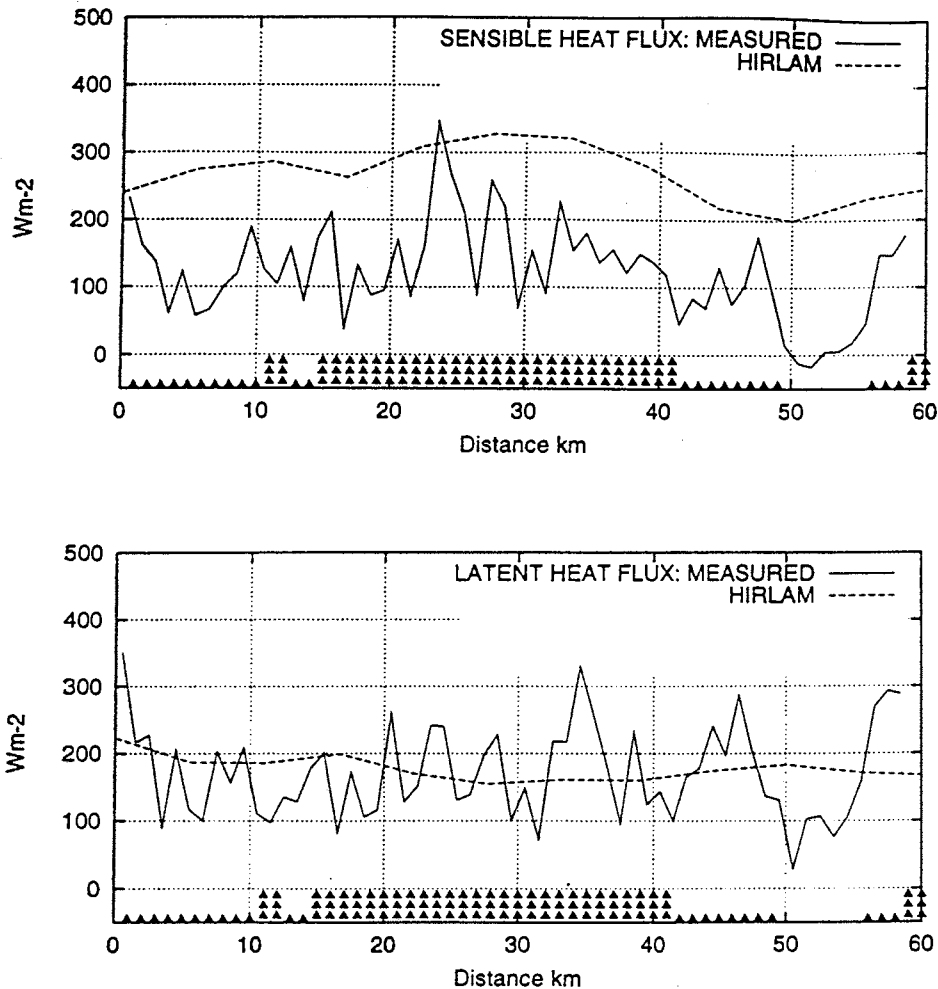
Figure 3. Aircraft-measured sensible and latent heat fluxes at a height of 100 m along the flight path Tisby - Tämnaren on 13 June 1994 compared to whole-grid square surface fluxes forecast with HIRLAM averaged over the subgrid surfaces in each grid box along the flight path. No triangle, one triangle and three stacked triangles mean lake, open land and forest respectively.

Storage of sensible heat due to warming of the boundary layer also gives some contribution.

The use of initial soil moisture from a routine hydrological model gave improved agreement with measured surface fluxes and radiosonde temperature and humidity profiles compared to initializing from routine HIRLAM surface data. For correct estimation of the moisture content and the height of the mixed PBL, it was found necessary to make a realistic estimation of the initial soil moisture rather than using predetermined assumptions. Further tests should cover extended periods over which the soil moisture has varied between extreme dry and wet conditions.

The straightforward flux-averaging approach, using weighting according to sub-grid area fractions, seemed to be appropriate for obtaining representative fluxes for the model grid square. A prerequisite, however, is a detailed classification of land use with realistic partitioning between the most contrasting land surface types. The increase in the horizontal grid

resolution of operational atmospheric models has set new demands particularly for more detailed parameterisation of the land surface processes as well as for more detailed and explicit representation of the varying surface types. The present experiment with HIRLAM was one step forward in attempts to make realistic account of the interaction between the heterogeneous landscape and the atmosphere. Overall, the system of detailed surface classification and the ISBA scheme for vegetation and soil processes implemented here in HIRLAM using a 5.5 km grid resolution seemed appropriate for the boreal land surface.

REFERENCES.

Bringfelt, B., 1996, Tests of a new land surface treatment in HIRLAM. HIRLAM Technical Report No. 23.

Collins, D. and Avissar, R., 1994. An evaluation with the Fourier Amplitude Sensitivity Test (FAST) of which land-surface parameters are of greatest importance for atmospheric modelling. J. of Climate, 7, 681-703.

Ducoudre, N. I., Laval, K. and Perrier, A., 1993. SECHIBA a new set of parametrizations of the hydrologic exchanges at the land-atmosphere interface within the LMD atmospheric general circulation model. J. of Climate, 6, 248-273.

Frech, M. and Jochum, A., 2000. Flux aggregation methods compared to aircraft measurements in the surface layer. To be published in a NOPEX Special issue of Agricultural and Forest Meteorology.

Halldin, S., Gottschalk, L., Gryning, S.E., Jochum, A., Lundin, L..C., and Van de Griend, A.A., 2000. Energy, water and carbon exchange in a boreal forest - NOPEX experiences. To be published in a NOPEX Special issue of Agricultural and Forest Meteorology.

Halldin, S., Gottschalk, L., van de Griend, A.A., Gryning, S.E., Heikinheimo, M., Högström, U., Jochum, A., Lundin, L..C., 1995. Science Plan for NOPEX. Technical Report No. 12, Uppsala University, NOPEX Central Office, Uppsala, 38 pp.

Källén, E. (ed.) 1996. HIRLAM Documentation Manual, System 2.5. SMHI Norrköping. (Available from SMHI, S-60176 Norrköping, Sweden).

Noilhan, J. and Planton, S., 1989, A simple Parametrization of Land Surface Processes for Meteorological Models. Mon. Wea. Rev., 117: 536-549.

Viterbo, P., 1996. The Representation of Surface Processes in General Circulation Models. European Centre for Medium-Range Weather Forecasts, Reading, UK. Doctoral Thesis.

What can we learn from LITFASS with regard to

the modelling of surface fluxes ?

F. Beyrich

Meteorologisches Observatorium Lindenberg - Deutscher Wetterdienst,
D-15864 Lindenberg, Germany

1. Introduction

The LITFASS-project of DWD (Müller et al., 1995) has been launched in 1995 with the background to intensify the experimental investigation of land surface - atmosphere interaction and boundary layer processes at DWD with direct respect to the treatment of these processes in numerical weather prediction (NWP) models. LITFASS is an acronym and stands for 'Lindenberg Inhomogeneous Terrain - Fluxes between Atmosphere and Surface: a Long-term Study'. The project has been designed in order to develop and to test a strategy for the determination and parameterization of the area-averaged turbulent fluxes of heat, momentum, and water vapour over a heterogeneous surface. These fluxes shall be representative for a horizontal scale of about 10 km corresponding to the size of a grid cell in the present operational numerical weather prediction model of the DWD.

LITFASS consists of three components:
- the development of a non-hydrostatic micro-α-scale model with a grid-size of 100 m (the LITFASS Local Model - LLM)
- experimental investigations of land surface - atmosphere exchange processes and boundary layer structure within a 20 km x 20 km area around the Meteorological Observatory Lindenberg (MOL)
- operation of a data base (LITFASS data base) as an interface between measurement and modeling activities.

The link between these three components is illustrated in Figure 1. The LLM shall be used to compute area-averaged fluxes based on a detailed high-resolution physico-geographical description of the model area, a data assimilation strategy taking into account the heterogeneity in the meteorological forcing conditions (mainly through the distribution of radiation and precipitation) and an advanced turbulence parameterization scheme properly considering the three-dimensionality of turbulence and the form drag induced by high vegetation or in built-up areas.

The measurements in the Lindenberg area serve to provide the meteorological forcing of the LLM at the lateral (profiles of wind, temperature, and humidity) and lower boundaries (radiation, precipitation), and also to provide model validation parameters (from the atmosphere and from the soil) both at single points over typical locally homogeneous types of surface and regionally integrated values from suitable experimental techniques or simple models (similarity theory, budget considerations).

As can be seen from Figure 1 and from this short description, the link between experimental and modelling activities is very strong and appears to be an imminent part of the project. At present, the LITFASS project is at the transition between the preparation and implementation phases. The overall project strategy has been tested for the first time in connection with the LITFASS-98 experiment, which took place in the Lindenberg area during May / June, 1998.
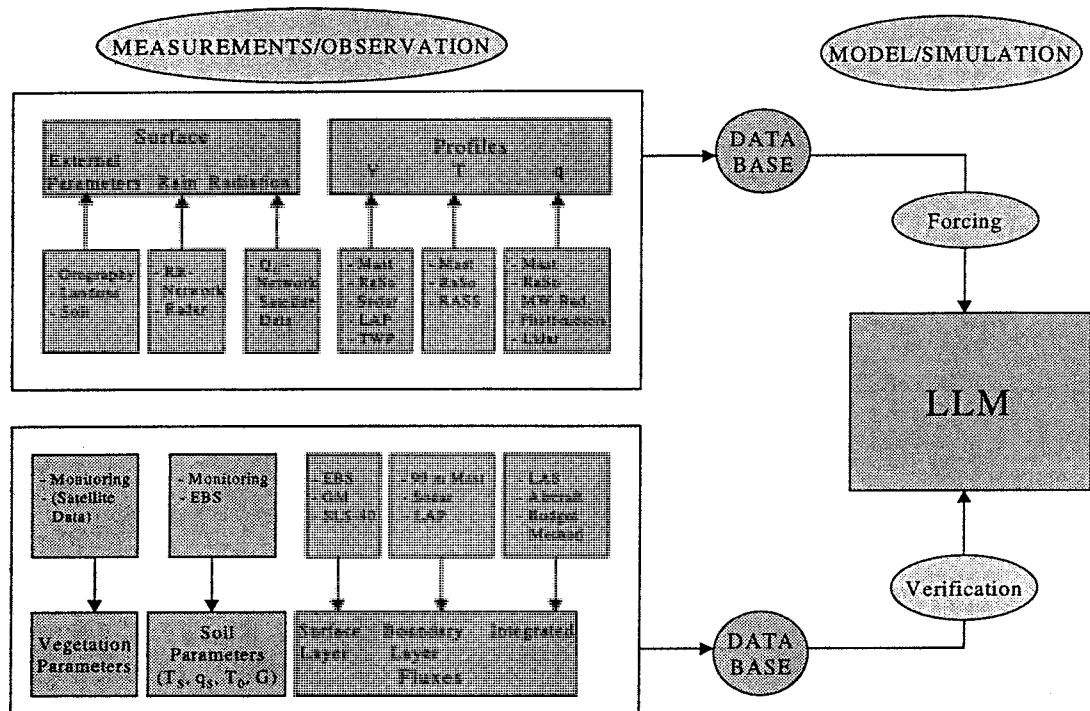
Figure 1
The general project strategy of LITFASS

The modelling activities connected with the experiment are currently performed at DWD. Instead of giving a comprehensive overview on the LITFASS-98 experiment, a few aspects concerning the link between observation and simulation will be discussed in some detail in the following sections.

2. Surface heterogeneity

The LITFASS area is characterized by a strong degree of surface heterogeneity with agricultural fields and forests being the dominating landuse classes (each covers about 42 % of the area). The distribution of different landuse types across the area is quite irregular. More than 12,000 basic landuse areas (patches) have been identified in the 20*20 km^2 area. About half of these patches have a size smaller than the LLM grid resolution, and the biggest area element covers about 3*3 km^2.

The typical patch scale lies in the range between 10^2 to 10^3 m. Detailed datasets of orography, landuse and soil types with a 100 m spatial resolution have been produced to provide the description of the lower model boundary for the LLM. For the agricultural fields, the actual kind of landuse has been updated every year since 1997. In addition to this basic information (which remains constant over a time of at least several months), a lot of soil and vegetation parameters characterizing the exchange processes at the land-atmosphere interface have a pronounced seasonal or even diurnal cycle, like soil moisture, vegetation height, fractional vegetation cover, leaf area index etc. Models often use standard values taken from the literature for these parameters and sometimes do not distinguish between different types of agricultural plants. In reality, e.g., the fractional vegetation cover in June (during the LITFASS-98 experiment) may vary between less than 10 % (for maize) and

higher then 90 % (for rape). During the LITFASS-98 experiment, an effort was made to monitor some of these parameters (soil moisture, vegetation height, LAI) on a weekly basis for a number of representative test sites, which turned out to be a man-power intensive task. A sample result from this activity is shown in Figure 2.
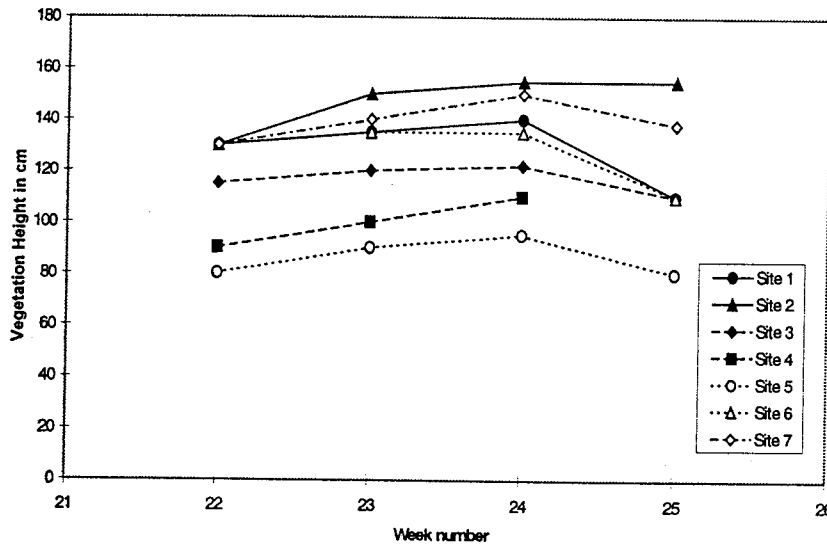

Figure 2
Vegetation height at different Triticale fields in the LITFASS area during the LITFASS-98 experiment

Figure 2 demonstrates that even for a given crop type, vegetation parameters may easily vary by a factor of two or more in a given area. It is not yet clear, how relevant local uncertainties in the soil and vegetation parameters are for the determination of areally averaged atmospheric quantities. Sensitivity studies with a mesoscale model (e.g., the LLM) are highly needed to answer this question and modellers are requested to provide the relevant limits of uncertainty concerning both the necessary accuracy of single parameters and the significance of scales. This is also needed to decide on the future efforts to be made for determining soil and vegetation parameters.

3. Fluxes over heterogeneous landscape

Flux determination is the central focus of the LITFASS project. During LITFASS-98, different measurement techniques have been employed to derive flux values which are representative for different spatial scales and different types of surface. This broad spectrum of sampling and footprint scales covered by the different methods is illustrated in Table 1.

Table 1 – Characteristics of the flux measurement systems

Method	during LITFASS-98 operated by	Fluxes determined	continuous operation	sampling scale	Footprint scale
single leaf evaporation (LiCor)	PIK	L_vE	no	10^{-2} m	--
eddy correlation (sonic)	MOL, GKSS, KNMI,U_DD U_BT	M, H, l_vE	(yes)	10^{-1} m	$10^1..10^2$ m
profile measurements (mast)	MOL	M, H, l_vE	(yes)	10^1 m	$10^2..10^3$ m
remote sensing systems (wind profiler, sodar, lidar)	MOL, U_HH	M, H, l_vE	(yes)	$10^1 .. 10^2$ m	$10^3..10^4$ m
small-aperture scintillometer	GKSS	M, H	(yes)	10^2 m	$10^1..10^2$ m
large aperture scintillometer	WAU	H	yes	10^3 m	$10^3..10^4$ m
(bulk) mixed layer model	NIMH	H	no	10^3 m	$10^3..10^4$ m
slow aircraft (Helipod, DO128)	U_H, Aerodata	M, H, l_vE	no	10^4 m	$10^3..10^4$ m
fast aircraft (Falcon)	DLR	M, H, l_vE	no	10^5 m	$10^3..10^4$ m

Short names stand for the following institutions:
Meteorologisches Observatorium Lindenberg (MOL), GKSS-Forschungszentrum Geesthacht (GKSS), Koninklijk Nederlands Meteorologiisch Instituut De Bilt (KNMI), Landbouw-Universiteit Wageningen (WAU), Potsdam-Institut für Klimafolgenforschung (PIK), Deutsches Zentrum für Luft- und Raumfahrt Oberpfaffenhofen (DLR), National Institute for Meteorology and Hydrology Sofia (NIMH), Universität Dresden (U_DD), Universität Hamburg (U_HH), Universität Hannover (U_H), Universität Bayreuth (U_BT), Fa. Aerodata Braunschweig (Aerodata)
Symbols for the fluxes are: M = momentum flux, H = sensible heat flux, l_vE = latent heat flux

Analysis and interpretation of the flux measurements from the different systems is still in progress. As a preliminary result, the diurnal cycle of the heat flux for the 18th of June, 1998, as derived from different methods is shown in Figure 3.
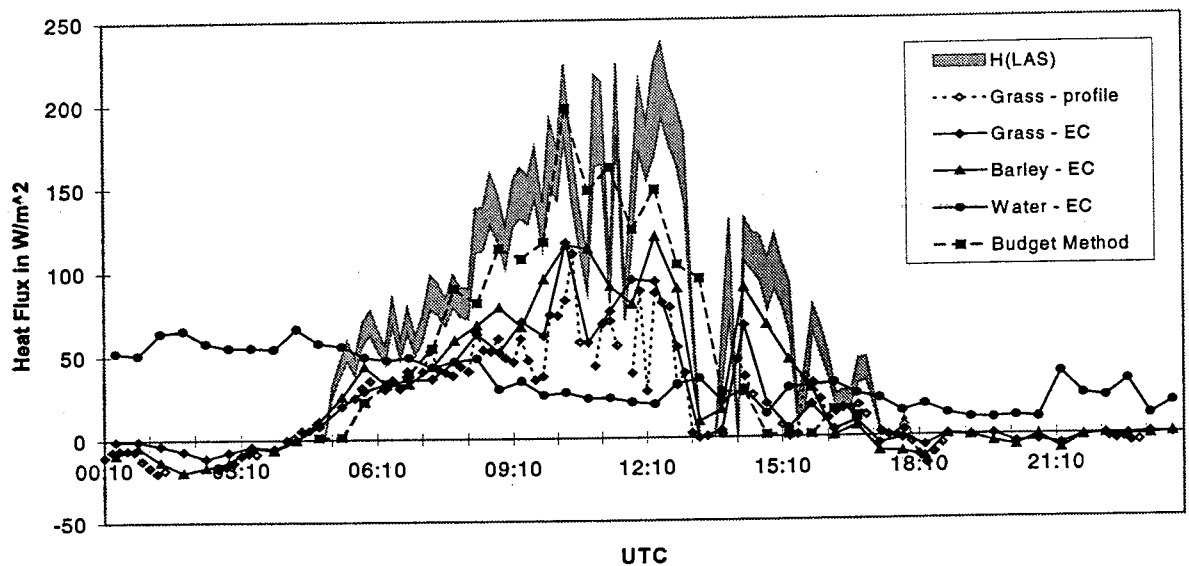

Figure 3
Diurnal cycle of heat flux in the LITFASS area for June 18, 1998

The eddy correlation and profile based fluxes over grass agree well in their magnitude. The local measurements show a tendency towards slightly higher values over the barley field when compared to the grassland site, even if the values are in the same order of magnitude. A significantly different diurnal behaviour and also magnitude of the heat flux must be noticed over the lake. The water was warmer than the air over all the day resulting in an upward heat flux which was strongest at the beginning of the night. This comparison demonstrates the necessity to cover the different typical land-use classes in the study area with direct measurements of the energy budget components in order to assess their relative contribution to the area-averaged flux. Therefore, a network of micrometeorological stations is currently set into operation within LITFASS and is planned to provide operational data from the beginning of BRIDGE, i.e., from January 2000. When compared with the local fluxes, the regionally representative heat flux values from the large-aperture scintillometer and from the mixing height method (supporting each other in magnitude) tend to be significantly higher than those measured over low vegetation. This might be due to higher sensible heat fluxes over the mainly forested western parts of the LITFASS area which find a reflection in the integrating measurements. This difference between local and regional flux values illustrates the importance of defining suitable aggregation and averaging algorithms for the comparison of measured fluxes with fluxes computed in 3d-mesoscale grid models.

4. Model forcing

The typical way to drive a mesoscale model is the nesting in a larger-scale (continental to global scale) model. The LLM with a model domain of 20*20 km^2 and a grid resolution of 100 m is at the transition between the mesoscale and the

microscale. First tests had been made to drive the LLM with output fields from the DM which currently has a grid resolution of 14 km. It turned out that the difference in the scales between DM and LLM was too big to obtain reliable results (note that the LLM model domain just covers one DM grid box plus a lateral margin zone). Small errors in the DM (phase errors, erroneous fields) thus dominated the complete output of the LLM. It was therefore concluded that for the diagnostic purposes of LITFASS, the LLM needs to be driven by observations. This means to provide forcing data at the surface and at the lateral boundaries with corresponding spatial and temporal resolution from measurements as indicated in the upper left part of Figure 1.

Different work packages have been derived within LITFASS from this request. Forcing from the surface requires a prescription of the areal distribution of available energy (radiation) and available water (precipitation, soil moisture). Global radiation and precipitation are therefore measured at 10 and 20 sites, respectively, in the LITFASS area. Interpolation schemes are used to produce two-dimensional fields from this point measurements. Currently, investigations are performed to use satellite data and weather radar data, respectively, which are adjusted to the data from the surface observation networks in order to obtain a more detailed areal description of these forcing parameters. However, first case studies have shown, that small-scale adjustment of weather radar data is still problematic for situations with highly variable convective precipitation.

To provide the necessary model input at the lateral boundaries of the LLM, the vertical profiles of wind, temperature and humidity have to be given. This can be achieved on the basis of the different direct and remote vertical sounding systems which are in operation at MOL (towers, radiosonde, wind profiler / RASS, sodar /

RASS, microwave radiometer profiler - during the LITFASS-98 experiment also Raman ~ and differential absorption lidars for water vapour profiling were employed). However, non of these systems is able to provide profiles over the full height range requested and with a time resolution of about one hour. It is therefore necessary to combine the data from the different systems in a suitable way. A number of problems does immediately show up when thinking about the realisation of this task:

a) How to determine the most reliable values of any parameter in those height regions where data from different systems are available but usually do not show the same values ?

b) Is it possible to combine the measurements done at the boundary layer field site of MOL within the lowest few hundreds of meters with the profile measurements performed at the observatory site - both sites are about 5 km away from each other and differ in sea level altitude by 30 to 40 m ?

c) Is it possible and justified to put the same vertical profiles at each of the lateral model boundaries ?

d) What is the effect of providing hourly profiles based on measurements with different sounding systems when compared to a linaer interpolation between subsequent radiosonde ascents on the model results ?

A special work package named "Composite Profiling" has been defined in order to answer these questions and to develop reliable algorithms for the provision of the necessary model input data.

5. Long-term measurements vs. field experiments

The LITFASS-98 experiment definitely gave a comprehensive dataset which is suitable to test several aspects of the LITFASS project strategy and to develop the algorithms for data analysis and interpretation from both the measurement and the modelling component of the project. However, although the weather conditions during the experiment did vary quite a lot, only a small spectrum of weather situations typical for a midlatitude site during summer could be covered. E.g., there was observed during the three-weeks core period of the experiment not even one single clear-sky day.

On the other side, the overall goal of LITFASS is to contribute to the development and validation of parameterizations used in numerical weather forecasting (and climate) models. These paramterizations need to be validated for a significant spectrum of weather conditions during all seasons of the year, and even a variety of extreme events needs to be covered. This means that continuous and comprehensive land surface - atmosphere interaction monitoring programs are necessary for the purpose of model validation. Field experiments are definitely well suited for process studies (provided you are lucky to meet the process you want to study), but they can not replace the monitoring programs.

Reference
Müller, E., Foken, Th., Heise, E., Majewski, D., 1995: "LITFASS" - a nucleus for a BALTEX field experiment. *DWD, Forschung und Entwicklung, Arbeitsergebnisse*, No. 33, 17 pp., App.

Parameterization of soil and surface processes in SWECLIM

Michael Tjernström*
Stockholm University/SWECLIM

1. INTRODUCTION

SWECLIM is a national Swedish regional climate modeling program, and its goal is to provide accurate, authoritative and timely estimates of the regional effects, in Sweden, of a globally changing climate. In particular, SWE-CLIM should provide scenarios, data and tools that makes it possible for users to assess their climate sensitivity, in order to be able to adapt. This means that the data should be made available to government and industry in a way that they can use, and that the quality of the scenarios in addition to be high, must be quantified. SWECLIM is organized with one climate modeling center, the Rossby Centre at SMHI, and several university groups that participate with basic research. One aim is to work across the traditional boundaries between the climate-oriented disciplines; integration of meteorology, hydrology and oceanography is strongly encouraged in the program.

The main agent in this work is dynamical downscaling; results from a General Circulation Model (GCM) is used at the lateral boundaries to drive a regional model. The regional model is essentially a HIRLAM-derivative. The climate version (Rossby Centre regional Atmospheric climate model, RCA), is based on the parallellized version of HIRLAM v2.7 (Källén 1996), thus the starting point for the model physics is that of the "old" operational HIRLAM model, with some minor modifications (Rummukainen et al. 1998). It is for practical reasons necessary to have a model that runs on a parallel computer. Since climate modeling, to some degree in contrast to weather prediction, is essentially a boundary-value problem, and data assimilation is impossible, the behavior of the physics package is critical. Even small systematic errors will rapidly show up in long integrations (here meaning years). This is naturally a problem, but can also be utilized to benefit model development. This sensitivity makes climate simulations ideal for testing of new parameterizations. In the future, RCA will be coupled to a fully three-dimensional ocean model for the Botnic, Baltic and North Seas, which is currently being completed.

The climate scenarios were here set up as 10 year time-slice experiments. The RCA is driven for ten years by forcing from a GCM in two different setups, one present climate control run and a $2*CO_2$ future climate run, representing conditions around mid-twentyfirst century. Both GCM results are portions taken from longer global simulations.

* *Corresponding author address:* Michael Tjernström, Department of Meteorology, Stockholm University, S-106 91 Stockholm, Sweden. email: michaelt@misu.su.se

2. THE FIRST SCENARIO (RCA0)

For the first scenario the Hadley Centre HadCM2 GCM results were used at the lateral boundaries and nested down to ~ 44 km in RCA. In the HIRLAM formulation for soil temperature and humidity ("Force-Restore") has two dynamic layers and one relaxation layer that uses climatology in weather prediction mode. Here, deep soil temperature and humidity from HadCM2 was used as a climatological forcing in the relaxation layer. Transfer of water in the soil only occurs through a diffusion-like formulation, similar to the heat flux formulation for temperature. Initially, some problems concerning the treatment of lake and sea surfaces had to be addressed. In northern Fennoscandia, the low-level temperature and humidity climate is very sensitive to how these-water surfaces are treated, in particular to the timing and amount of ice in winter. This became clear because HadCM2 does not resolve lakes, while RCA treats lakes as surface fractions. The lakes then take on interpolated sea-surface temperature (SST) from the climate model as a surface temperature. In HadCM2, the Baltic Sea are firstly to warm and secondly, ice never develops. Thus an "ice proxy" was developed to allow ice formation to influence the climate.

Although many aspects of the control climate in this scenario are surprisingly accurate (Räisänen 1999), it was immediately obvious that the way the lakes and the soil, in particular the soil water, was treated needed an upgrade. It was obvious that the HadCM2 SST, used also for lakes and the Baltic Sea when ice is not present, was unrealistic for this region and that the result is quite sensitive to this. The relaxation of the soil water to the HadCM2 values also left the water budget unclosed; i.e. net precipitation-evaporation-runoff was large. Evaporation was somewhat unrealistically low and it lacked the "observed" north-south gradient. The annual precipitation cycle was also less well described; the precipitation was to uniformly distributed over the year, although the annual average precipitation was quite well modeled. Even comparing to local stations, the precipitation appear quite reasonable.

2. THE SECOND SCENARIO (RCA1)

For the next scenario, the simulations were nested in two steps: from the GCM to ~ 88 km, and then to ~ 22 km. For the full two-step nesting, forcing was used from the HadCM2. In addition one ~ 88 km scenario was run using forcing from the Max-Planck institute (ECHAM4/OPYC3) OAGCM. While the soil temperature/water scheme in RCA was updated, all changes were kept such that the model structure in the RCA/HIRLAM code could be maintained,

to facilitate a simple implementation. In summary, the changes in the new scheme are:

- The relaxation of soil water to the GCM values was removed. The corresponding temperature relaxation was, however, kept unchanged.
- A simple but dynamic model for the lakes and for the Baltic Seas, including ice, was implemented.
- Hydraulic and thermal diffusivities in the soil are made dependent on soil texture and soil water.
- A realistic runoff formulation from the hydrological HBV model is implemented. This allows the water from precipitation and snow melt to flow down through the soil, rather than be transferred by diffusion only.
- Evapotranspiration from plants during the growing season is modeled with a stomatal resistance that is a function of "Leaf Area Index", air temperature and soil water stress.
- Evapotranspiration is modeled so that a fraction of the actual evapotranspiration is taken from the deeper layer, the root zone, and the rest from the upper layer, using ISBA-features; this loosely describes the action of a canopy.
- Soil freezing is introduced in the lower layer.

3 THE ANNUAL CYCLE

Figure 1 shows the simulated present-climate temperatures, reduced to sea level, and precipitation for the Nordic region, compared to the Climate Research Unit (CRU) data for the period 1961-90, for different versions, resolutions and GCM forcing. It is immediately clear from the temperatures shown here, that there is a significant difference between the runs forced with HadCM2 and ECHAM4, where the latter appear much closer to CRU. It seems clear that the RCA differences in temperature for the two scenario experiments are imported from the GCM and that the HadCM2 has a cold bias for the Nordic region, while the ECHAM4 model lies closer to CRU. Still, the RCA results are also closer to CRU than the corresponding GCM results; in this respect, RCA provides an improvement. However, there appears to be very little difference in temperature that can be traced back to the changes in the surface parameterization between RCA0 and RCA1. There is a small but significant difference between RCA0 and RCA1, while driven by HadCM2 at ~ 88 km during winter, where the latter is closer to CRU. This could be due to the implementation of the dynamic lake/ice model, providing a more realistic surface temperature and ice climate in winter, but could also be a result of soil freezing. The difference disappears, however, when nesting RCA1 into itself down to ~ 22 km. The reason for this remains to be investigated in detail.

The corresponding results for precipitation show a more scattered picture. First, it is clear that all scenario runs have a problem with the annual cycle, which is too flat. Second, the annual mean seems to become larger while the annual distribution improves, as the resolution

is improved. Third, it appears that RCA provides (erroneously) larger annual precipitation but a better annual cycle when forced by ECHAM4 than by HadCM2. It seems
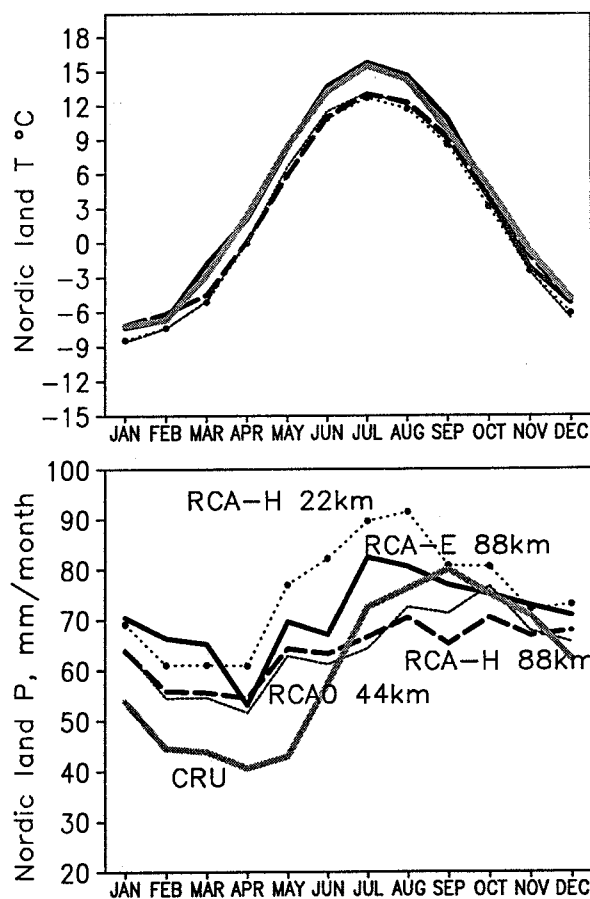

Figure 1. Annual variation of the monthly averaged two-meter temperature and precipitation for present climate (CRU, thick gray line) and simulation results, showing RCA0 (~ 44 km, thin dotted); RCA1 using HadCM2 forcing at ~ 88 km (thick dashed) and ~ 22 km (thin dotted with markers); RCA1 using ECHAM4 forcing at ~ 88 km (thick solid).
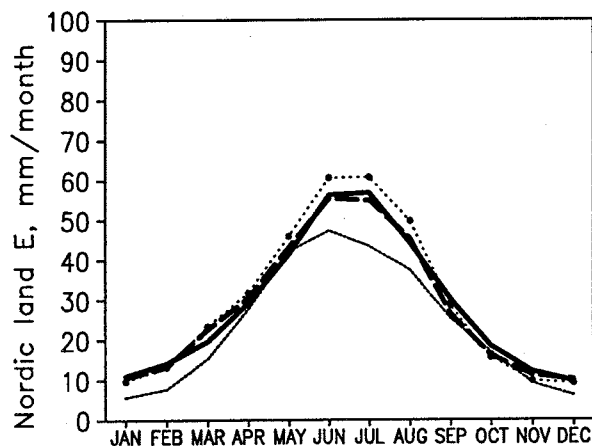

Figure 2. As Figure 1 but for evaporation, except that there is no climate dataset - see the text for a discussion.
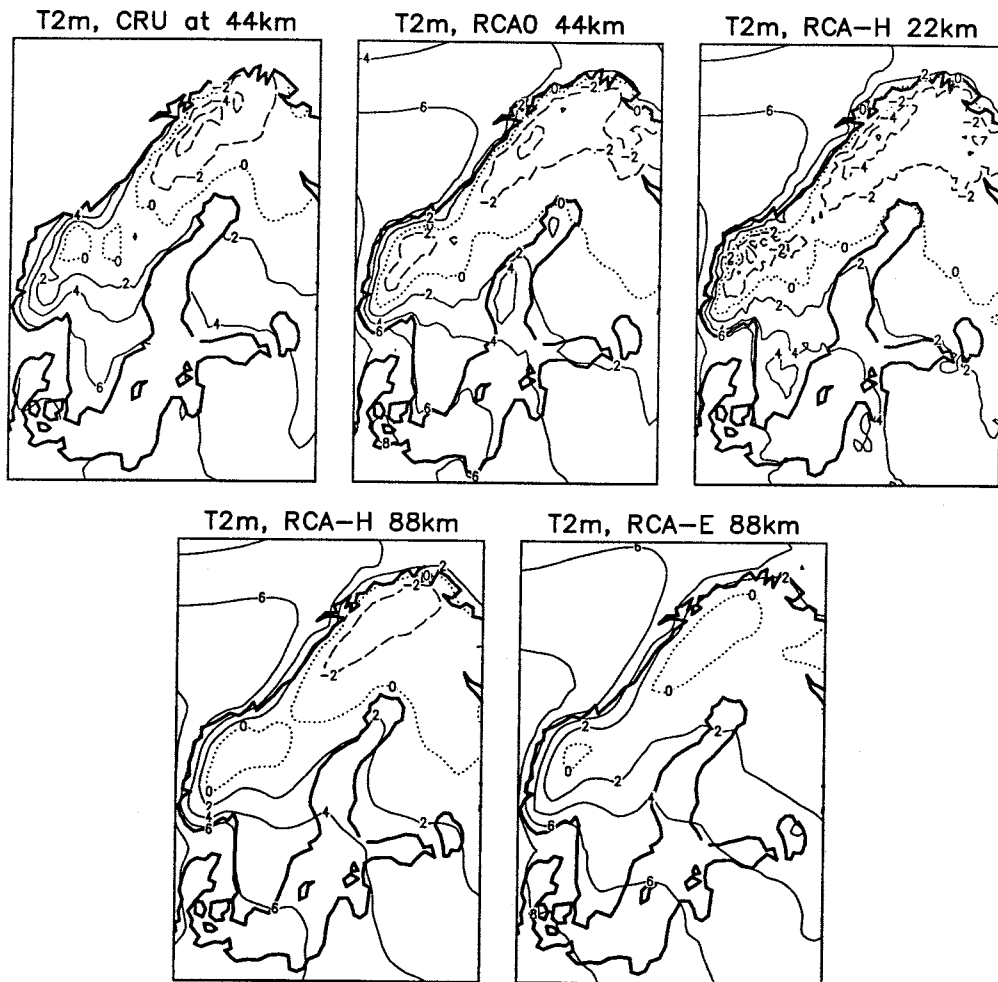
Figure 3 Contour maps of two meter temperature for the different simulations and for present climate (CRU). Note that the temperatures are not corrected for terrain height differences as a consequence of resolution differences.

clear that improving the spatial resolution improves the annual cycle but also generates more precipitation and, by comparing RCA0 at ~ 44 km with RCA1 at ~ 88 km (notably with differences in some parameterizations, but not in those for precipitation and clouds), it seems that the resolution has to be better than ~ 44 km to make any significant difference.

A comparison between simulated evaporation and the corresponding climate is precarious because of the lack of good quality measurements. Climatological evaporation is usually estimated as the residual between measured precipitation and runoff. Accepting values based on such principles, RCA0 has a too low evaporation, and furthermore lacks the observed north-south gradient. The results in RCA1 is better in both respects. As there is notably a very small difference between results forced with different GCM, the changes must be due to the improved parameterization. It is only when increasing the resolution further that the evaporation also increases more. This is presumably due to the more vigorous hydrological cycle: e.g. increased precipitation.

4. SPATIAL DISTRIBUTION

The contours of the two-meter annual average temperature, shown in Figure 3, illustrate the relative success of these simulations. Comparing the patterns of the simulated temperature to that in the CRU data, they appear quite similar. Also, it again illustrates the differences between runs driven by HadCM2 and ECHAM4. While the patterns in CRU and RCA0 are quite similar, RCA0 is significantly colder, by about 2 °C. Changing the surface parameterization, as in RCA1-H at ~ 88 km, alters very little, except the lesser details in the coarser run. Note, however, the differences in temperature over the Sea of Botnia, between RCA0 and RCA1, both driven by HadCM2. This is most certainly an effect of simulating the SST, rather than taking it from the driving model. This illustrate clearly the importance of a correct treatment of lake and sea surfaces for a regional climate simulation. Increasing the resolution, as in RCA1-H at ~ 22 km, mostly adds geographical detail; cf. e.g. the colder region in central southern Sweden. Simulations using ECHAM4, on the other hand, are notably warmer; compare for example the ~ 88 km results from

RCA1-H and RCA1-E. It seems clear that the RCA temperature cannot deviate significantly from that in the GCM. How much of this that is caused by forcing from the lateral boundaries and how much that is due to the HIRLAM soil scheme, where the GCM deep soil temperature is used to force the climatological layer, is not clear.

Figure 4 shows contours of annual average precipitation for the same runs as in Figure 3. It is clear that the regional model is capable of realistically resolving the strong precipitation gradient across the Scandinavian mountains. It also shows the observed climatological maximum at the west coast of Sweden. However, at ~ 44 km, the resolution is still not quite sufficient to create the strong gradient that is observed. Altering the surface parameterization (e.g. RCA1-H at ~ 88 km) changes the precipitation only marginally, compared to RCA0 at ~ 44 km, while also increasing the resolution (RCA1-H at ~ 22 km) clearly adds the desired detail, see e.g. the shape of the maximum at southwestern Norway. On the other hand, this also increases the total amount of precipitation almost everywhere. Simulations using ECHAM4 at the boundary seems to generate more precipitation than the corresponding HadCM2 experiment. It must be remembered, however, that observations of precipitation, in particular in the Nordic climate

with significant amounts of snow and over sea, are difficult. Many other features thus remain uncorroborated. For example, the run using ECHAM4 forcing appears to have a much higher precipitation over the Baltic states.

Herein lies a fundamental problem in dynamical downscaling of precipitation; moist parameterizations in GCMs are tuned to provide a reasonably accurate annual average precipitation but fail, presumably due to poor resolution of the orography, to provide neither spatial detail nor a correct annual cycle. When such fields are fed into a relatively coarse resolution regional model (e.g. RCA0) at the lateral boundaries, only slight improvements occur on average, while there is a substantial, but for hydrological purposes insufficient, improvement in spatial distribution. Improving the resolution in the regional model further - beyond ~ 40 km seems to be a critical stage in these results - improves the annual cycle, but also increases the annual precipitation to larger values than what is observed and simulated in the driving GCM. At the heart of this problem lies the tuning of the moist parameterizations in the GCM. Due to the poorly resolved orography, it has to be tuned, in order to predict a realistic annual average precipitation, however, that tuning is not optimal for the regional model, where the orography is represented better.
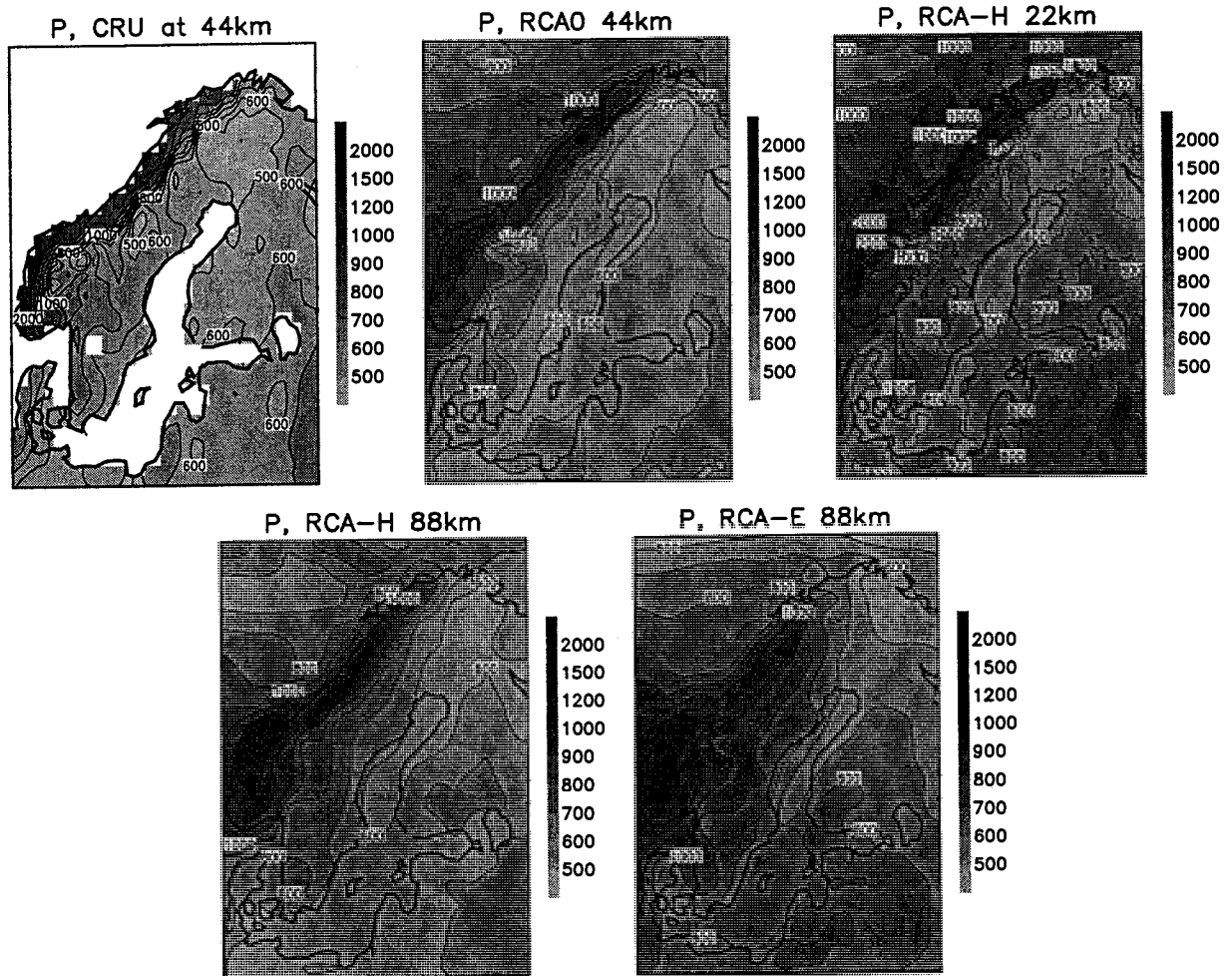

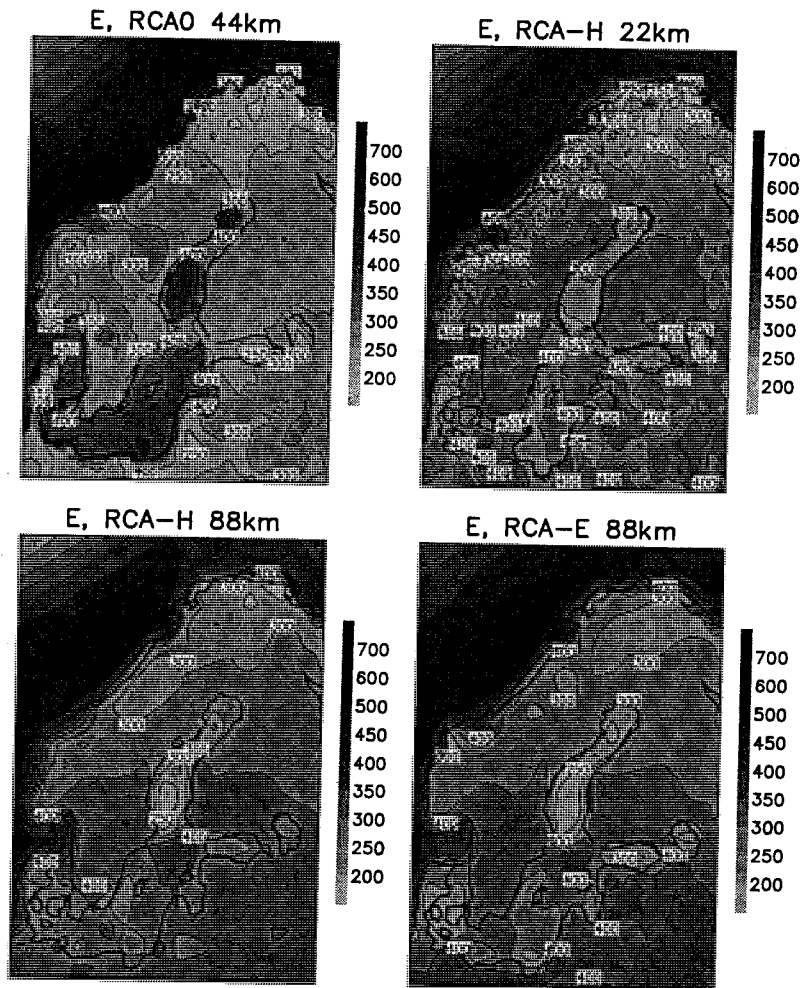Figure 4. The same as Figure 3. but for precipitation.

58

Figure 5. Same as Figure 3, but for evaporation. Note that there is CRU dataset for evaporation.

It appears that one has the choice of either having a too large annual precipitation in the regional model (using similar schemes in the inner and outer models) or of having boundary relaxation problems (retuning the parameterization in the inner model to provide better results) thus making the models incompatible at the boundaries. The solution to this problem remains unclear, but must surely be at the focus in regional modeling studies in the years to come.

Reliable estimates of evaporation are difficult to obtain, other than for shorter periods at specific locations during field experiments. However, judging from estimates based on the residual of measured precipitation and run-off, the RCA0 results are to low and lack the observed north-south gradient. Although somewhat patchy, the evaporation here is ~ 300 mm annually over much of Sweden. The new surface scheme (in RCA1) improves both these problems and the results, already at ~ 88 km resolution while using HadCM2 forcing, appears more realistic. Increasing the resolution adds detail but changes the magnitudes only marginally.

One significant difference between RC0 and RCA1 is found over the Botnic sea. Here the evaporation drops from over 400 mm in RCA0 to less than 250 mm in RCA1. This is a clear effect of adding a more realistic dynamic lake/sea model providing a better SST and a more realistic ice cover. The differences between forcing from HadCM2 and ECHAM4 are small. The structures are very similar, except for over the Baltic states, where the evaporation is somewhat higher in the latter simulation, presumably due to the increased precipitation (se above).

5. CONCLUSIONS

Starting from very minor changes to the HIRLAM v2.7 physics, the first SWECLIM 10-year time-slice regional climate dynamical downscaling experiments were performed in 1998. These runs were forced at the lateral boundary by GCM results from HadCM2. The results were quite encouraging, although it was immediately clear that some model features needed immediate attention. In a second experiment during 1999, a double nesting technique was developed that allowed climate simulations down to a nominal resolution of ~ 22 km. This is a necessary resolution for meaningful hydrological scenarios.

In the first scenario, several deficiencies in the surface parameterization were noticed. It appeared clear that an explicit treatment of lake and sea surfaces was necessary. In particular the timing of the ice is very important. Also,

59

the use of deep soil water content from the GCM to force the RCA deepest climatological layer resulted in a severe loss of water from the model, while the evaporation was too small and lacked north-south gradient. All the runoff appeared from the top soil layer, since soil water was only allowed to penetrate the soil through diffusion. Vegetation was in the old scheme only represented by a change in surface roughness and albedo. When the routines for these processes were updated in combination with explicit modeling of the lake and sea surfaces, in simulations with higher resolution, many results were improved. In particular worth noticing is that several of the new features in the model were introduced across traditional discipline boundaries. For example, the lake/sea model is a simplified slab or column oceanographic model that was directly coupled dynamically to the RCA, and the new soil water treatment was taken more or less directly from the hydrological HBV-model.

RCA improves the regional climate description over using interpolated values directly from the forcing GCM. This is particularly true for temperature, also for precipitation and less certain (in a statistical sense) for other variables, e.g. cloud cover and wind speed. Without this feature, this exercise would have been quite pointless. The results indicate that with the present model setup, the low-level temperature is forced strongly by the GCM, so that the temperature results were significantly different using HadCM2 or ECHAM4. Precipitation is also somewhat sensitive to which GCM forcing that is used, but significantly less so than for the temperature. Instead, the critical feature for precipitation is the model resolution. Practically all GCMs suffer from a poorly described annual cycle. This is true also for RCA at coarse resolution. However, as resolution is improved, not only does RCA provide very realistic horizontal gradients, but the proper annual cycle also starts to appear at resolutions better than ~ 40 km. Unfortunately, this happens at the expense of the average annual precipitation, which becomes to large as the hydrological cycle becomes more vigorous. The evaporation, on the other hand, seems to be controlled mostly by the choice of surface parameterization. The runoff estimates (not shown) were also improved by implementing some HBV properties directly in to the soil water routines. Providing a coupled dynamical model for the lake and sea surfaces is also critical, in particular on the Botnic Bay and Sea. Here a realistic description of the ice cover is critical, and the regional climate is presumably very sensitive. It is expected that this feature is very important in the climate-change simulations, as the ice cover here might change drastically in a warmer climate.

It is also suggested that the use of climate simulations is very efficient for developing new parameterizations. Systematic errors, that can easily be hidden by the data assimilation in weather prediction mode, appear clearly in a climate simulation over several years. It is also clear, however, that much caution is needed here. This is partly due to the fact that some of the processes are more sensitive to resolution, other to the climate that is imported from the

GCM and others still to the actual physical description. The practice of interfacing new schemes from other models is thus advised against, since one looses control over the sensitive balance between different processes, which can be retained while developing all routines in the same model framework.

New schemes should ideally be built on a process basis, comparing the parameters of the scheme against measurements of the same parameter. Evaluating e.g. a new turbulence scheme, using forecast scores of surface pressure or two-meter temperature runs a serious risk of obscuring the actual results, since these variables are the result of a multitude of processes in addition to the turbulence scheme itself. Feedback between processes cannot be ignored.

A particular problem that has to be addressed in the future is that of running downscaling experiments using driving models with different physics than in the regional model. It is illustrated here, that for example moist physics in a GCM is tuned to provide accurate annual average precipitation, while annual cycle and spatial distribution is sacrificed. Adding horizontal resolution in the regional model alleviates this at the cost of overestimating annual precipitation. Thus smooth fields over the boundary relaxation zone can sometimes not be combined with an accurate behavior within the regional model. The ability of the regional model to improve the regional climate over that of the GCM should always lie at the heart of the problem. No other criteria can, in the long run, motivate this approach.

References

Källén, E., 1996: HIRLAM Documentation manual, System 2.5. SMHI Norrköping (Available from SMHI, S-60176 Norrköping Sweden).

Rummukainen, M., J. Räisänen, A. Ullerstig, B. Bringfelt, U. Hansson. P. Graham and U. Willén, 1998: RCA - Rossby Centre regional Atmospheric climate model: Model description and results from the first multi-year simulation. SMHI Report No. 83.

Räisänen, J., M. Rummukainen, A. Ullerstig, B. Bringfelt, U. Hansson, and U. Willén, 1999: The first Rossby Centre Regional Climate Scenario - Dynamical downscaling of CO_2 induced climate change in the HadCM2 GCM. SMHI Report No. 85.

A hydrological perspective on unification of meteorological and hydrological land surface models

Sten Bergström, Göran Lindström and Marie Gardelin
Swedish Meteorological and Hydrological Institute
sten.bergstrom@smhi.se, goran.lindstrom@smhi.se, marie.gardelin@smhi.se

Although hydrologists and meteorologists have a common interest in developing better routines for surface parameterisation there is still a long way to go before harmony is reached between the hydrology in climate models and hydrological models. Within BALTEX, and in particular in NEWBALTIC II, we are trying to unite the meteorological and hydrological model traditions and come out with a synthesis in the end. This is also one of the present tasks of the Swedish programme for regional climate modelling, SWECLIM. Experience has shown that the macro-scale runoff modelling problem, on the Baltic basin scale, can be solved rather pragmatically with existing conceptual hydrological models. More advanced models are, however, needed to bridge the scientific gap between meteorology and hydrology. This development process requires an intensified use of field data for the internal validation of the individual components of land parameterisation schemes in order, among others, to overcome the problems related to compensating errors. The models must also be capable of addressing sub-grid or sub-basin variability in a heterogeneous landscape in a realistic, but still practical manner. Finally it is of utmost importance to pay attention to the complexity chain in this modelling process.

Meteorological and hydrological surface parameterisations

The most important difference between meteorological and hydrological approaches is that the meteorological models primarily focus on the energy exchange at the land surface, while the water balance, and often just river runoff are the basic goals of hydrological modelling. The time resolution is another difference. Hydrologists normally work with a resolution of 24 hours or hours, while the solution of the energy balance of meteorological models requires higher resolutions.

In hydrology relatively simple conceptual models, with empirically derived functions for water fluxes, is the most commonly used approach, while theoretically derived equations for vertical fluxes of water and energy is the tradition in meteorological modelling. A large difference between the hydrological and meteorological problem is the strong non-linearity in the meteorological approach, since the energy exchange at the surface has strong feedbacks into the atmosphere. As a result of the conceptual hydrological modelling approach, validation is a logical step after calibration of the model parameters. Validation of the energy exchange in the meteorological models is more complex, since the turbulent fluxes are difficult to measure, and have large sub-grid variations. The hydrological models focus on the catchment and descriptions of the horizontal variability within a catchment, while the meteorological models are based on grid squares with treatment of sub-grid processes by empirical relationships. The fact that meteorology uses the grid-square as primary unit, while hydrology uses the catchment is, however, of little significance. The reason for using catchments in hydrology is simply ease of model application and validation. The

approach to physical description of the system should be the same, no matter whether the area is a square or whatever irregular shape. Fig.1. illustrates typical differences in meteorological and hydrological model thinking. The latter, represented by the Swedish HBV model (Bergström, 1995), is illustrated in more detail in Fig. 2., where the following basic features can be identified.

- The basin is divided into sub-basins if its complexity so requires.
- Major lakes are modelled explicitly, while smaller lakes are integrated in the saturated zone of the model.

- Each sub-basin is divided into elevation zones.
- Each elevation zone is divided into open land and forests.
- Snow accumulation can be distributed statistically in each elevation zone (this option is normally used above the timberline).
- Water is stored as snow, capillary water in the snow, soil moisture, groundwater (saturated zone) and in lakes.
- Generated runoff from the saturated zone is routed through the lakes and the river system.
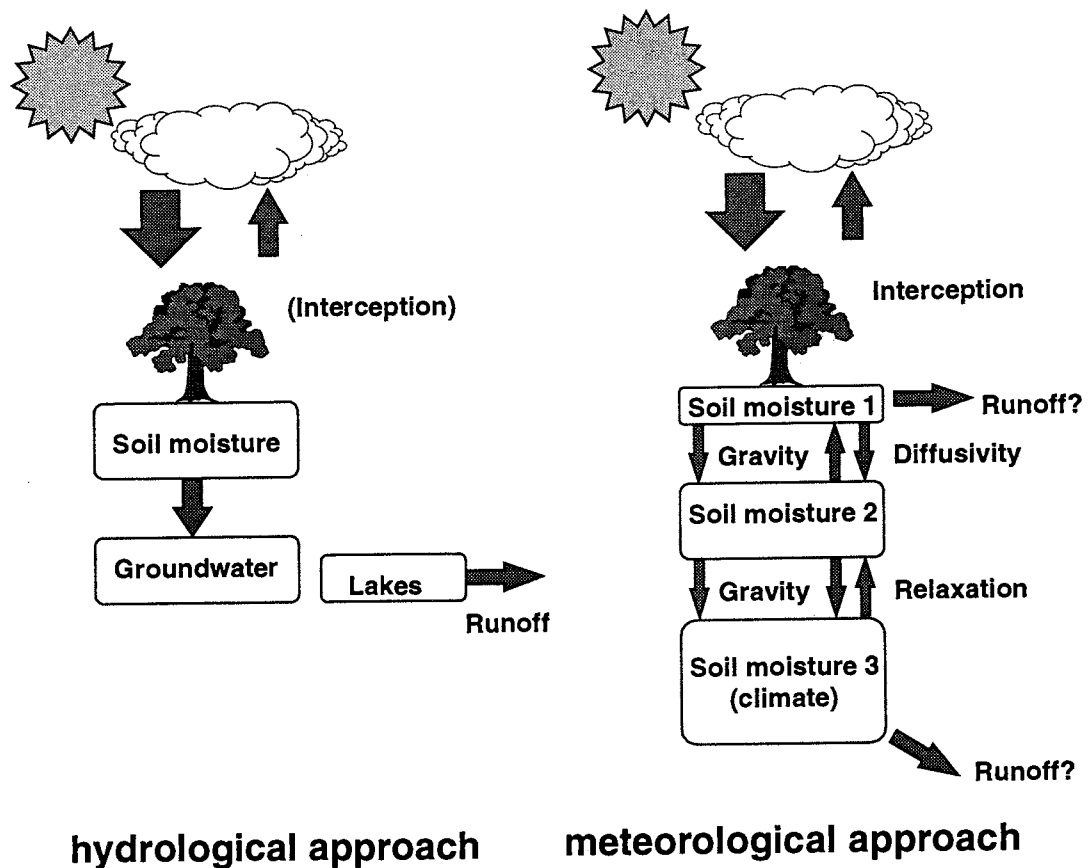

hydrological approach   **meteorological approach**

Fig. 1.   *Schematic illustration of typical hydrological and meteorological approaches to surface parameterisation.*
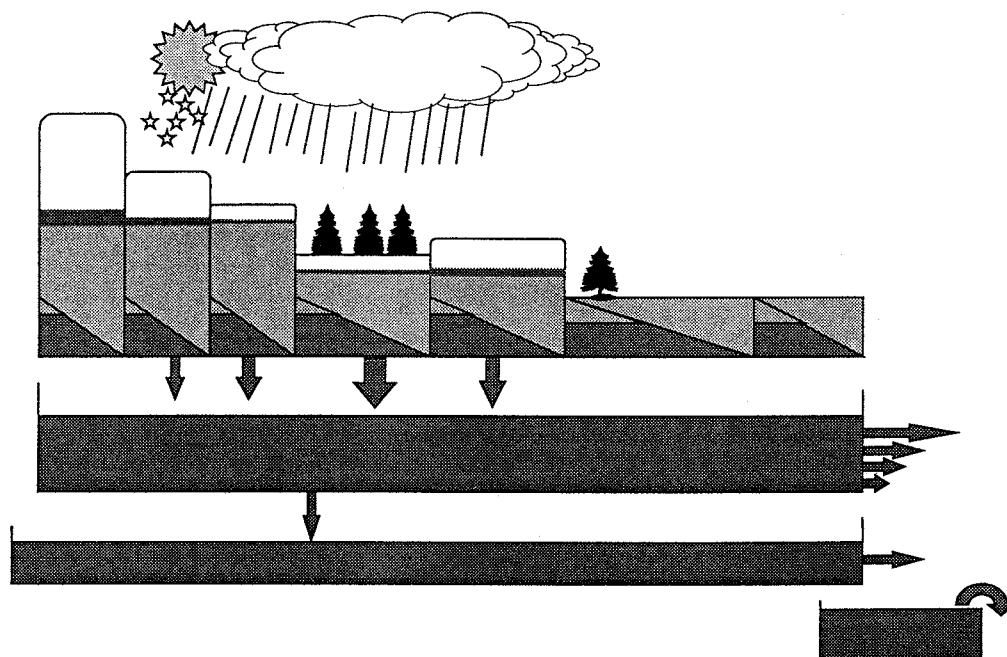
Fig. 2.   *Schematic presentation of the HBV model structure for one sub-basin, three elevation zones, two land classes and one major lake at the outlet. Note the statistical distribution of snow above the timberline at the highest elevations.*

The soil moisture routine of the HBV model was introduced as early as in 1972. It is based on a variable parameter approach, which has been showed to be a very robust and relatively scale independent means of modelling soil moisture dynamics under heterogeneous conditions. The starting point is the simple and traditional bucket theory, which assumes that no vertical drainage occurs in the soil until its field capacity is reached. The novelty was that the variability in soil conditions is considered. This variability is a joint result of variable antecedent rainfall and snowmelt conditions, as well as variable geological conditions. The result is a much less rigid relationship between soil moisture status and runoff generation, than is possible to obtain with the bucket theory. In fact, this work has proved that the bucket theory is inadequate.

The variable parameter approach was introduced into climate modelling by Dümenil and Todini (1992). Just recently has the HIRLAM scheme of the regional climate model at the Rossby Centre been modified to account for this effect. So we have examples of unification of hydrological and meteorological approaches. In this case it was possible, as the scheme is insensitive to the shape of the unit area. It doesn't matter whether it is a grid-square or shaped as a sub-basin.

While it seems relatively straightforward to combine the modelling schools in soil-moisture parameterisations it is a bit more difficult when it comes to snow. Even though the hydrological snow models, with their degree-day tradition, often are described as simple in contrast to the more sophisticated physically based schemes of the meteorological schemes a closer look at Fig. 2 may support the opposite opinion. The elevation zoning and lapse rates, which have become hydrological standard, are very difficult to transfer to climate models without an unacceptable increase in complexity and computer time requirements. Add to this variable vegetation cover, statistical snow

distribution used to illustrate snow-drifts, water–holding capacity of snow and the hydrological models suddenly turns out to be very comprehensive! We have to realise that a proper parameterisation of snow has to cope with the fact that we simultaneously may have three seasons in a mountainous grid cell, namely winter, spring and summer.

The conclusion from unification work on snow modelling, just initiated at the Rossby Centre, is that it is difficult to reach the degree of sophistication of hydrological models when it comes to the areal discretisation of snow processes.

Compromises are needed to maintain a reasonable complexity in the climate model. One simplification which is studied is to relate the snow covered fraction of a basin to the amount of remaining snow rather than to the snow amount itself. In this way a clearer relation is achieved and the same relation can be used in different basins (Fig. 3). The need for distribution into elevation zones and the statistical snow distribution within a grid square is partly overcome by this approach. A similar treatment of snow accumulation as a function of the different temperatures at different altitudes in a grid square is also being tested.
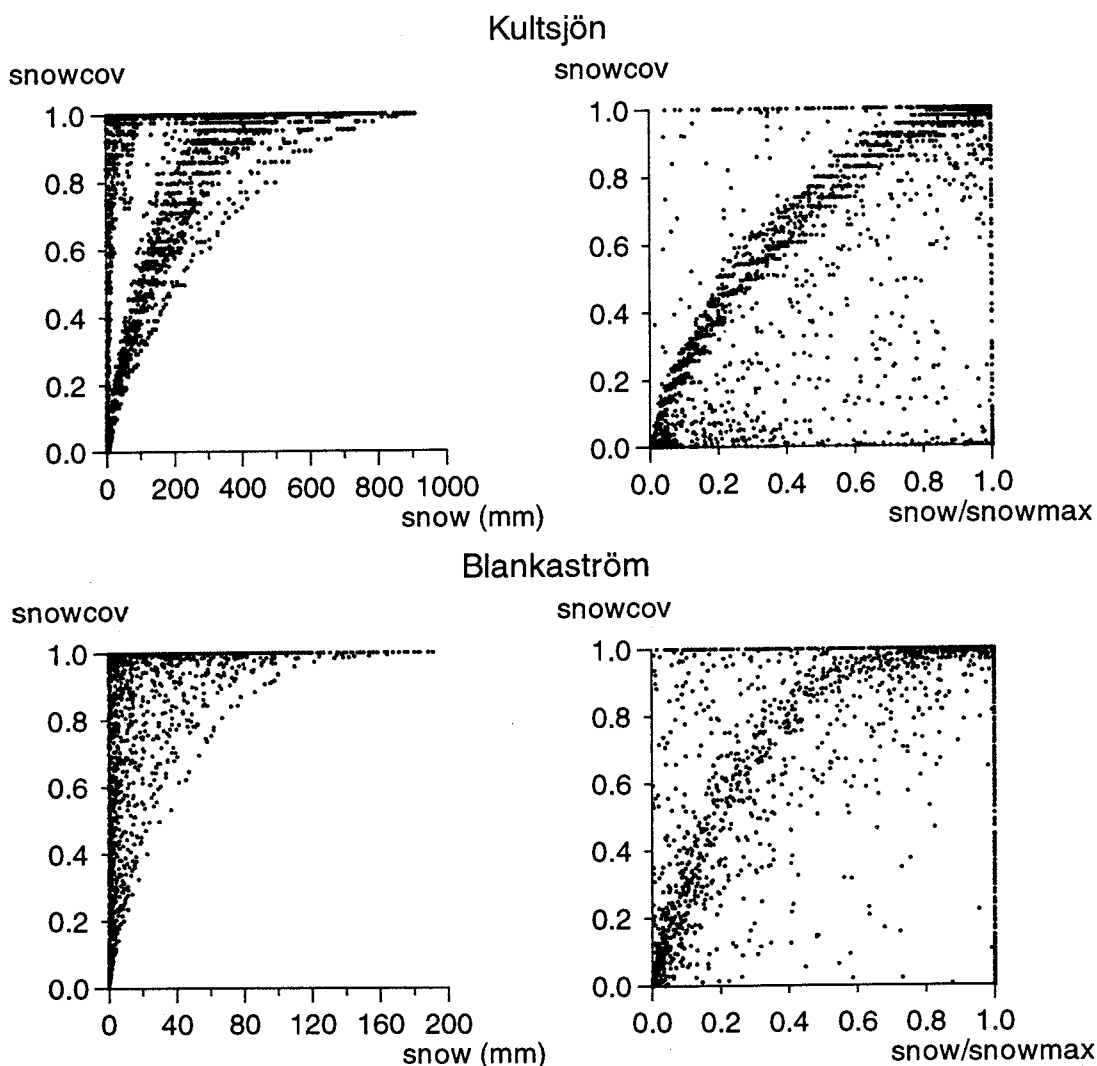

Fig. 3.   Snow-covered fraction of the Kultsjön and Blankaström basins (in northern and southern Sweden respectively) versus snow amount. Left: versus current snow pack, right: versus the current snowpack as a fraction of the maximum snow pack so far during the winter season. Analysis of results by the HBV model.

Is there a scale problem?

The HBV model has been applied under a great variability of physiographic settings and at a wide range of scales. It seems like its parameterisation is fairly robust, as it has been possible to calibrate the basic model without any great changes of its structure. Lately the model was applied to the entire catchment of the Baltic Sea (Bergström and Graham, 1998; Graham, 1999). This work was carried out within the NEWBALTIC project and was initiated, not without scientific hesitation and criticism. Is it possible to model such a large basin and is it meaningful? Retrospectively we can see that it was possible and had a meaning. The work gave us opportunities for more in-depth comparisons between hydrological and meteorological approaches as we now had a scale at which we could meet. The results show that the two approaches differ a lot and that the risk for compensating errors in land parameterisations has to be considered seriously (Graham et al., 1998). The work further provided us with a near real time model for simulation of river runoff to the Baltic Sea, which is very useful for oceanographers, now as river runoff data are becoming less available in the area.

Pay attention to the complexity chain when marrying models!

Another fundamental conclusion, which can be drawn from the integration work between hydrology and meteorology is that we have to pay more attention to the complexity chain in modelling. This means that fully physically based distributed model components successively can be aggregated into statistically distributed descriptions and lumped approaches, but it is very difficult to go the other way around. This process is shown schematically in Fig. 4, which illustrates how this chain looks at
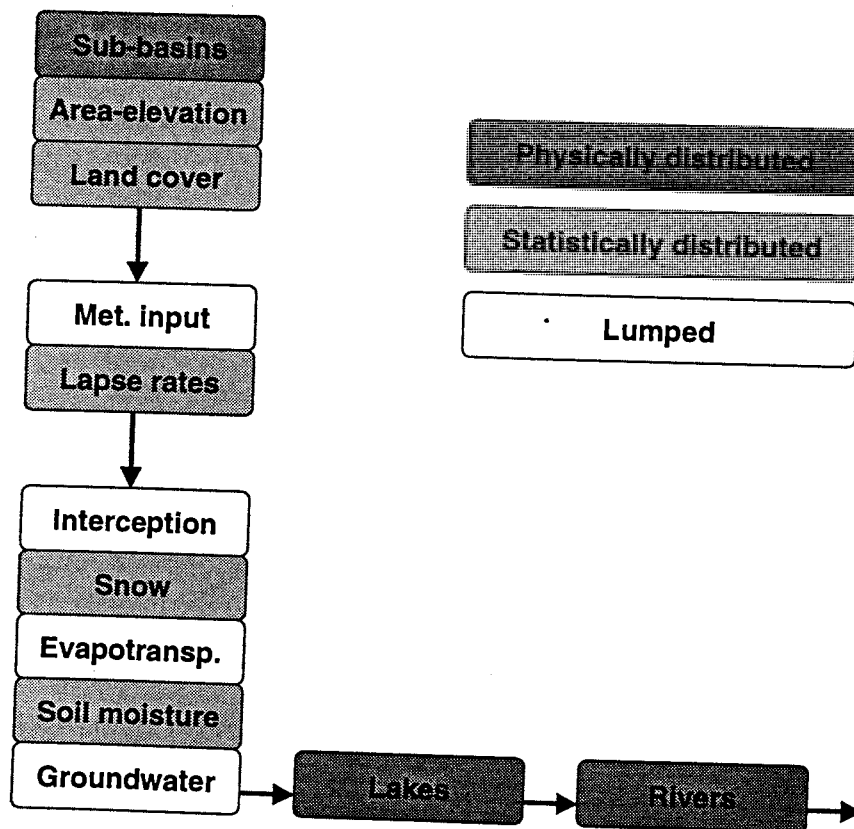

Fig. 4. *The complexity chain as identified in the HBV model, which is typical for many hydrological models.*

present in the HBV model. It reveals that there is a tendency to go from higher to lower degrees of sophistication although some inconsistencies can be identified. We should disregard routing in lakes and rivers as this is based on local additional information and therefore a shift towards more physical methods can be justified. When we start mixing modelling components, there is an obvious risk that we run into interface problems if the principles for model distribution are in disharmony.

Conclusions

There is a common interest among climate modellers and hydrologists in better surface parameterisations. This is a key subject for the BALTEX research programme and other continental scale experiments within GEWEX. It is also in focus within the Swedish research programme for regional climate modelling, SWECLIM.

Attempts to unite the hydrological and meteorological modelling traditions are under way and some encouraging results have been reported as concerns the variability parameter approach in soil moisture parameterisation. It seems like the unification of the snow parameterisation is more difficult. It is not easy to transfer the hydrological tradition of detailed description of snow in the landscape to climate models, without great simplifications. Such work is in progress.

One common problem in all modelling is the risk for compensating errors. This might block further development, as improvement in one process description falsely may be interpreted as a failure, if we do not get rid of a compensating error simultaneously. To cope with this problem we have to pay more attention to internal process validation in our models in the future. The application of a hydrological model to a continental scale basin has also a great potential in this respect as it offers opportunities to review how the physical processes are modelled and behave.

Finally the concept of a complexity chain helps avoiding inconsistency traps in unified modelling. This means that the degree of discrimination should be logical and normally follow a declining scale through the modelling process. If we do not pay attention to the complexity chain we may develop a monster and not a model!

References

Bergström, S. (1995) The HBV model. In: Singh, V. P. (Ed.). Computer Models of Watershed Hydrology, Water Resources Publications.

Bergström, S. and Graham, L.P. (1998) On the scale problem in soil moisture modelling. Journal of Hydrology, 211, pp. 253-265.

Dümenil, L. and Todini, E. (1992) A rainfall-runoff scheme for use in the Hamburg climate models. In: O'Kane, J.P. (Ed.). Advances in Theoretical Hydrology. Elsevier, Amsterdam, pp. 129-157

Graham, L.P. (1999) Modeling Runoff to the Baltic Sea. Ambio, in press.

Graham, L.P., Bergström, S. and Jacob, D. (1998) A discussion of land parameterization in hydrologic and climate models - example from the Baltic Sea Basin. Cont. to the Second International Conference on Climate and Water. Espoo, Finland, 17-20 August.

Runoff simulations for BALTEX

Bart van den Hurk, KNMI, the Netherlands, e-mail: hurk@knmi.nl

September 29, 1999

1. Introduction

Runoff is an important component in the regional hydrological cycle of the Baltic Sea catchment area. Calculations with the ECHAM4 climate model indicate that 40% of annual precipitation falling on land surface enters the Baltic Sea as runoff (Bengtsson, 1998).

The intensity of land surface runoff and its phasing in time and place are relevant for electric power planning, forecasts of flooding events and fresh water inflow. Therefore, an accurate simulation of runoff is of importance. Since weather phenomena are major precursors for land surface runoff, embedding the process of runoff in climate and weather models has gained interest in the last decade. Simulation of runoff in large scale meteorological models is carried out using several different approaches.

In one approach, the soil column is divided in a set of discrete, vertically stacked layers. Runoff occurs when the infiltration rate as a result of precipitation and snowmelt exceeds the capacity of the (shallow) top soil layer, or by the process of leakage of water from the bottom soil layer. In this approach, surface runoff only occurs when the complete top layer is (nearly) saturated with water. The latest ECMWF land surface scheme (Viterbo and Beljaars, 1995) uses this approach.

Alternatively, Dümenil and Todini (1992) appreciate the horizontal variability of soil saturation on a spatial scale comparable to a climate model gridbox. A portion a of the gridbox is assumed to be fully saturated, and produces runoff when additional infiltration occurs. a depends on the relative saturation of the total soil column, and the variability of the land surface orography, yielding more runoff in steep terrain. In addition to this surface runoff, a similar deep water leakage is included as mentioned above. This scheme is implemented in the ECHAM4 climate model.

Quite different is the approach in a distributed hydrological model, such as HBV (Lindstrom et al. (1997). In HBV, detailed information about the orography, soil moisture storage capacity and soil physical parameters is combined with an external forcing of rain- and snowfall and evaporation in order to simulate the catchment runoff. Calibration on river flow data is usually performed. A detailed version of HBV for the Baltic Sea catchment is constructed (Graham, 1999).

In this study, we use simulations of HBV, and the surface schemes of ECMWF and ECHAM4 in order to evaluate the characteristics and skill of these schemes in terms of runoff. The study focusses on daily totals for the whole Baltic Sea catchment in a single growing season March - October 1995. We will use HBV as "verification material", since it is calibrated to the specific area and forced with observed rain- and snowfall. The two surface schemes are embedded in a common regional climate model called RACMO (Christensen et al., 1996), situated over the Baltic area at 1/6° grid resolution. Atmospheric fields in RACMO are initialized using ECMWF operational analyses, and also lateral boundaries are taken from ECMWF.

2. Scheme characteristics

In the ECMWF surface scheme, soil characteristics are similar everywhere. Deep water runoff is a function of the relative saturation in the lowest model layer. When initialized at field capacity (set at 0.353 m^3/m^3), the runoff will result in a cumulative water loss of about 40 mm after 10 days. As the water level decreases, runoff decreases.

In the ECHAM scheme, the soil depth is variable over the domain. The average depth in the Baltic catchment is ±0.30m. When soil moisture is initialized at full saturation for a 0.3 m deep layer, cumulative water loss due to runoff will be ap-

proximately 15 mm after 10 days; initialization at field capacity (defined as 75% of saturation) will result in a water loss of only 0.2 mm. Deep water runoff is thus a steep function of relative water content. *Surface* runoff is related to the infiltration rate and the subgrid-variability, and in practice dominates the runoff process for all non-flat areas.

3. Simulated runoff

Figure 1 shows the results of average runoff (expressed in mm/day) in the Baltic Sea catchment as calculated by HBV, RACMO with the layered ECMWF land surface scheme, and two versions of RACMO with the variable infiltration ECHAM4 land surface scheme. The latter two version differ in the amount of soil water used to initialize the simulations.

The first ECHAM4 simulation was started with soil water initialized at field capacity (75% of full saturation). The runoff calculated for March 1995 appeared to be very low (see figure), as a result of the steep decrease of runoff with decreasing water content. To increase the runoff to values comparable to HBV and ECMWF, the simulation was cancelled and a new run was started with initial soil water at saturation. Also shown are simulations carried out with RACMO and the ECMWF surface scheme for the so-called PIDCAP simulation between 1 August and 31 October 1995 (Bengtsson, 1998), in which soil moisture initialization appeared a sensitive and uncertain issue.

From this figure the following can be deduced:

- The ECMWF model shows a runoff curve which is much smoother than the results predicted by the HBV-scheme. Surface runoff, occuring after heavy precipitation or snow melt events, is never simulated in the ECMWF-scheme. This is a result of the requirement that a complete 7 cm slab over the full grid box must be saturated with water before surface runoff can occur, which never happens. Moreover, the ECMWF curve shows a general delay of the major runoff events compared to the HBV-output. This is a result of the fact that water leaking out of the soil reservoir has to travel through a deep soil layer before stored leaving the soil as runoff.

- The ECHAM4 scheme initialized at saturation follows the peaks in the HBV-output reasonably. The extremes are higher than in the HBV-simulation, and as a result, the dry-down period is likely to be reached a bit earlier.

4. Cumulative budgets

A comparison between the cumulative hydrological budget terms is shown in figures 2a-2c for each of the HBV, ECMWF and ECHAM4 runs. For HBV only runoff and precipitation are available at this moment.

Although not large, some noticeable differences between the schemes can be concluded from this figure:

- The precipitation in the HBV run is some 10 % lower than either of the two RACMO runs. This is due to the use of uncorrected raingauges as input to HBV.

- The ECMWF runoff is 35 mm larger than the ECHAM4 runoff, in spite of the lack of surface runoff. This is a result of the choice of the hydraulic conductivity in the model. The HBV-runoff, accumulated until 1 Nov 1995, is 8 mm higher than ECHAM4.

- Owing to the increased runoff, the ECMWF-scheme produces 69 mm *less evaporation* and 57 mm *less precipitation*. A positive feedback is present here, since the reduction in evaporation exceeds the increase in runoff, comparing ECMWF to ECHAM4.

5. Timescales

As shown in figure 1, the two RACMO schemes have a different runoff time scale. In ECHAM4, surface runoff with short timescales seems dominant, while in the ECMWF scheme, runoff is filtered as the water passes through a slab of soil. Moreover, in the season under study runoff is affected by a combination of snow melt and precipitation. Snow accumulation forms a delay of runoff after precipitation events.

In the current section we explore the timescales in the HBV-record and the RACMO simulations, by calculating the instantaneous and lagged correlation coefficient between simulated runoff and

a given forcing. The lagged correlation coefficient $r_{F,R}(L)$ is defined as

$$r_{F,R}(L) = r_{F(t),R(t+L)} \qquad (1)$$

where F is the forcing, R is runoff and L is the delay in days relative to initial time t.

Figure 3 shows lagged correlation coefficients derived from the HBV, ECHAM and ECMWF results. Shown are correlations of runoff to total precipitation, liquid precipitation, snow melt and snow fall. Liquid precipitation is the total precipitation minus snowfall. It was not (yet) available from the HBV-simulation, but instead it was calculated using the relative snow precipitation derived from the RACMO-ECHAM4 simulation.

From the HBV-plot, the correlation for each of the forcings is highest when no time lag is used. Only for snow fall a small secondary maximum seems present at a lag of 20 days, related to the time between snow fall and snow melt. Surprisingly, the correlation with liquid precipitation is lower than the total precipitation, and becomes negative. This is a result of the dominant signal of the snow melt. In figure 4 the lagged correlations are shown for the months June-October, where snow is largely absent.

The correlation signature of the ECHAM4 scheme resembles the HBV output rather well: a dominant peak related to snow melt at no lag, a secondary maximum of snow fall after 20 - 25 days, and smaller (and negative) correlations to total and liquid precipitation.

The ECMWF picture, on the other hand, looks very different. Here the snow melt is again the dominant process, but a clear filtered lag of approximately 10 days is seen. The correlation to snow fall increases monotonically, and also no (unlagged) correlation with precipitation is visible.

From this figure we can conclude that on a seasonal timescale snow melt and snowfall processes dominate the runoff spectrum, and that this occurs via a fast responding surface runoff process.

In the snow-free months (figure 4) it is shown that also the correlation between precipitation and runoff is optimal when no timelag is applied. From the HBV-simulations the fall of the initial slope is slightly steeper than in the ECHAM

simulation, but the qualitative correspondence is clear. The ECMWF scheme does not show this fast response to precipitation at all, for reasons discussed before.

6. Conclusions

This study reveals that:

- The runoff produced by the ECMWF scheme has no surface component, and is therefore much smoother and delayed compared to the ECHAM4 and HBV-simulations

- In spite of the absence of surface runoff, the ECMWF scheme produces a bit more runoff than the HBV and ECHAM4 models do. This leads to a decrease in land surface evaporation and a decrease in precipitation over land. The decrease in evaporation exceeds the increase in runoff, indicating a positive feedback.

- The ECHAM4 scheme has a spectral signature which compares quite well to the HBV-simulations. The initialization obviously forms a sensitive issue.

- On a catchment scale, fast processes (related to surface runoff) dominate the runoff characteristics. This is the case for both snow melt and (liquid) precipitation.

References
Bengtsson, L. (ed) (1998): *Numerical studies of the energy and water cycle of the Baltic Region*; End report EU-project ENV4-CT95-0072.

Christensen, J.H., O.B. Christensen, P. Lopez, E. van Meijgaard and M. Botzet (1996): *The HIRHAM4 Re-*

gional Atmospheric Climate Model; Danish Meteorol. Institute, Copenhagen, Scientific Report 96-4, 51 pp.

Dümenil, L. and E. Todini (1992): A rainfall-runoff scheme for use in the Hamburg climate model; in: *Adv. Theor. Hydrology*, J.P. O'Kane (*Ed.*); European Geoph. Soc. Series on Hydrological Sciences, Vol. 1, Elsevier Science Publishers, Amsterdam, pp. 129-157.

Graham, P. (1999): Modelling runoff to the Baltic Sea; *Ambio* **28**, 328-334.

Lindstrom, G., B. Johansson, M. Persson, M. Gardelin and S. Bergstrom (1997): Development and test of the distributed HBV-96 hydrological model; *J. Hydrol.* **201**, 272-288.

Viterbo, P. and A.C.M. Beljaars (1995): An improved land surface parametrization scheme in the ECMWF model and its validation; *J. Climate* **8**, 2716-2748.
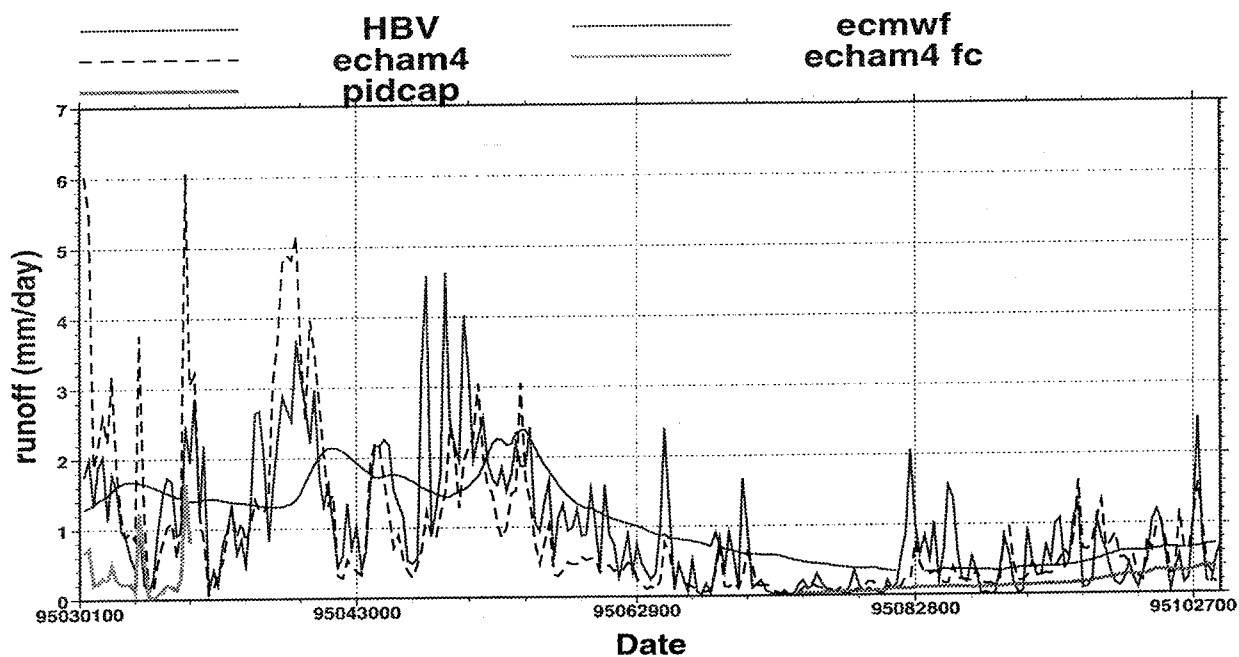
BALTEX land total runoff

Figure 1: Total runoff simulated by the HBV-model, RACMO with the ECMWF surface scheme (labeled "ecmwf"), RACMO with the ECHAM4 surface scheme (labeled "echam4"), and anoter ECHAM4 simulation initialized at 75% of soil saturation, assumed to be field capacity (labeled "echam4 fc"). Also shown are ecmwf-results carried out in the so-called PIDCAP model intercomparison (see text).
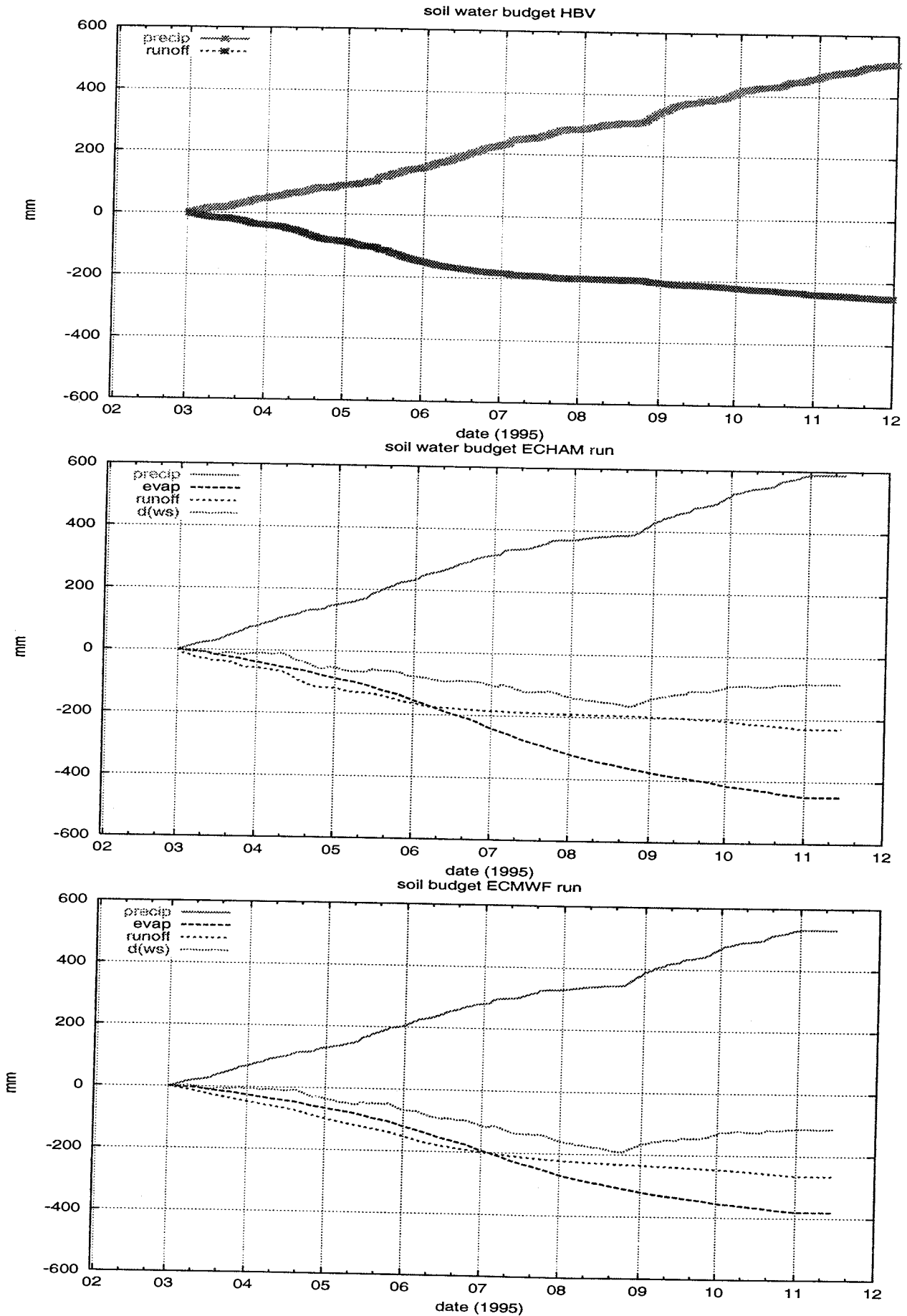
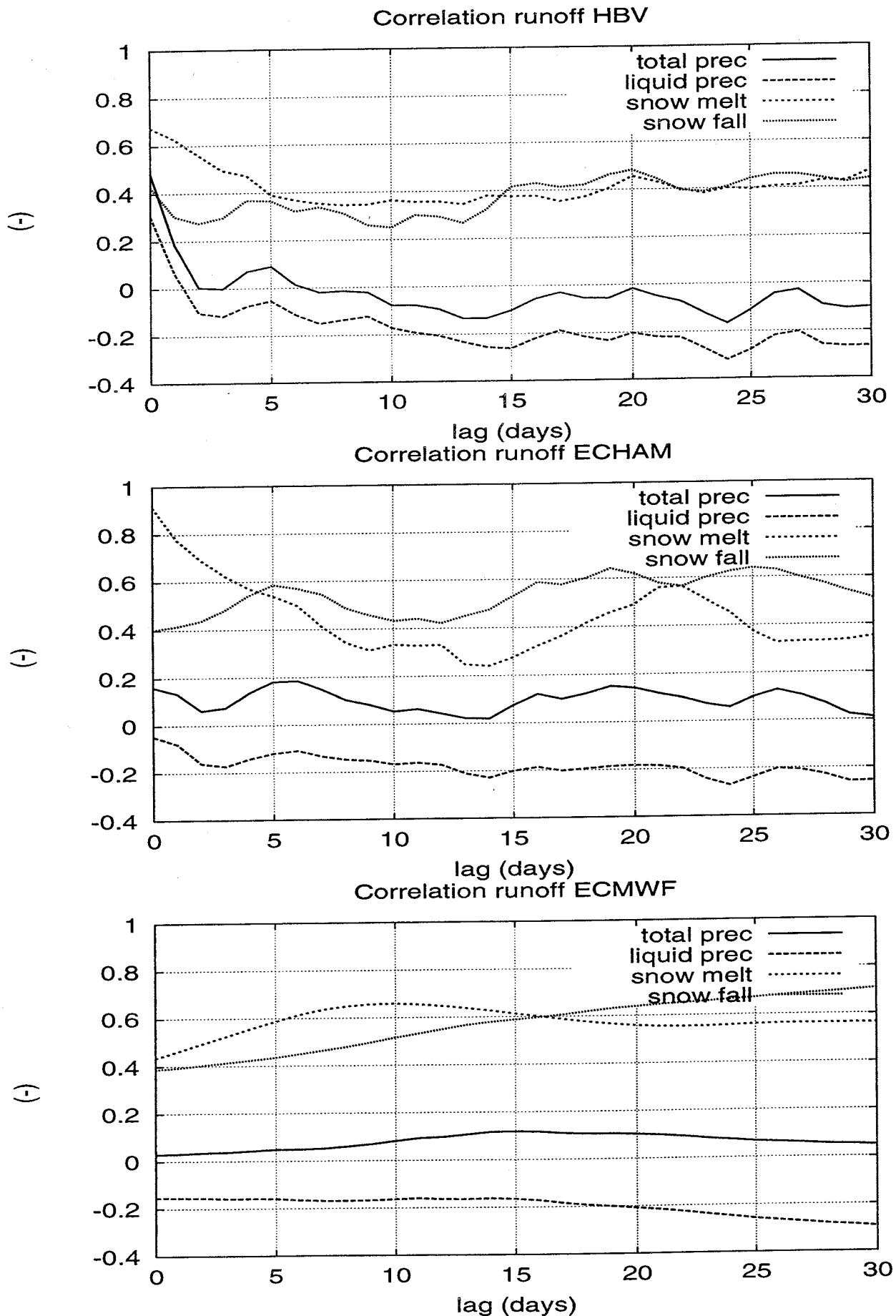Figure 2: Hydrological budgets of simulations with HBV, ECHAM4 and ECMWF.

Figure 3: Lagged correlation coefficients between runoff and total precipitation, liquid precipitation, snow fall and snow melt derived from simulations with HBV, ECHAM4 and ECMWF.
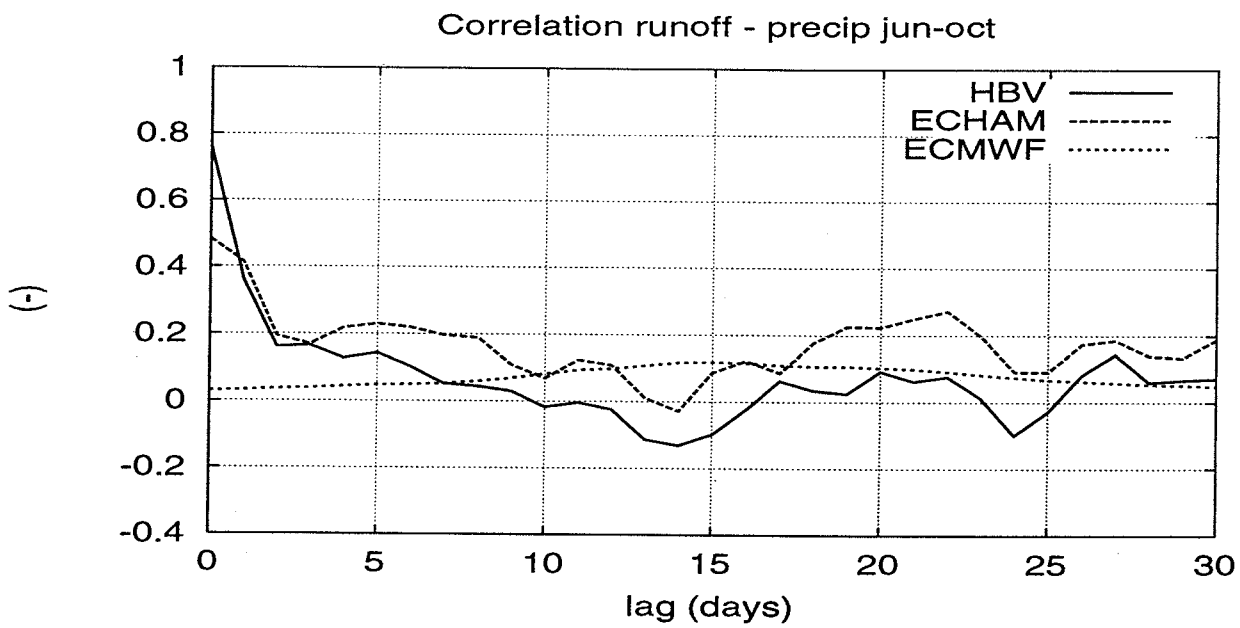
Figure 4: Lagged correlation coefficients between runoff and total precipitation for the largely snow-free months June - October.

Shaping of the basic climatic and hydrologic parameters on the Polish Lowland on the basis of the Warta River basin

Prof. dr hab. inż. Piotr Kowalczak

Institute of Meteorology and Water Management

Poznań Branch

The Warta River (A=54528,7 km^2) is the main tributary of the Odra River. The hydrological and climatic ratio in the river basin of Warta is typical for the Polish Lowland and is characterised – especially in case of hydrology – by a great area and time variability. The region is predominated by agriculture, although there are two big industry centres which have a great influence on the shaping of water resources in the river basin (lignite mines in Bełchatów and Konin). The river flows through big urban areas (Poznań, Gorzów, Konin).
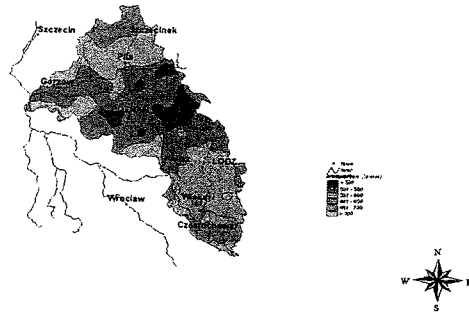
The river source is located in the upland region. The northern tributaries of the Warta River (Gwda and Drawa) also flow from the upland regions. The rest of the river basin is located in the lowland.

The climate of the Warta River basin has features of the transitory climate typical for Poland. Since the analysed area is mainly located in the west part of the county, it is characterised by the great participation of the oceanic features: lower temperature amplitudes, early spring and summer,

relatively short winter. Because of the great meridional and parallel expansion as one moves to the north and north-west borders of the analysed region, one finds greater influence of the sea features being the effect of the influence of the Baltic Sea (greater cloud cover, cooler summer). However, as one moves to the east borders of the basin one finds more influence of the continental features (longer and colder winter), whereas in the south-east part of the region one finds greater influence of the upland area (greater precipitation and diversification of the climate conditions depending on the height and exposure).
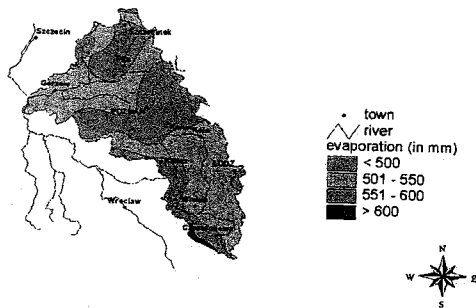
Selected climatic parameters are presented in Fig. 1 and Fig. 2.

Fig. 1. Average annual precipitation rate in the Warta River basin (1931-60)

Fig. 2. Average annual area evaporation in the Warta River basin (1931-60).

The annual activity of the cyclone systems is the cause of the precipitation throughout the year. However, in the summer, when clouds are thicker and more watery, the precipitation is greater which is typical for the continental regions. The precipitation is also much dependant on the upheaval of the given region over the sea level. High sums of the annual precipitation – over 600 mm - appear in the central part of the Pomorskie Lakeland. These areas are open to the predominating influence of the west winds. The central part of the river basin is located in

the 'precipitation shade' and has smaller precipitation rate (below 550 mm). In the Poznań, Gniezno, and Kujawy Lakeland the totals precipitation are about 470 – 480 mm. These are the lowest average annual totals atmospheric precipitation in Poland. Moving to the south, these rates gradually get higher together with the greater influence of orography, so that in the region of the Cracow-Częstochowa Upland the precipitation rates are above 650 mm.

The winter precipitation, despite the great frequency (14–19 days a month), is much less efficient than the less frequent but more abundant summer precipitation (10-16 days). The atmospheric precipitation is one of the most variable elements of climate. Sometimes monthly totals of precipitation can be even close to 0 mm in the central part of the river basin. However, in the summer the monthly precipitation can exceed 200 mm, especially in the northern and southern parts of the Warta basin. The highest twenty-four hours precipitation in the summer, especially in the Kujawy Lakeland, can exceed 100 mm. At the same time however, there exist rather inconvenient for agriculture atmospheric droughts connected with the existence of long (sometimes several weeks) periods without rain at all.

In the region of the Warta River basin part of the precipitation appears in the form of snow. This phenomenon appears from October till May, with the maximum frequency from December till February. The average annual number of days with snowfall in the analysed region has been calculated to less than 30 days

in the central-west part of the region, and over 40 days in the north and south part of the region.

Similar spatial distribution has the average annual number of days with snow cover. It rates from less than 40 days in the central-west part to over 60 days in the south-east, and over 70 days in the north-east part. The greatest thickness of the snow cover is noted on the second half of the winter – in February it can exceed 30 cm. The average maximum annual water supply in the snow cover contains from below 30 mm locally and in the central and south-west part of the basin, to over 50 mm in the region of the Cracow-Częstochowa Upland.

The average annual area evaporation, calculated as the difference between the precipitation and the runoff, has been estimated in the area of The Warta River basin from below 400 mm in the west part, to over 450 mm in the central-south and south part. The average annual potential evaporation during the vegetation period from April to October totals from below 650 mm in the Kujawy Lakeland and in the north part of the Sieradz Basin, to over 750 mm in the Leszno Lakeland. The mentioned sums of the potential evaporation are higher than the average annual sums of precipitation (excluding the basin border regions), which means that the analysed region is characterised by a great aridity.

The hydrologic ratios in the Warta River basin are more complex and are affected by the variable precipitation distribution, difference in the land development, and also by

the specific system of the region specific runoff also shaped by the specific natural underground drainage (The Warsaw-Berlin Pradolina).

Average annual specific runoff in the Warta River basin (1951-80).
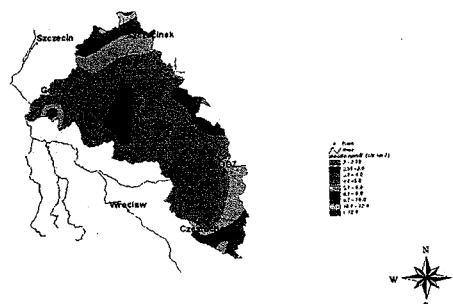
Fig. 3. Average annual specific runoff in the Warta River basin (1951-80)

The Fig. 3 clearly presents the significant area diversification of the runoff, which is range between 12,0 l/s km² in the Gwda basin, to below 2,0 l/s km² in the Upper Noteć Basin.

In case of extreme runoffs the diversification is greater despite the lowland character of the basin. The runoff values are presented in Table 1.

Table 1. Basic basin parameters

No	River	Section	Drainage area km²	Spec. Runoff (1951-80) (l/s km²)		
				Low	Medium	High
1	Warta	Działoszyn	4088,5	2,76	5,65	21,08
2	Warta	Konin	13351,1	1,86	4,2	18,29
3	Warta	Poznań	25910,9	1,34	3,9	13,74
4	Noteć	Nakło Z.	4097,6	0,85	2,61	5,05
5	Noteć	Estuary to Warta	17330,5	2,38	4,46	8,12
6	Drawa	Estuary to Noteć	3296,5	3,85	6,09	9,37
7	Gwda	Estuary to Noteć	4942,8	2,59	5,52	11,05
8	Warta	Estuary to Odra	54528,7	1,86	4,04	9,07

The Warta basin is located in the area where there is a clear border between the lake and non-lake region in Poland, which is connected with the last Baltic glaciation. The Fig. 4

presents the lake rate of the Warta basin in %/100km². The influence of the lakes in the Warta basin on the shaping of the runoff is diversified and results mainly from the ways of the lake management. However, in case of the basins located in the Upper Noteć Basin the influence of the climatic factors is also important (low totals of precipitation, influence of the underground drainage).


Lake location (in %/100 km2) in the Warta River basin.
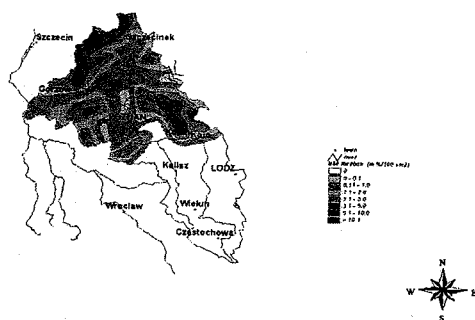
Fig. 4. Lake location (in % /100 km²) in the Warta River basin.

Figures 5,6,7 present the values of the average annual temperatures, annual totals atmospheric precipitation and average annual runoffs in the period from 1891 to 1995 for Poznań (the basin centre).

As the figure 5 clearly presents, there is no statistically significant trend of the average annual temperatures. Similarly, the annual totals atmospheric precipitation (Fig. 6) has no statistically significant trend either. However, beginning with 1940's there has been noticed an increased amplitude of the precipitation. The trend lines of the unitary runoffs suggest a small increase of the average annual runoff with a significantly greater diversification of the 10 summer mobile averages in comparison with the values calculated for the atmospheric precipitation.

Fig. 5. Average annual air temperature
Poznań 1891-1995
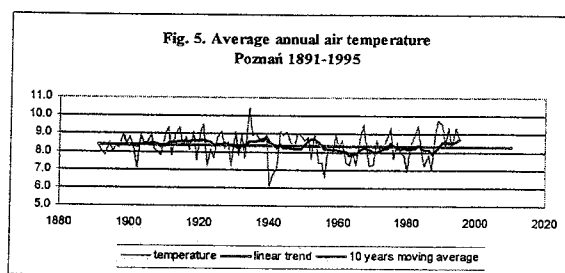
Fig. 6. Annual totals atmospheric precipitation
Poznań 1981-1995
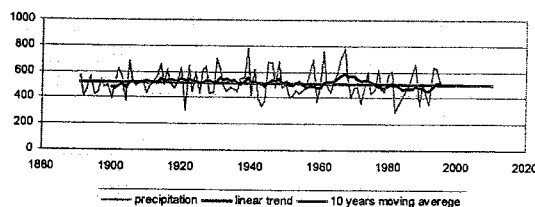
Fig. 7. Average annual runoff of the Warta River
in the Poznań section 1891-1995
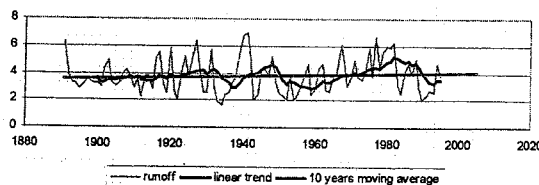
On the effects of lakes on energy and water fluxes

Nicole Mölders, Institut für Meteorologie, Universität Leipzig, Stephanstraße 3, D-04103 Leipzig, Germany
moelders@curie.meteo.uni-leipzig.de

1. Introduction

Evaporation is the conversion from the liquid phase of water to its vapor phase. Evaporation from free water surfaces depends on the energy supply, the water vapor deficit of the atmosphere, and the exchange of surface air with surrounding atmospheric air. In the last decades, several authors developed methods to estimate evaporation from streams, lakes, water reservoirs and oceans. These methods can be divided into (1) empirical methods, (2) water budget methods, (3), energy-budget methods, and (4) mass transfer methods (e.g., Burman and Pochop 1994). In atmospheric models, usually empirical methods applying the predicted meteorological quantities and based, in general, upon *Dalton*'s law and energy-budget methods are the most frequently used procedures to calculate evaporation from free water surfaces (e.g., Kramm and Foken 1998) when the waters are resolved by the model grid resolution. Obviously the approaches for the interfacial sublayer play an important role in the determination of evaporation from waters. For instance, using *Sheppard*'s (1958) approach provides nearly 50 % higher water vapor fluxes than *Reichardt*'s (1951) approach (see Kramm and Foken 1998). Therefore, Kramm and Foken (1998) concluded that parameterization schemes of the interfacial sublayer have to be validated not only on the basis of laboratory data as *Reichardt*'s approach, but also on data from field experiments.

Besides the treatment of the interfacial sublayer, in numerical modeling, the grid horizontal resolution leads to further difficulty in determining evaporation from lakes. In meteorological models, the horizontal grid resolution is often much coarser than that required to represent streams, small lakes and water reservoirs. Thus, waters are often of subgrid-scale with respect to the model resolution. A grid element of a mesoscale meteorological model encompasses several square kilometer for which the dominant land-use type is usually taken to be the representative one to determine the water and energy fluxes at the interface water/land-atmosphere. Applying this strategy neglects the effects of subgrid-scale waters on the distribution of near-surface atmospheric conditions. The resulting deviations in the near-surface water vapor and air temperature distributions may also affect cloud and precipitation formation (e.g., Mölders 1999a) and runoff by complicate non-linear feedback mechanisms.

Obviously, a better representation of the surface characteristics may be achieved by a finer grid resolution. Unfortunately, limitations of model parameterizations and computer performance as well as the availability of data to initialize the model restrict this possibility (Mölders and Raabe 1996). This article presents a strategy to consider lakes on a finer grid-resolution than that used in the atmospheric model.

2. Parameterization to consider subgrid-scale lake effects

The explicit subgrid-scheme, first suggested by Seth et al. (1994) for the global scale, was adapted for the meso-β-scale (Mölders et al. 1996) to consider subgrid-scale lake effects. Herein, a higher resolution grid (in my study 1×1 km^2) consisting of N (= 25 in my study) subgrid cells per grid cell (5×5 km^2) is defined in the soil and at the surface of the model (Fig. 1). These subgrid cells are assumed to be homogeneously covered by either waters or their individual vegetation and soil types. Unique energy and hydrological budgets (Eqs. 1 to 4) are maintained for each subgrid cell using the subgrid cell surface characteristics and micro climate at the representative location. This means that, in

each subgrid cell, the fluxes are calculated with its own near-surface meteorological forcing in the immediate vicinity of the interface earth-atmosphere and with its own subgrid water surface temperature or its own subgrid soil temperatures and soil wetness. These quantities are stored for each subgrid cell and serve to determine these quantities in the next time step. In the mth subgrid cell of the jth grid cell, net radiation, Q, soil heat flux, G, the fluxes of sensible, H, and latent heat, LE, are, therefore, given by (Mölders et al. 1996)

$$Q_{m,j} = -S_{m,j}(1-\alpha_{m,j}) - \varepsilon_{m,j}L_{m,j} + \varepsilon_{m,j}\sigma T_{sm,j}^4 \quad (1)$$

$$G_{m,j} = \begin{cases} -\lambda_{m,j}\partial T_{gm,j} / \partial z & \text{for land} \\ Q_{m,j} + L_vE_{m,j} + H_{m,j} & \text{for water} \end{cases} \quad (2)$$

$$H_{m,j} = \rho c_p C_{hm,j}u_{rj} (\Theta_{gm,j} - \Theta_{rj}) \quad (3)$$

$$L_vE_{m,j} = \begin{cases} \dfrac{\rho L_v C_{qm,j}u_{rj} (q_{sm,j}(T_{fm,j}) - q_{rj}) g_{sm,j}}{g_{sm,j} + C_{qm,j}u_{rj}} & \text{vegetation} \\ \rho L_v C_{qm,j}u_{rj} (q_{sm,j}(T_{gm,j}) - q_{rj}) f_{m,j} & \text{bare soil} \\ \rho L_v C_{qm,j}u_{rj} (q_{sm,j}(T_{wm,j}) - q_{rj}) & \text{water} \end{cases} \quad (4)$$

where the subscripts r, g, and w stand for the reference height (located at the first half level in 10 m height above ground), the ground and the water surface. The potential temperature, temperature, specific humidity, specific humidity of saturation and wind are denoted as Θ, T, q, q_s, and u, respectively. Furthermore, ρ, α, ε, λ, σ, z, S and L stand for the density of air, the albedo, the emissivity of the surface, the soil thermal conductivity, the Stephan-Boltzmann constant, the depth of the upper soil layer, the shortwave and longwave radiation. The specific heat at constant pressure and latent heat of condensation are denoted as c_p and L_v, respectively. Furthermore, C_h and C_q are the transfer coefficients for heat and water vapor, g_s is the canopy conductivity that depends on the maximal evaporative conductivity, in-

solation, water vapor deficit, air temperature, and soil wetness factor, f (e.g., Deardorff 1978). The dimensionless drag and transfer coefficients, C_d, C_h, and C_q, read for stable conditions

$$\begin{Bmatrix} C_h \\ C_q \end{Bmatrix} = \begin{Bmatrix} 1 / (C_d^{1/2}B_h^{-1} + 1) \\ 1 / (C_d^{1/2}B_q^{-1} + 1) \end{Bmatrix} C_d \quad (5)$$

and for unstable conditions

$$\begin{Bmatrix} C_h \\ C_q \end{Bmatrix} = \begin{Bmatrix} 1/(C_d^{1/2}B_h^{-1} + F_m^{-1/2}) \\ 1/(C_d^{1/2}B_q^{-1} + F_m^{-1/2}) \end{Bmatrix} C_d \quad (6)$$

(Mölders 1998), where the drag coefficient for momentum is given by

$$C_d = \kappa^2 F_m / (\ln (z_r/z_0) \ln (z_r/z_0)) . \quad (7)$$

Herein, the B_h^{-1} and B_q^{-1} are the sublayer-*Stanton* numbers for heat and moisture which, in the present study, are calculated according to Garratt and Hicks (1973) by

$$B_h^{-1} = 1/\kappa \ln(z_0/z_{0h}) \quad (8)$$

and

$$B_q^{-1} = 1/\kappa \ln(z_0/z_{0q}) . \quad (9)$$

Note that Kramm et al. (1996) give a detailed discussion on determining sublayer-*Stanton* numbers for heat and matter. The roughness length for heat z_{0h} and moisture z_{0q} are given by (Brussart 1975, Hicks 1985, Eppel et al. 1995)

$$z_{0q} = \begin{cases} z_0/\exp(2.3) & \text{vegetation} \\ z_0/\exp(36.34(u_*z_0)^{1/4}-2) & \text{elsewhere,} \end{cases} \quad (10)$$

$$z_{0h} = \begin{cases} z_0/\exp(2.3) & \text{vegetation} \\ z_0/\exp(39.53(u_*z_0)^{1/4}-2) & \text{elsewhere.} \end{cases} \quad (11)$$

Here, the roughness-length z_0 depends on the land-use for vegetative, urban or bare surfaces. Furthermore, the stability functions $F_{m,h,q}$ are given by the parametric model of Kramm et al. (1995)

81

$$F_m = \begin{cases} (1 - \gamma_1 Ri_b)^2 & Ri_{cr} \geq Ri_b > 0 \\ (1 - \gamma_2 Ri)^{1/2} & Ri < 0 \end{cases}$$

$$(12)$$

$$F_h = \begin{cases} F_m & Ri_{cr} \geq Ri_b > 0 \\ F_m^{3/2} & Ri < 0 \end{cases}$$

$$(13)$$

which is based on the *Monin-Obukhov* similarity theory. Here, Ri, Ri_b and Ri_{cr} are the *Richardson* number, the bulk-*Richardson* number, and the critical *Richardson* number, respectively. Furthermore, $\gamma_1 = \gamma_3 \approx 5$, $\gamma_2 = \gamma_4 \approx 16$ and $F_q = F_h$ are assumed (e.g., Garratt, 1992). Note that Kramm et al. (1995; their Fig. 1) showed that this parameterization of the stability functions is exactly the analytical solution in the stable case and it matches more closely the analytical solution than that of Louis (1979) in the unstable case.

The coupling to the jth atmospheric grid cell is realized by arithmetically averaging the individual subgrid cell fluxes and quantities of states, $F_{m,j}^k$, to provide the grid cell values

$$F_j^k = \frac{1}{N} \sum_{m=1}^{N} F_{m,j}^k \quad , \quad (14)$$

where the index k stands for the fluxes and the quantities of state (L_vE, H, G, Q, f, T_g, Θ, q).

A fundamental assumption of this strategy is that the subgrid-scale near-surface meteorological forcing, which is experienced by the surface, is important in determining the net exchange of heat, moisture and momentum at the interface earth-atmosphere (Mölders et al. 1996). This means that no interaction between the different landuse types exists. Since in the explicit subgrid strategy, the grid cells of the atmospheric model are explicitly broken down, the spatial location of each subgrid flux is known (Fig. 1).

Like in Seth et al. (1994) the average grid cell values of wind speed and surface pressure are used for all subgrid cells. This means that the explicit subgrid

scheme ignores subgrid-scale dynamical effects related to the surface heterogeneity, for instance, directed flows caused by topography or lake-breeze effects. Moreover, it also neglects advective effects accompanied by occasionally observed internal boundary layers (e.g., Raabe 1983, 1991, Garratt 1992, Hupfer and Raabe 1994) and interaction between the energy budgets of the different landuse types.
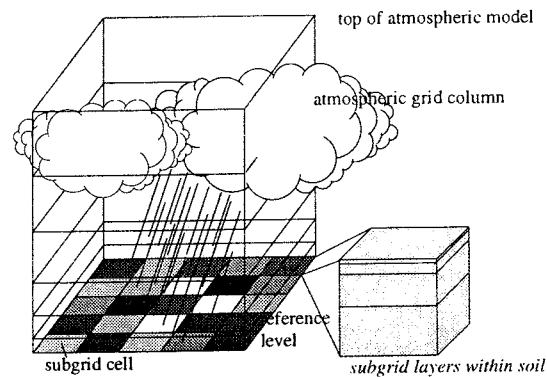

Fig. 1. Schematic view of the explicit subgrid scheme (modified after Mölders et al. 1999).

3. Design of the study

Numerical experiments were carried out using a mesoscale β meteorological model (GESIMA; see Kapitza and Eppel 1992, Eppel et al. 1995), where the same surface exchange and turbulence parameterization schemes are embedded into the strategies mentioned above to ensure that differences in the results are only affected by these different strategies. Moreover, simulations using the explicit subgrid-scheme with and without lakes were carried out to elaborate the effect of subgrid-scale lakes alone. In doing so, subgrid-scale water reservoirs were added that totally amount to 417 km². All three simulations were performed for Northern Saxony and Southern Brandenburg (see Mölders 1998, her Fig. 1 for land-use distribution of the model domain) for a typical day in spring.

The temperature and moisture states in the system earth-atmosphere evolve by fluxes which themselves depend on those states. The resultant non-linear dynamical system has modes of variability and statis-

tical signatures that depend on the inter-actions of the energy and water budget (Entekhabi and Brubaker 1995). To evaluate the statistical behavior of the effects of the strategies, frequency distributions of the model state quantities, the water and energy fluxes as well as the cloud and pre-cipitating particles were determined for the entire simulation time on the basis of the hourly data provided by each of the three simulations.

4. Results

4.1 General aspects of lakes

In spring and early summer, water surface temperatures are cooler than the surface temperatures of the surrounding land dur-ing the daytime. Note that the opposite is true at night as well as in autumn and early winter. The aforementioned discrepancy leads to a stabilization by day and a labili-zation by night. During the night, the addi-tional warm water-surfaces result in greater vertical components of the wind-vector than those obtained over the cultivated land at the same place in the reference land-scape (= landscape without additional lakes). At daytime, the vertical component is reduced in those grid-cells where lakes exists as compared to the same locations in the landscape without additional lakes.
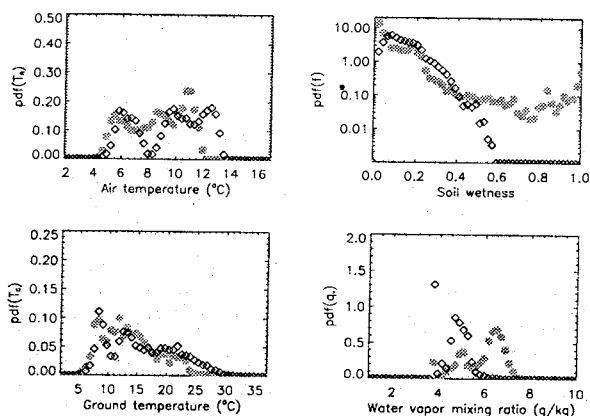

Fig. 2. Comparison of the probability density functions of near-surface air temperatures, soil wetness, ground temperatures and wa-ter vapor mixing ratios (upper left to lower right) as obtained by the simulation with the strategy of dominant land-use (grey dots) and the explicit subgrid scheme (= simulation without additional lakes; dia-monds).

In addition to different energetic and hydrological behavior, the surface characteristics of land and water differ in roughness and terrain-elevation. These differences may affect vertical mixing and the stability of the atmospheric boundary layer (ABL). Thus, besides the differenting evaporation from lakes, lakes may modify evapotranspiration at their lee-side borders by the altered micrometeorological condi-tions (wind, temperature, humidity, etc.) of the air mass that passed over the water. Note that moisture convergence may be significantly altered by the lower aerody-namical roughness of the water than land if the lake is of sufficient size (cf. Figs. 3, 10 in Mölders 1999b).

4.2 The effect of subgrid scale hetero-geneity

The probability of higher values of near-surface air temperatures and surface tem-peratures will increase if subgrid-scale surface heterogeneity is included (Fig. 2). Moreover, the probability for high wind speeds grows when considering subgrid-scale surface heterogeneity. Although locally large differences in the vertical wind component occur between the simu-lations with and without consideration of subgrid-scale heterogeneity, the distribu-tion of the probability density function of vertical velocity hardly changes. Consid-eration of subgrid-scale surface heteroge-neity results in a shift towards an increased probability for lower evapotranspiration (Figs. 3, 4), near-surface humidity (Fig. 2), mixing ratios of cloud water, rainwater and ice, precipitation rates as well as soil wet-ness (Fig. 2).

The probability of lower net radia-tion and lower soil heat fluxes increases when subgrid-scale surface heterogeneity is taken into account. The spatial and tempo-ral variability of latent heat fluxes rises due to heterogeneity. The joint probability density function calculated for the results with heterogeneity are skewed to larger sensible and lower latent heat fluxes as compared to those obtained by the simula-tion with the strategy of dominant land-use (Figs. 3, 4). The reasons are manifold. As

mentioned before, the soils are drier when heterogeneity is considered. Dry soils are associated with larger Bowen ratios (Figs. 3, 4). Usually, rising air temperatures lead to an increase in potential evapotranspiration. However, in both the simulations the potential evapotranspiration is not achieved and the actual evapotranspiration is even lower for the simulation with consideration of subgrid-scale heterogeneity than without.
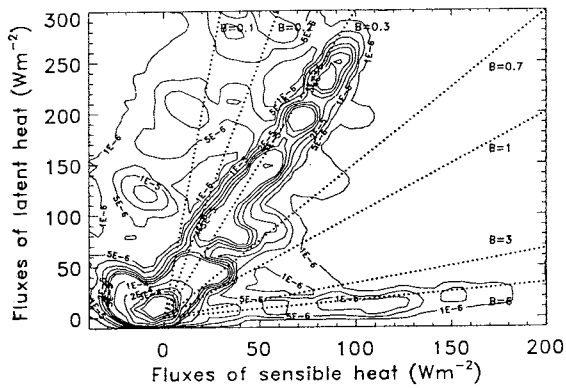

Fig. 3. Isolines of joint probability density functions for the surface fluxes of latent and sensible heat in the simulation using the strategy of dominant land-use. Lines of constant Bowen ratios are superimposed.
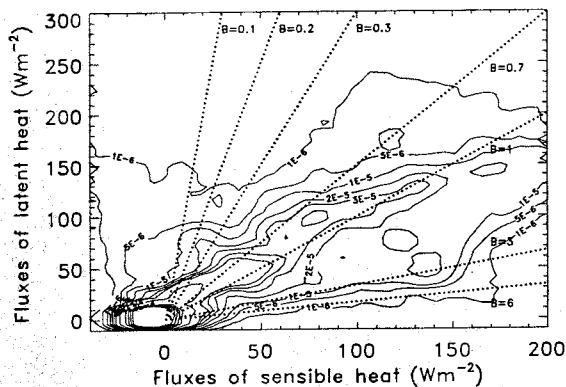

Fig. 4. Like Fig. 3, but for the simulation using the explicit subgrid scheme (= simulation without additional lakes).

4.3 Lake effects

This subsection illustrates the influence of additional lakes on energy and water fluxes. The probability density functions of surface temperature shift towards slightly lower values when lakes are added into the landscape. This change leads to similar behavior in the air temperatures (Fig. 5). Therefore, additional lakes result in both

significantly lower latent and sensible heat-fluxes as compared to the reference land-scape (see also Figs. 4, 6) to the benefit of the heat-fluxes in the diurnal course. Humidity is slightly reduced over the additional lakes during the daytime, because the lakes provide significantly less water to the atmosphere than the same areas in the reference landscape. Thus, the probability density functions of specific humidity shift towards lower values for the simulation with lakes than that without (Fig. 5). A further reason is that the water surfaces slightly cool the overlying air and the downwind surroundings of the waters. This effect reduces the water-vapor deficit. During the night, humidity increases (up to 0.3 g/kg) over the additional lakes and their environs due to the, on average, apprecia-bly warmer air (0.3 K and more) of the lower ABL than in the landscape without these additional lakes (see also Mölders 1998).
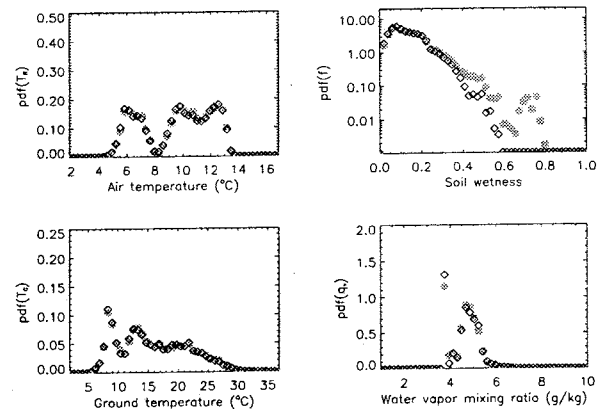

Fig. 5. Like Fig. 2, but for the simulation with (grey dots) and without additional lakes (diamonds).
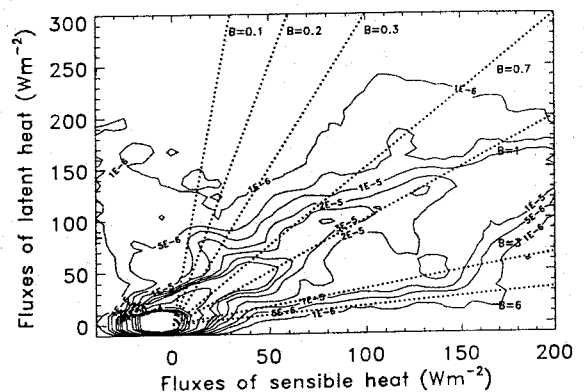

Fig. 6. Like Fig. 3, but for the simulation with additional lakes.

As a consequence of the reduced water supply to the atmosphere, cloudiness over the lakes during the daytime decreases in the simulations including additional lakes. The opposite is true at night. Furthermore, herein, the probability density functions shift towards lower as well as slightly higher mixing ratios of cloud water, rainwater, and ice as compared to the simulation without additional lakes. This means that the distribution of these quantities becomes wider with than without additional lakes. The presence of the lakes increases the domain-averaged 24h-accumulated precipitation from 1.3 mm to 1.7 mm.

The altered distributions of the probability density functions of cloud and precipitating particles and their varying times of development may be explained as follows: As compared to the reference landscape, the stabilization retards cloud and precipitation formation over the additional lakes during the morning and early afternoon. This means that, here, precipitating particles form much later in the afternoon than in the reference landscape. At that time, the evaporation from lakes exceeds the evapotranspiration taking place at these areas in the reference landscape. This higher water supply leads to higher precipitation rates in the late afternoon for the simulation that includes additional lakes. Note that, in both landscapes, the formation of precipitation particles starts at nearly the same time in the regions far away from the land-use changes. As a secondary effect, differences in advection of heat and humidity lead to further differences in the water and energy fluxes.

In the simulation with additional lakes, the lower air temperatures reduce the evapotranspiration until the early afternoon as compared to the simulation with the reference landscape. Therefore, the soil-wetness-factors increase downwind of the additional lakes as compared to those obtained by the simulation with the reference landscape. As a consequence of the higher precipitation rates in the simulation with additional lakes, soil-wetness increases in the late afternoon.

In summary, the additional lakes strongly affect the water-cycle in their environs. The presence of lakes retards precipitation formation in spring. In the late afternoon, when precipitation starts to reach the ground, the incoming energy is already low. Hence, in a landscape with lakes, precipitation contributes more to infiltration and runoff than to evapotranspiration.

5. Conclusions

The results substantiate that neglecting of lake effects, for instance by the strategy of dominant land-use, may provide inadequate results. Moreover, the results illustrate that even subgrid-scale small lakes may affect water and energy fluxes, the variables of state as well as cloud and precipitation formation. Considering these findings, it may be concluded that parameterizations of lake effects have to be further developed and included in meso-scale meteorological models. The approaches used in these parameterizations, of course, have to be evaluated by field experiments. Moreover, the performance of these parameterizations should also be evaluated indirectly by evaluating the overall performance of the model with inclusion of lake effects.

Acknowledgments

References

Brussart, H.W., 1975. The roughness-length for water vapor, sensible heat and other scalars. *J. Atmos. Sci.* **32**, 2028-2031.

Burman, R., L.O. Pochop, 1994. *Evaporation, evapotranspiration and climatic data.* Developments in Atmospheric Sciences 22, Elsevier, Amsterdam, Lausanne, New York, Oxford, Shannon, Tokyo, pp. 278.

Deardorff, J.W., 1978. Efficient prediction of ground surface temperature and moisture, with

inclusion of a layer of vegetation. *J. Geophys. Res.* **84C**, 1889-1903.

Entekhabi, D., K.L. Brubaker, 1995. An analytical approach to modeling land-atmosphere interaction. 2. Stochastic formulation. *Water Resource Res.* **31**, 633-643.

Eppel, D.P., H. Kapitza, M. Claussen, D. Jacob, W. Koch, L. Levkov, H.-T. Mengelkamp, N. Werrmann, 1995. The non-hydrostatic mesoscale model GESIMA. Part II: Parameterizations and applications. *Contrib. Atmos. Phys.* **68**, 15-41.

Garratt, J.R., 1992. The internal boundary layer - a review. *Boundary Layer Meteorol.* **50**, 171-203.

Garrat, J.R., B.B. Hicks, 1973. Momentum, heat and water vapour transfer to and from natural and artificial surfaces. *Quart. J. Roy. Meteor. Soc.* **99**, 680-687.

Hicks, B.B., 1985. Applications of forest-atmosphere turbulent exchange information. In: Hutchison, B.A., B.B. Hicks (eds.) *The Forest-Atmosphere Interaction*, 631-644.

Hupfer, P. A. Raabe, 1994. Meteorological transition between land and sea in the microscale. *Meteorol. Zeitsch.* **44**, 100-103.

Kapitza, H., D.P. Eppel, 1992: The non-hydrostatic mesoscale model GESIMA. Part I: Dynamical equations and tests. *Contr. Phys. Atmos.* **65**, 129-146.

Kramm, G., R. Dlugi, G.J. Dollard, T. Foken, N. Mölders, H. Müller, W. Seiler, H. Sievering, 1995. On the dry deposition of ozone and reactive nitrogen compounds. *Atmos. Environ.* **29**, 3209-3231.

Kramm, G., T. Foken, N. Mölders, H. Müller, K.T. Paw U, 1996. On the determination of the sublayer Stanton numbers of heat and matter for different types of surfaces. *Contrib. Atmos. Phys.* **69**, 417-430.

Kramm, G., T. Foken, 1998. Uncertainty analysis on the evaporation at the sea surface. *BALTEX Publ.* **11**, 113-114.

Louis, J.-F., 1979. A parametric model of vertical eddy fluxes in the atmosphere. *Boundary Layer Met.* **17**, 187-202.

Mölders, N., A. Raabe, 1996. Numerical investigations on the influence of subgrid-scale surface heterogeneity on evapotranspiration and cloud processes. *J. Appl. Meteor.* **35**, 782-795.

Mölders, N., A. Raabe, G. Tetzlaff, 1996. A comparison of two strategies on land surface heterogeneity used in a mesoscale β meteorological model. *Tellus* **48A**, 733-749.

Mölders, N., 1998. Landscape changes over a region in East Germany and their impact upon the processes of its atmospheric water-cycle. *Meteor. Atmos. Phys.* **68**, 79-98.

Mölders, N., 1999a. Einfache und akkumulierte Landnutzungsänderungen und ihre Auswirkungen auf Evapotranspiration, Wolken- und Niederschlagsbildung. Wis. Mitt. Leipzig, **15** (Habil.Schrift).

Mölders, N., 1999b. On the effects of different flooding stages of the Odra and different land-use types on the local distributions of evapotranspiration, cloudiness and rainfall in the Brandenburg-Polish border area. *Contrib. Atmos. Phys.* **72**, 1-24.

Mölders, N., Raabe, A., Beckmann, T, 1999. A technique to downscale meteorological quantities for the use in hydrologic models - Description and first results. *IAHS Publ.* **254**, 89-98.

Raabe, A., 1983. On the relation between the drag coefficient and fetch above the sea in the case of off shore wind in the near-shore zone. *Z. Meteor.* **6**, 363-367.

Raabe, A., 1991. Die Höhe der internen Grenzschicht. *Z. Meteor.* **41**, 251-261.

Reichardt, H., 1951. Vollständige Darstellung der turbulenten Geschwindigkeitsverteilung in glatten Rohren. *Z. angewandte Mech.* **31**, 4188-4191.

Seth, A., F. Giorgi, R.E. Dickinson, 1994. Simulating fluxes from heterogeneous land surfaces: explicit subgrid method employing the biosphere-atmosphere transfer scheme (BATS). *J. Geophys. Res.* **99D**, 18651-18667.

Sheppard, P.A., 1958. Transfer across the Earth's surface and through the air above. *Quart. J. Roy. Meteor. Soc.* **84**, 205-244.

BASIS and air-ice coupling

Jouko Launiainen, Cheng Bin, Juha Uotila and Timo Vihma
Finnish Institute of Marine Research, Box 33, FIN-00931 Helsinki

1. Introduction

The Baltic-Air-Sea Ice Study (BALTEX-BASIS) is a sub-project of BALTEX. The overall objective of BASIS is

- to create and analyse an experimental data set for optimization and verification of coupled atmosphere-ice-ocean models.

BASIS is carried out as an EC funded project by Finnish, Swedish and German institutes[1]. The main experimental campaign was carried out in February-March 1998 (Launiainen, 1999).
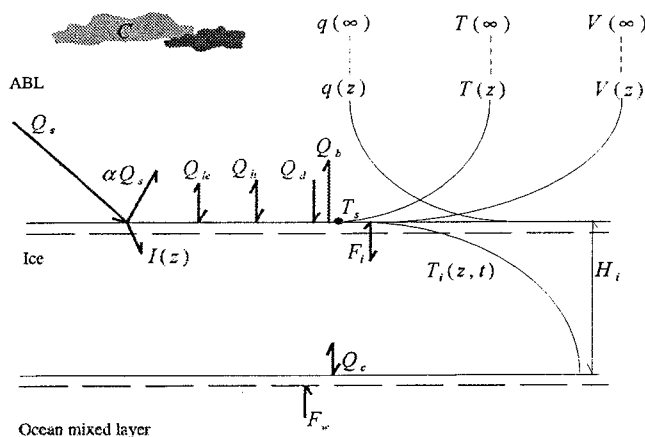
Air-ice-ocean coupling and modelling are important goals of the project. In the air-ice coupling, the primary quantities to be studied include the air-ice interfacial (surface) temperature, the fluxes of momentum, heat and water vapour (latent heat), and, the radiative fluxes. In this report, we introduce FIMR process studies of air-ice-ocean coupling and a few preliminary results based on the measurements carried out at the RV Aranda Ice Station during BASIS.

2. Measurements

The measurements focused on the air-ice coupling studies included direct eddy flux (sonic anemometer) measurements of momentum and sensible heat, and of wind and temperature measurements in a meteorological profile mast. The latter measurements allow us to calculate the fluxes of momentum and sensible heat, for comparison with the eddy flux observed results, by using the so-called gradient or level difference method based on the Monin-Obukhov similarity theory. No eddy flux or gradient measurements were made for determination of water vapour or latent heat flux. For this case, we will estimate that by using a single-level measurement of relative air humidity and an indirect "synthetic" method. In addition, various radiation fluxes were measured and in-ice/snow temperature measurements were collected by an ice temperature logging stick. Finally, water-ice fluxes of heat, momentum and salt were measured (by University of Hokkaido, Japan) with various eddy flux equipments below the ice. The varius observations are introduced in the BASIS Data Report (Launiainen, 1999).

ABL

$q(\infty)$ $T(\infty)$ $V(\infty)$

$q(z)$ $T(z)$ $V(z)$

Q_s

αQ_s Q_{le} Q_h Q_d Q_b

T_s

Ice $I(z)$ F_i

$T_i(z,t)$ H_i

Q_c

Ocean mixed layer F_w

ABL
Short-wave (Q_s, I) and long-wave (Q_d, Q_b) rad. fluxes

Turbulent fluxes of momentum, sensible heat (Q_h) and
latent heat (Q_{le})

Monin-Obukhov similarity

Surface heat balance and T_s *to be controlled by it*

ICE
Heat conduction (F_i)in snow and ice
Short-wave penetration ($q(z,t)$) in snow and ice

OBL
Heat flux (F_w) from ocean

Figure 1. Coupled FIMR 1D thermodynamic Air-Ice-Ocean Model.

3. Coupled model

For local process studies a one-dimensional coupled thermodynamic air-ice-ocean model (Launiainen and Cheng, 1998) is used. A schematic presentation of the model is given in Fig. 1.

The ice model has 10 to 30 layers in snow and ice totally, and the time step may be from 10 s upwards. Air and snow/ice are fully coupled in each time step calculation. The input data read: wind speed, temperature and moisture from any level (arbitrary and mutually different, if necessary) in the constant flux layer, say below 50 m, and short-wave radiation. If radiation data are not available, those will be calculated by standard formulae in the model. In addition, the initial ice thickness and snow thickness are given. The output data read:
- air-ice fluxes and atmospheric stratification
- atmospheric profiles of wind, temperature and moisture. The model can e.g. produce a surface layer inversion under negative surface radiation balance.

- ice thickness and in-ice temperature in various depths in ice.

As a module, the ice model has been coupled with a mesoscale atmospheric model.

In BASIS studies, the ice model was applied to and compared with measurements made from RV Aranda Ice Station.

4. Results

Fig. 2 gives the time series of the sensible heat flux derived by various methods. The direct eddy flux results are compared with results of the profile method and with the fluxes calculated by the coupled ice model. All the meteorological input data for the ice model were taken from a single-level data from the meteorological mast, and the three methods are in practice independent. In general, the agreement is good and the results are very promising. As to the momentum flux, not shown here, the various methods agree (surprisingly) well also. In this connection, we want to

emphasize that the wind and temperature sensors in the mast were (and have to be) especially carefully calibrated, for the level difference profile method which tends to be very liable to errors, peaks etc. However, the good general coherence of the level difference and ice model results with the eddy flux results supports to the overall validity of the Monin-Obukhov similarity theory.

As an example of the air-ice interaction characteristics, Fig. 3 gives the neutral drag coefficient $C_{DN}(10)$ as a function of the wind speed, as calculated from the basis of the sonic anemometer data in the Ice Station. The results show a drag coefficient of 1.2×10^{-3} in those conditions over a rather smooth sea ice in the Ice Station.

Fig. 4 shows a comparison of the time series of the observed and model estimated in-ice temperatures for the BASIS Ice Station data set. The comparison shows a rather good general agreement. The above justifies a good overall relevancy of the ice model construction and parameterizations and indicates its potential for process studies.

Finally, we may note that the above discussion is related to a local one-dimensional approach, strictly. In nature, a sea ice field usually consists of a mosaic of open water and ice floes of various thickness, and the field is therefore heterogeneous with respect to the surface temperature and roughness. Spatial averaging is therefore necessary to estimate regionally representative air-sea-ice fluxes, and several possibilities are available for the parameterization of them (Vihma, 1995). For the purpose, the FIMR thermodynamic model is coupled as a module with a mesoscale atmospheric model.

References:

Launiainen, J. and Cheng, B., Modelling of ice thermodynamics in natural water bodies. - Cold regions science and technology 27:153-178, 1998.

Launiainen, J. (Ed.): BALTEX-BASIS, BASIS-98 Data Report, International BALTEX Secretariat, Publication No. 14, 92 pp., 1999.

Vihma, T., Subgrid parameterization of surface heat and momentum fluxes over polar oceans, J. Geophys. Res., 100, 22 625-22 646, 1995.
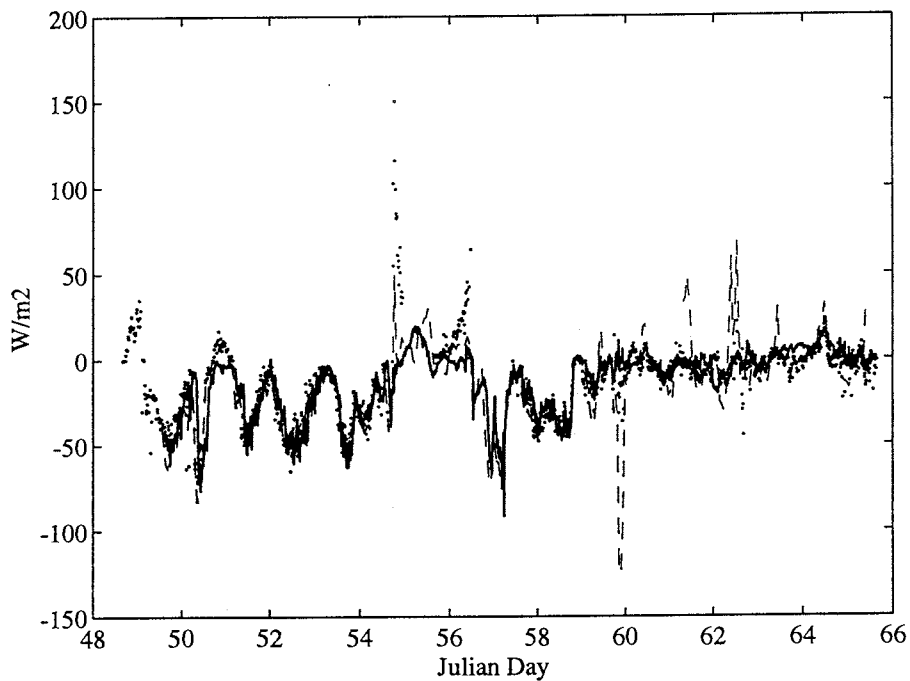
Figure 2. Sensible heat flux at Aranda Ice Station during BASIS as: measured by the sonic anemometer (dotted; 10 min values), calculated by profile the level-difference profile method (broken; hourly means) and, calculated by the coupled air-ice-ocean model (continuos; 10 min values).
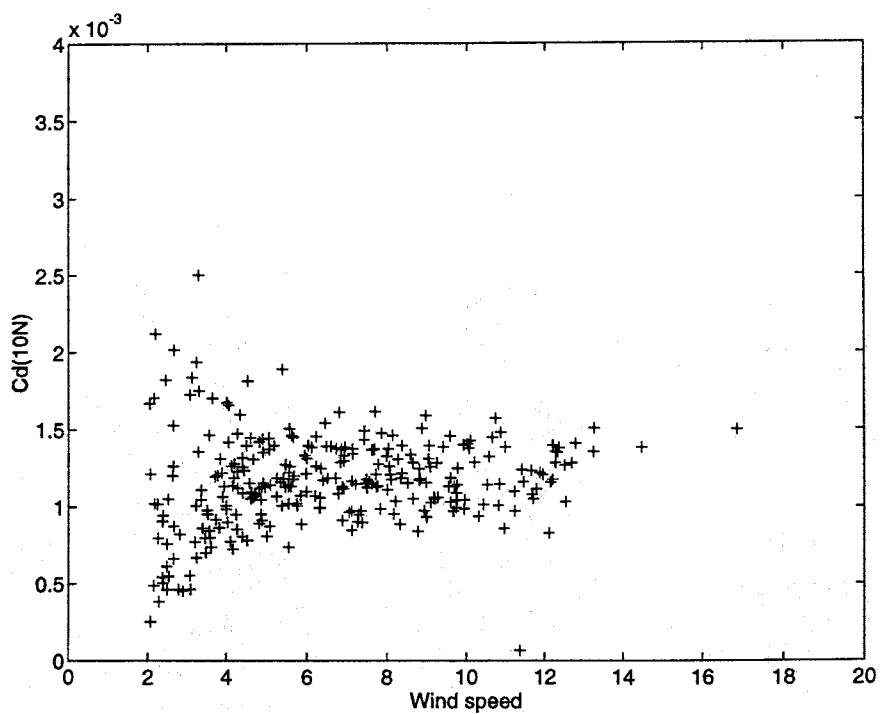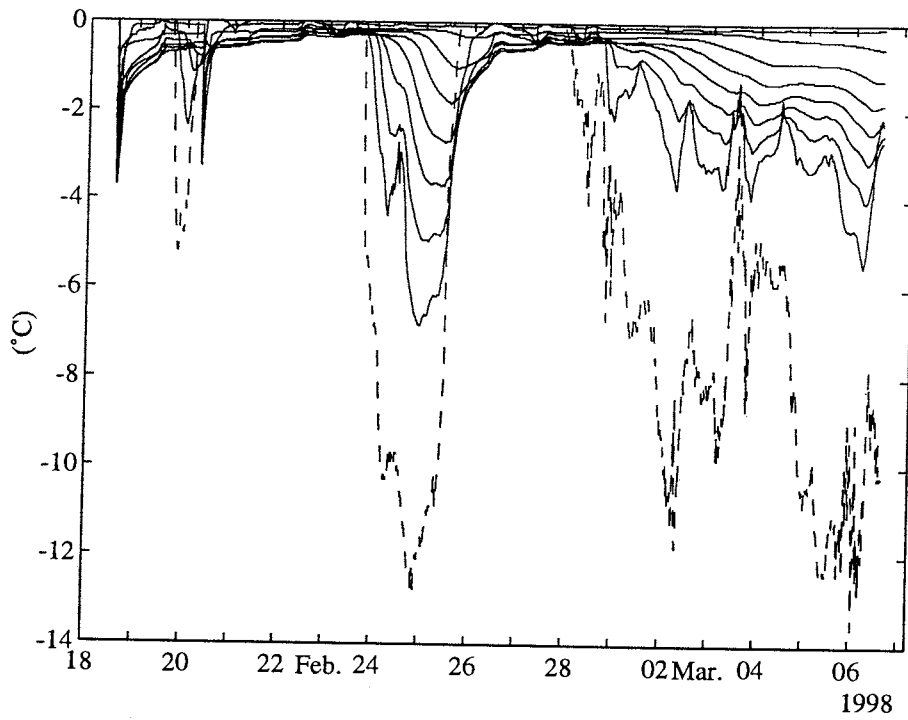Upward flux is positive.

Figure 3. Eddy flux measurements derived drag coefficient $C_{DN}(10)$ as a function of wind speed (m/s) at the Aranda Ice Station.
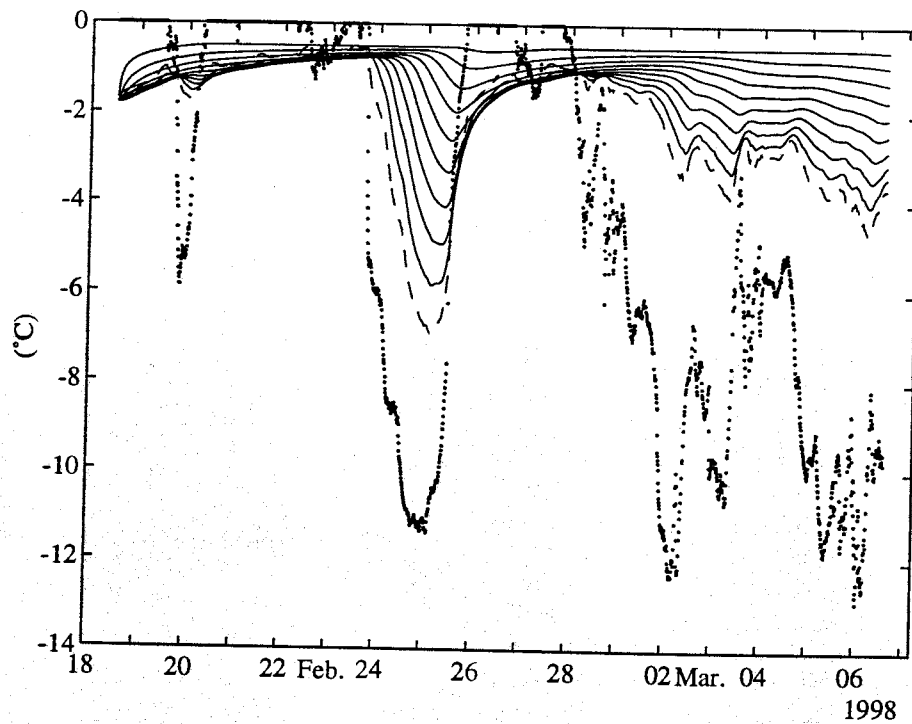
90

a)

b)

Figure 4. In-ice temperatures during BASIS:

    a) Air temperature (broken) and the observed temperatures in various depths (approx. 5 cm vertical intervals) in ice. The mean total ice thickness was 35 cm.

    b) Calculated temperatures by the coupled model. Dotted line gives the air-snow interface (i.e. surface) temperature. Dotted line is the snow-ice interface temperature and the continuos lines give in-ice temperatures in various depths.

Observation and modeling of surface fluxes over sea

Anna Rutgersson[1]

Department of Earth Sciences, Meteorology, University of Uppsala, Sweden.

Abstract. In this study direct measurements of latent heat flux at two sites within the Baltic Sea are compared with estimates using two different models. The models are the regional scale atmospheric model HIRLAM and the ocean model PROBE-Baltic. It is shown that both models clearly overestimates the latent heat flux. This overestimation can to a large extent be explained by errors in sea surface temperature and surface humidity. The flux calculation in the models are very sensitive to errors in mean parameters. The large deviations between models and measurements show the importance of verifying flux estimates from models.

1. Introduction

The water balance of the Baltic Sea is one main concern in the BALTEX research program (BALTEX, 1995). The balance is controlled by the net precipitation (precipitation minus evaporation), the river runoff and the in- and outflows through the Baltic Sea entrance area. The probably most unknown component of the water balance is the net precipitation, which has often been regarded as a residual term or has been neglected in the water balance. The project PEP in BALTEX (Pilot study of Precipitation and Evaporation in BALTEX) is investigating this problem using measurements and models for estimating precipitation and evaporation over the Baltic Sea. In *Omstedt and Rutgersson* [1999] the net precipitation differs by a factor of two when determined by different methods. Precipitation is probably the most uncertain parameter in the net precipitation, but also evaporation (or latent heat flux) is determined with great uncertainty. It is difficult to cover large areas with direct measurements, so latent heat flux needs to be determined either by measuring mean parameters at coastal stations or ships or by using models. It would appear easier to model surface fluxes over sea than over land due to less heterogeneity. But there are some

factors complicating the situation over sea:

- There are few measurements of mean parameters for verification of methods and also few flux studies, so theories are mostly developed over land areas.

- Sea surface temperature is often determined with great uncertainty.

- The lower boundary varies in time (waves and ice).

- Coastal problems, for example local circulation systems due to large horizontal gradients in roughness and temperature.

In this work the last two points will not be considered, but they are important factors for further studies. For the two first items coupled models could be a part of the solution of the problem and work is progressing in the area (*Gustafsson et al.* [1998] and *Hagedorn et al.* [1998]), but it is still of crucial importance to know that the models are describing correct fluxes. A comparison between measured and modeled sensible heat and momentum fluxes using the regional scale model HIRLAM was performed in *Rutgersson* [1999], showing a certain overestimation of both sensible heat and momentum flux in the model.

Few previous studies have been performed of the latent heat flux over the Baltic Sea. In *Gustafsson et al.* [1998] it was found that HIRLAM gives a too large latent heat flux.

[1]Currently at the Swedish Meteorological and Hydrological Institute (SMHI), SE-601 76 Norrköping, Sweden. (e-mail: Anna.Rutgersson@smhi.se)
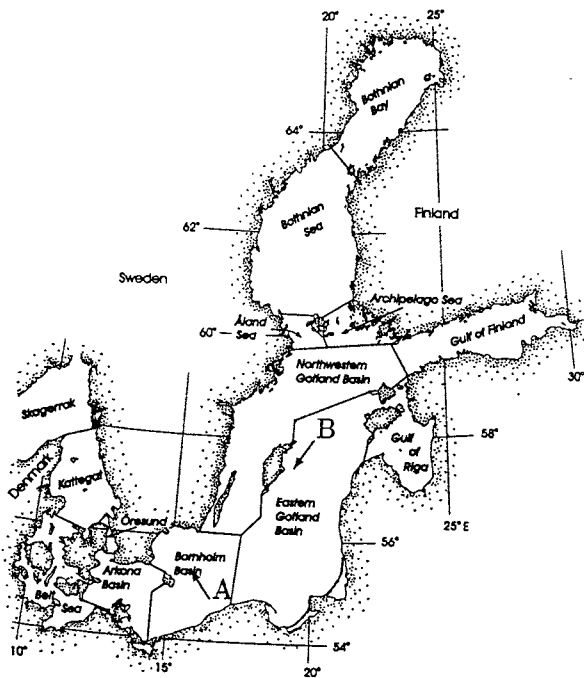
Figure 1. Map of the subbasins, *A* and *B* are the measuring sites.

Isemer and Lindau [1998] used voluntary ships for long-term estimates of evaporation and precipitation.

In this study, direct flux measurements of latent heat over the sea are compared with the fluxes given by two different models, one atmospheric model and one ocean model. The sensitivity of the models due to errors in mean parameters is also investigated. It should be noted that the model are not independent since atmospheric information from the HIRLAM model is used as input to the ocean model.

2. Measurements

Two measuring sites within the Baltic Sea have been used. A small island north of Bornholm, Christiansö, *A* on the map in Figure 1 and an island east of Gotland, Östergarnsholm, *B* on the map.

2.1. The Christiansö site

At site A, Christiansö, a 10 m high mast has been erected on a very small is-

land near the main island Christiansö. The mast is instrumented with a SOLENT sonic anemometer and an Ophir open path instrument for measuring humidity fluctuations. The site is exposed to winds from the approximate sector $120^\circ - 300^\circ$ over south. For the sector $180 - 270^\circ$ the winds have passed Bornholm which is ~ 20 km away. This can to some extent disturb the measurements, but Bornholm is a small island, and this is not expected to have very large influence. Synoptic data are taken at Christiansö Fyr some hundred meters from the site and sea surface temperature is measured in the waters outside the island.

2.2. The Östergarnsholm site

Site B, Östergarnsholm, is a small very flat island 4 km east of Gotland. A 30 meter tower has been raised at the southern tip of the island. The sector 60-220 degrees has more than 150 km of undisturbed upwind fetch. The instrumentation and measuring site are described with more details in *Smedman et al.* [1999].

Turbulent fluxes are determined using two different methods. For a short period the high quality MiUU-instrument was used giving reliable measurements. During May and October some measurements of relatively high quality was obtained using a LiCOR system [*Grelle and Lindroth*, 1996]. Only data from these periods have been used in this study.

3. Models

3.1. HIRLAM

The HIRLAM forecast model is a 3-dimensional limited area model covering the northern part of Europe. A detailed description of the model can be found in *Källén* [1996]. HIRLAM is based on the primitive equations with horizontal velocity components, temperature, humidity and surface pressure as prognostic variables. In the present study data from the HIRLAM version used operationally at SMHI have

been used. The horizontal resolution for the data is (22 × 22) km and in the vertical 31 levels are used. The vertical diffusion scheme is based on non-local first order turbulent closure. The surface turbulent fluxes are determined from mean model parameters using a bulk formulation:

$$\tau = \rho C_D u_z^2$$

$$H = \rho c_p C_H u_z (\theta_s - \theta_z) \qquad (1)$$

$$E = \rho C_E u_z (q_s - q_z)$$

τ, H and E describe the vertical turbulent fluxes of momentum, sensible and latent heat, ρ is the air density and c_p the specific heat capacity of air. u_z, θ_z and q_z are mean wind, potential temperature and humidity at level z and θ_s and q_s are the potential temperature and humidity at the surface. C_D, C_H and C_E are the transfer coefficients for momentum, sensible and latent heat. The transfer coefficients are described in *Louis* [1979] and *Louis et al.* [1982]. For sea surface temperature (SST) and ice cover rather sparse measurements from the Baltic Sea are used in combination with satellite data.

For the comparison the HIRLAM 100 % sea grid point closest to each site is used.

3.2. PROBE-Baltic

The PROBE-Baltic ocean model [*Omstedt and Nyberg*, 1996] is a basin model for the Baltic Sea. The model is divided into 13 sub-basins (Figure 1) and as meteorological input to the model, data from HIRLAM is used with a time resolution of three hours. River runoff as observed monthly means is included and the model calculates the horizontal mean properties of e g sea surface temperature, ice concentration and thickness in each sub-basin. The turbulent fluxes are calculated from a bulk formulation, Equation (1). The neutral transfer coefficient for momentum are described in *WAMDI* [1988]. The bulk transfer coefficients C_H and C_E are revised from the original PROBE-Baltic scheme, using
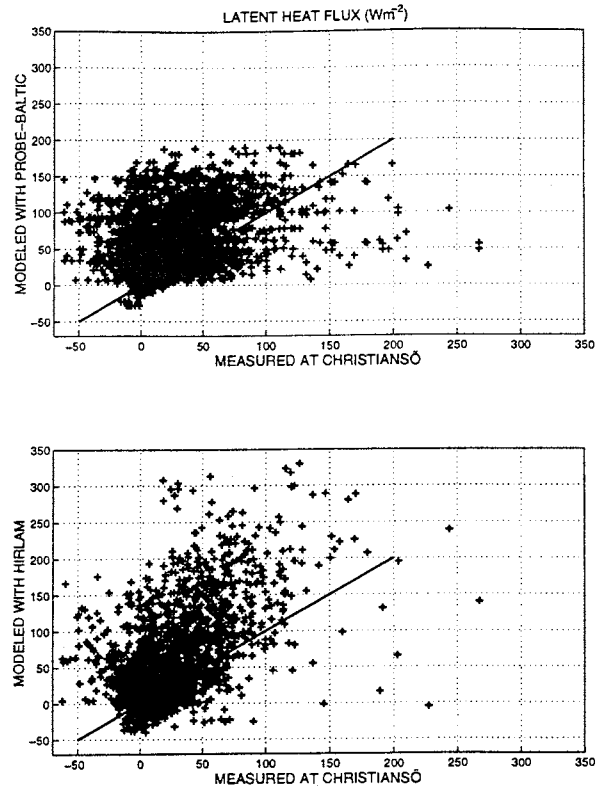

Figure 2. Latent heat flux in (Wm^{-2}) for the period May 1998 to December 1998. Crosses are the data and solid line the one to one relation. Measurements are compared with (a) the PROBE-Baltic model and (b) the HIRLAM model.

DeCosmo et al. [1996] for the neutral values. A simplified version of the scheme described in *Launiainen* [1995] is used for the stability functions. The main difference to the scheme described in *Launiainen* [1995] is the description of the roughness length which in the present model is a function of the neutral values of the transfer coefficients.

For the comparison with data the Bornholm Basin is used for Site A and Eastern Gotland Basin for Site B. Only data when both measurements and models have undisturbed winds from the sea sector are used (120-300° resp 60-220°).
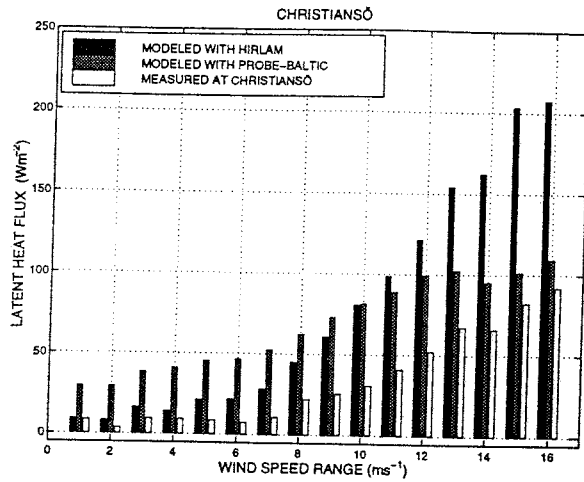
94

Figure 3. Latent heat flux in (Wm^{-2}) divided into wind speed ranges. Data are from Christiansö for the period May 1998 to December 1998. Note that there are rather few data for the highest wind speed range.

4. Results

4.1. Comparison

In Figure 2a the measured latent heat flux at Christiansö and the modeled flux with PROBE-Baltic can be seen, and in Figure 2b fluxes measured and modeled with HIRLAM. Both models show a great scatter and overestimate the latent heat flux. In Figure 3 the data are divided into measured wind speed ranges and the latent heat flux is averaged for each range. It can be seen that PROBE-Baltic generally overestimates for all ranges whereas the overestimation in HIRLAM is more pronounced for higher wind speeds.

From Figures 2 and 3 and also Table 1 where some statistics of the fluxes can be seen it is clear that both the models overestimate latent heat flux for this site and this period. The difference between measurements and models can be explained by several factors, some will be discusse in the next Section.

Table 1. Statistics for the different parameters at Christiansö. Number of data is denoted n, r_0 is the correlation coefficient, *bias* is mean difference and *rms* the root-mean-square error. U and T are measured at 10 m, q at 2 m. In PROBE-Balitc U representing 10 m and T and q for 2 meters are used. In HIRLAM all parameters are recalculated to 10 m.

	PROBE-Baltic	HIRLAM
U_{10} (m/s) $n = 2433$	$r_0 = 0.88$ $bias = -0.4$ $rms = 1.68$	$r_0 = 0.89$ $bias = 0.4$ $rms = 1.7$
T $(^\circ C)$ $n = 2104$	$r_0 = 0.94$ $bias = 0.4$ $rms = 1.25$	$r_0 = 0.91$ $bias = -0.1$ $rms = 1.3$
q (g/kg) $n = 440$	$r_0 = 0.85$ $bias = -0.48$ $rms = 1.22$	$r_0 = 0.95$ $bias = -0.83$ $rms = 1.07$
SST $(^\circ C)$ $n = 79$	$r_0 = 0.98$ $bias = 1.90$ $rms = 2.01$	$r_0 = 0.86$ $bias = 0.26$ $rms = 1.69$
H (W/m^2) $n = 2433$	$r_0 = 0.77$ $bias = 9.3$ $rms = 27.1$	$r_0 = 0.83$ $bias = -1.8$ $rms = 21.0$
E (W/m^2) $n = 2433$	$r_0 = 0.53$ $bias = 38.8$ $rms = 52.7$	$r_0 = 0.57$ $bias = 28.0$ $rms = 59.4$

Table 2. Sensitivity of parameterization scheme to changes in mean parameters at Christiansö. Averaged fluxes in (W/m^2).

meas	modeled		
	org	*SST-1*	*SST-1 q+1*
H=13.4 E=22.9	H=23.0 E=65.3	H=11.7 E=47.0	H=11.7 E=34.1

95

4.2. Causes of errors

4.2.1. Mean parameters

The most obvious source of error is the mean parameters used in the models. In Table 1 some statistics of the various parameters can be seen. It should here be noted that the humidity data are taken at the synoptic station at Christiansö Fyr, there is a certain areal separation to the other data. The synoptic site is not quite as exposed and thus perhaps slightly too dry. This would make the difference to the models even greater. The parameter most difficult to determine is in general SST. In Figure 4 the SST can be seen. PROBE-Baltic clearly overestimates SST by more than one degree, this also explains the overestimation of sensible heat flux by PROBE-Baltic. The average agreement is better for HIRLAM but the variations in SST are unrealistically large on short time-scales, due to the interpolation technique used for determining SST in HIRLAM. This will give an unrealistic high scatter in the latent heat flux.

The bias for the mean parameters seems to be within what can be expected from such models, apart from the erroneous SST. We then need to consider how certain error affects the fluxes. To study the sensitivity in the fluxes to errors in mean parameters the heat flux scheme from in PROBE-Baltic is used together with model parameters.

In Table 2 the averaged fluxes after these tests can be seen. When decreasing the SST one degree the sensible heat flux decreased by 50% and is in good agreement with the measured flux, the latent heat flux is decreased by 30%. Increasing specific humidity by 0.5 g/kg decrease the latent heat flux by another 30%, and the calculations are closer to measurements.

The sensitivity for the scheme used in HIRLAM is similar. It should also be noted that this is not a test of the models since it is no model simulation, it is merely a test of the sensitivity in the parameteriza-
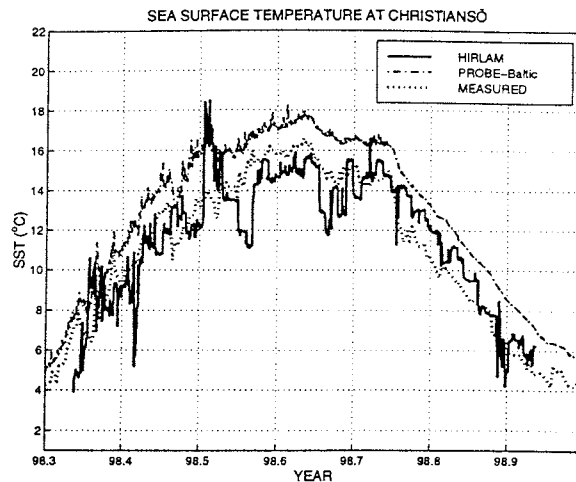

Figure 4. Sea surface temperatures for the period May 1998 to December 1998. Solid line is the HIRLAM model, dashed is the PROBE-Baltic model and dotted is measured outside Christiansö
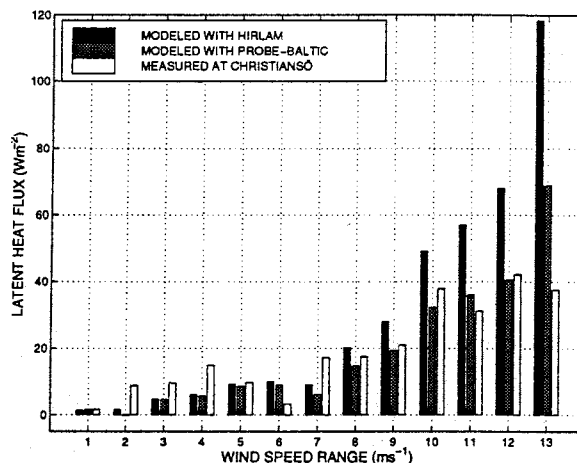

Figure 5. Averages of latent heat flux for measured wind speed ranges. Measured mean parameters are used as input in the parameterization schemes used in HIRLAM and PROBE-Baltic respectively.

tion scheme. The model response to these changes is not studied.

4.2.2. Parameterization scheme

When dealing with errors in SST of the order of 2 degrees the result is not very sensitive to coefficients in the parameterization scheme. But a scheme giving systematic errors due to the parameterization
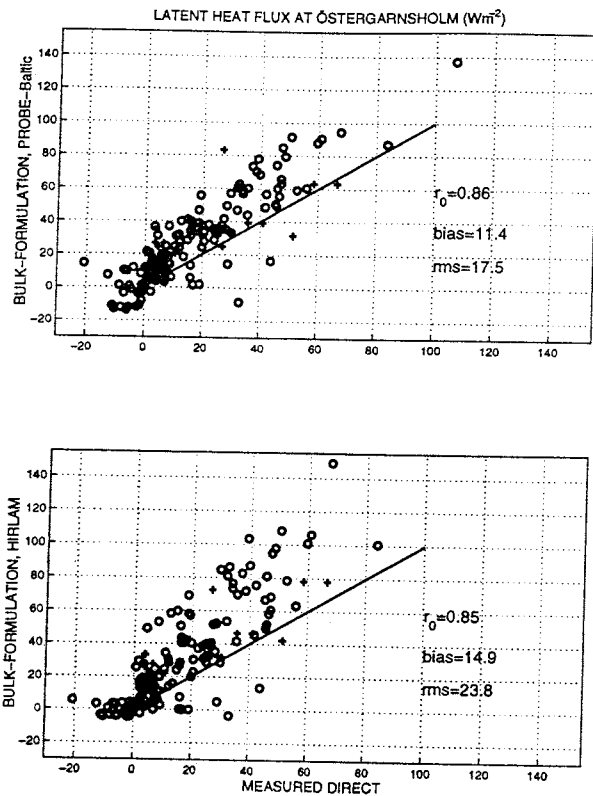
Figure 6. Latent heat flux calculated by bulk formulas (a) as in PROBE-Baltic and (b) as in HIRLAM, compared with measurements from Östergarnsholm. Crosses use the MiUU-turbulence instrument and circles the LiCOR system.

still give large systematic errors. For example the scheme used in HIRLAM can be questioned for high wind speeds. In Figure 5 the schemes used in the two models are tested using measured mean parameters at Christiansö as input, this will give a new data set which is not directly comparable to Table 2. The data is divided into measured wind speed ranges.

Average values for the measured latent heat flux is $18\ Wm^{-2}$, modeled as in PROBE-Baltic give $15\ Wm^{-2}$ and as in HIRLAM $23\ Wm^{-2}$, the scheme used in HIRLAM clearly overestimates fluxes at higher winds. Also data from Östergarnsholm are used to test the two schemes. In Figure 6 results for two different measuring setups are used. For this data both schemes give too high la-

tent heat flux, but it is a more clear signal using the scheme from HIRLAM.

From the parameterization tests together with Figure 3 it can be concluded that the wind speed dependence in the transfer coefficient for humidity, C_E, gives too large latent heat flux at high winds. It is otherwise difficult to draw any further conclusions. The areal separation of the measurements of humidity to the others at Christiansö results in a too large scatter for any more careful examination. Figure 6 (a) with high quality data indicates that also the parameterization scheme used in PROBE-Baltic results in too high latent heat fluxes.

4.2.3. Measurement quality

When it comes to comparing measurements and models, the question about quality of measurements naturally arises. This problem can be divided into two parts. Representativity of measurements and measurement errors.

The assumption is that a single point measurement represents an area average in the model. For the HIRLAM comparison this is not a too great assumption since the measurements represent a footprint of the conditions several kilometers upwind the measuring site. Only data with on-shore winds are used and neither of the two sites are believed to be very influenced by upwelling, so the surface is relatively homogeneous in space. Hourly averages of measurements are used, not to include smaller scale phenomenon. For the PROBE-Baltic this is perhaps a more questionable assumption since the PROBE-Baltic basins are of the order of hundreds of square kilometers. But still since both measuring sites are quite in the middle of each basin, and not very close to large upwelling areas, the conditions are assumed to be rather homogeneous in space. However, the problem with representativity can explain some of the deviations in SST for PROBE-Baltic.

The problem with measurement errors is also hard to answer. It is difficult to verify flux measurements over sea. Since statis-

tical turbulence parameters, for the data used in the present study, look reasonable (not shown here) there is really no reason to question the measurements.

5. Discussion and conclusions

At Christiansö the two models overestimate latent heat flux, this is in general agreements with earlier findings from HIRLAM by *Gustafsson et al.* [1998] and also for the sensible heat fluxes at Östergarnsholm [*Rutgersson*, 1999]. In Figure 7 examples of soundings before and after the passing over the Bothnian Bay are shown, the agreement is good before passing the Bothnian Bay, but the model is too humid in the lower layers after. Further investigation is needed to see if this is a general feature or not. Explanations for this can in HIRLAM be surface parameterization - but also the turbulence parameterization. If the turbulence is too efficient in transporting humidity away from the surface, we will have a too dry surface and too large latent heat fluxes. Since the PROBE-Baltic model is driven by meteorological parameters from HIRLAM a too dry HIRLAM will also influence the latent heat fluxes in PROBE-Baltic.

The mean parameters are of critical importance for the resulting fluxes and the accuracy in SST and low level temperature and humidity needs to be very high. In *Fairall et al.* [1996] it was shown that the accuracy of temperatures need to be 0.2 K and of humidity 0.2 g/kg to give fluxes within 10 %.

The conclusions from this study can be summarized as follows:

- The two models clearly overestimate latent heat flux at Christiansö. A possible explanation is too dry surface layers over sea.

- The latent heat flux is extremely sensitive to errors in SST and surface humidity. An accuracy of some tenths of degrees and some tenths of g/kg
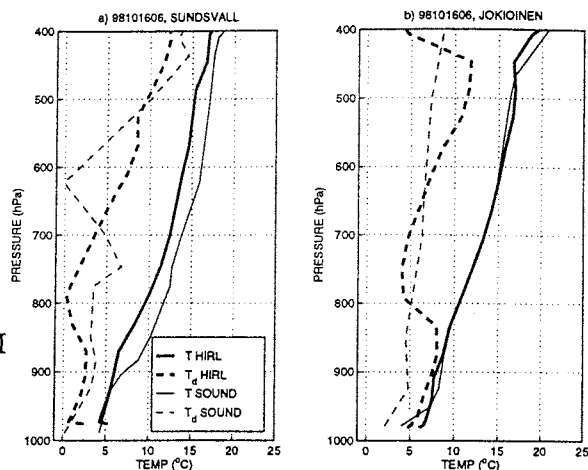
Figure 7. Vertical profiles of temperature and dew point temperature at a) Sundsvall and b) Jokioinen. Sundsvall is situated on the Swedish side of the Bothnian Bay and Jokioinen on the Finnish side.

is needed for accurate flux estimates. This seems however to be far from the accuracy in present atmosphere and ocean models applied to the Baltic Sea.

- It is also important to have a good parameterization scheme. The scheme used in HIRLAM was shown to overestimate fluxes at high wind speeds.

- The lack of agreement between models and measurements indicate the need of further development of models before drawing further conclusions concerning heat and water budgets.

The overestimation of the latent heat flux in this study is clearly seen north of Bornholm for both models. It is perhaps too early to generalize this feature to all Baltic Sea and other models, but it is likely that this is the case.

References

DeCosmo, J., K. B. Katsaros, S. D. Smith, R. J. Anderson, W. A. Oost, K. Bumke, and H. Chadwick, Air-sea exchange of water vapor and sensible heat: The HEXOS results, *J. Geophys. Res.*, *101*, 12,001–12,016, 1996.

Fairall, C. W., E. F. Bradley, D. P. Rogers, J. B. Edson, and G. S. Young, Bulk parameterization of air-sea fluxes for Tropical Ocean-Global Atmosphere Coupled-Ocean Atmosphere Response Experiment, *J. Geophys. Res*, *101*, 3747–3764, 1996.

Grelle, A., and A. Lindroth, Eddy-correlation system for long-term monitoring of fluxes of heat water and CO_2, *Global Change Biology*, *2*, 297–307, 1996.

Gustafsson, N., L. Nyberg, and A. Omstedt, Coupling High Resolution Atmosphere and Ocean Models for the Baltic Sea, *Mon. Wea. Rev.*, *126*, 2822–2846, 1998.

Hagedorn, R., D. Jacob, and A. Lehman, A Coupled High Resolution Atmosphere-Ocean Model for the BALTEX Region, in *Conference Preceedings of the Second Study Conference on BALTEX*, pp. 66–67, International BALTEX Secretariat Publication, 1998.

Isemer, H., and R. Lindau, Climatological estimates of precipitation and evaporation over the Baltic Proper based on COADS, in *Conference Preceedings of the Second Study Conference on BALTEX*, pp. 80–81, International BALTEX Secretariat Publication, 1998.

Källén, E., *Hirlam Documentation Manual. System 2.5*, SMHI, Norrköping, 1996.

Launiainen, J., Derivation of the relationship between the Obukhov stability parameter and the bulk Richardson number for flux profiles, *Bound.-Layer Meteor.*, *76*, 165–179, 1995.

Louis, J. F., A parametric model of vertical eddy fluxes in the atmosphere, *Bound.-Layer Meteor.*, *17*, 187–202, 1979.

Louis, J. F., M. Tiedtke, and J. F. Geleyn, A short history of the PBL parameterization at ECMWF, in *Proc. ECMWF Workshop on boundary-layer parameterization*, pp. 59–79, ECMWF, 1982.

Omstedt, A., and L. Nyberg, Response of Baltic Sea ice to seasonal, interannual forcing and climate change, *Tellus*, *48A*, 644–662, 1996.

Omstedt, A., and A. Rutgersson, Closing the water and heat cycles of the Baltic Sea, *Accepted for publ. in Contr. Atm. Phys.*, 1999.

Rutgersson, A., A comparison between measured and modeled sensible heat and momentum fluxes using a High Resolution Limited Area Model (HIRLAM), *Accepted for publ. in Contr. Atm. Phys.*, 1999.

Smedman, A.-S., U. Högström, H. Bergström, A. Rutgersson, K. Kahma, and H. Pettersson, A case-study of air-sea interaction during swell conditions, Accepted for publ. in *J. Geophys. Res.*, 1999.

WAMDI, The WAM Model. A third generation ocean wave prediction model, *J. Phys. Oceanogr.*, *18*, 1775–1810, 1988.

A. Rutgersson, Department of Meteorology, Uppsala University, Sweden.

Revision of the surface flux parameterization over sea in HIRLAM: Theory and results

Niels Woetmann Nielsen DMI, Copenhagen

1. INTRODUCTION

The present parameterization of surface fluxes in HIRLAM over sea does not include the smooth surface regime. Instead a lower limit is set for the roughness length (currently $1.5 \cdot 10^{-5}$m). The roughness length for momentum, z_{0M}, is calculated from Charnock's formula, with a constant of proportionallity equal to 0.0032. It is further assumed that the roughness lengths for sensible heat and moisture are identical to z_{0M}. Observations as well as theoretical work indicate that this is not the case.

The minimum constraint on z_{0M} together with the applied stability functions ensures that the fluxes of sensible heat and moisture have non-zero values in free convection. However, the latter values depend on the minimum value chosen for z_{0M}. This minimum value also in general imply that free convection (unrealistically) occurs at a mean wind speed greater than zero.

A revised parameterization of surface fluxes over sea without the shortcomings listed above has been developed for the HIRLAM model. Details about this model is given in Källén (1996).

2. ROUGH AND SMOOTH SEA SURFACE

In the revised scheme there is a distinction between a smooth and rough sea. For near-surface wind speeds $\leq$ 3 m/s the sea is considered to be smooth with roughness lengths $z_{0\gamma} = r_\gamma \cdot \nu / u_*$ ($\gamma = $ m (momentum), h (heat) and q (moisture)) with $r_m = 0.11$, $r_h = 0.2$ and $r_q = 0.3$. For near-surface wind speeds $\geq$ 5 m/s the sea is considered to be rough with $z_{0m} = \beta \cdot u_*^2/g$ (Charnock's relation) with $\beta = 0.014$ over the open sea and $\beta = 0.032$ in coastal waters (fraction of sea ≤ 1). In the transition zone an interpolation formula depending on wind speed is applied. In the rough regime the roughness lengths for heat and moisture are given by (Garratt, 1992)

$$\ln \frac{z_{0m}}{z_{0h}} = c_h Re_*^{1/4} - 2, \tag{1}$$

$$\ln \frac{z_{0m}}{z_{0q}} = \ln \frac{z_{0m}}{z_{0h}} - c_q Re_*^{1/4}, \tag{2}$$

in which Re_* (the roughness Reynolds number) is defined as

$$Re_* = \frac{z_{0m} u_*}{\nu}, \tag{3}$$

Over rough sea $c_h = 2.48, c_q = 0.20$ and over smooth sea $c_h = 2.43, c_q = 0.70$.

3. FREE CONVECTION AND 1D RESULTS

A free convection limit in accordance with laboratory measurements (e.g. Deardorff et al., 1969) is obtained by modifying the stability function in (4) (Louis et al., 1981)

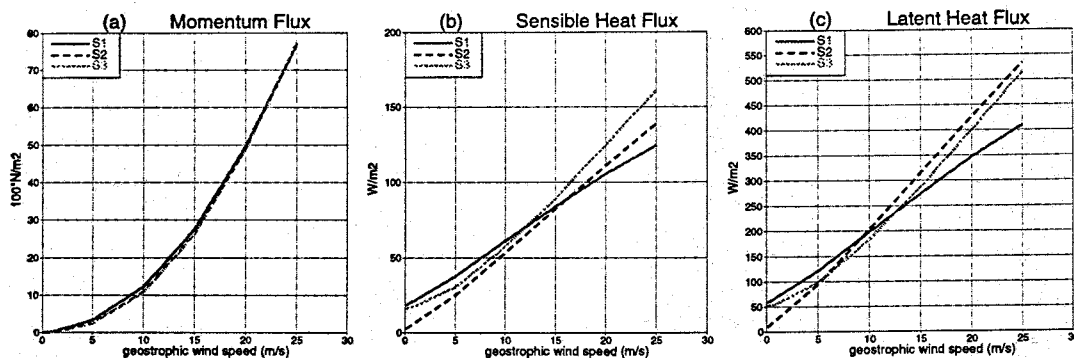$$f_\gamma = 1 + \frac{a_\gamma \cdot Ri}{1 + b_\gamma \cdot C_{mN} \cdot (Ri \cdot z/z_{0m})^{1/2}} \tag{4}$$

FIG. 1: Surface fluxes over sea as a function of geostrophic wind speed (at $60°N$) from the parameterization schemes S1 (full), S2 (dashed) and S3 (dotted), see text for details. a: momentum flux (N/m^2) , b: sensible heat flux (W/m^2) and c: latent heat flux (W/m^2). In the calculations $\Delta\theta_v = 5.1°$ C, $\Delta q = 5.9$ g/kg and $\theta_{vs} = 286.3$ K.
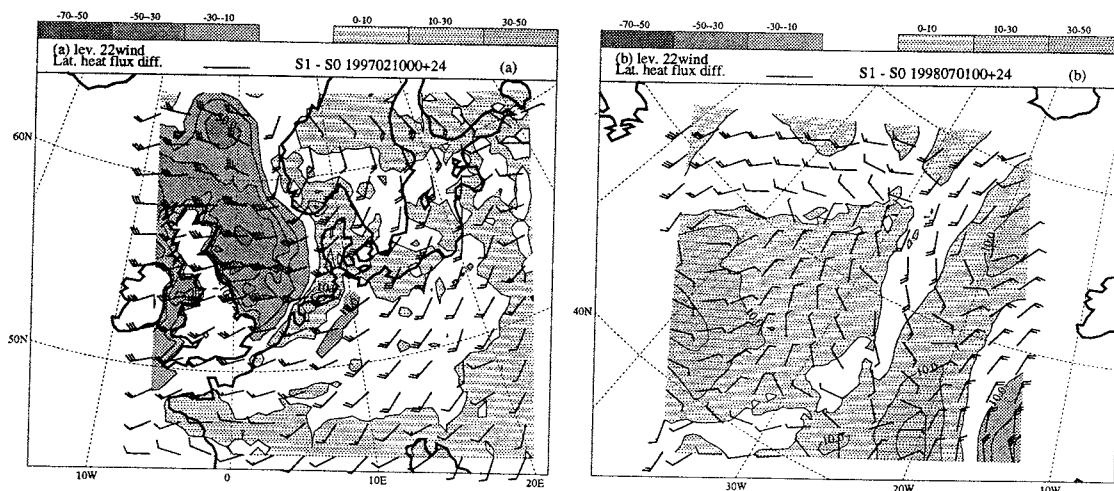
FIG. 2: Difference $S1$-$S0$ in surface latent heat flux of two parallel forecasts $S1$ and $S0$ (see text for details) together with wind velocity (WMO standard) at the lowest model level in $S1$. Negative flux differences ($\leq$-10 W/m^2) are shaded and positive differences are hatched. Contour interval is 10 W/m^2. a: 24 hours forecast from 00 UTC, 10 February 1997 , b: 24 hours forecast from 00 UTC, 1 July 1998.

in which a_m=6, a_h=a_q=9 and b_γ=45, Ri is a surface layer bulk Richardson number and C_{mN} the momentum drag coefficient in neutral stratification. The modification to the stability function in (4) consists of a replacement of C_{mN} with $C_{\gamma N}$ and z_{0m} in the square root term with another length scale d_γ. The definition of $C_{\gamma N}$ is

$$C_{\gamma N} = C_{mN}\left(1 + \ln\frac{z_{0m}}{z_{0\gamma}} / \ln\frac{z}{z_{0m}}\right)^{-1}, \qquad (5)$$

and the definition of d_γ is

$$d_\gamma = \left(\delta_H \cdot Pr^{-2/3} \cdot e_\gamma\right)^2 \cdot \nu/u_{FC}, \qquad (6)$$

in which $\delta_H \approx 0.17$, Pr is the Prandtl number, ν is the molecular kinematic coefficient of viscosity, e_γ is a constant ($e_m = 7.5 \cdot Pr^{4/3}$, $e_h = e_q = 5$.) and $u_{FC} = (g/\theta_v \cdot \Delta\theta_v \cdot \nu)^{1/3}$. Figure 1 shows an example of surface momentum, heat and moisture (latent heat) fluxes, as function of geostrophic wind speed, produced by the revised scheme (S1) in a 1-dimensional (1D) version of HIRLAM. For comparison the figure also includes results form two alternative parameterizations, respectively Makin and Perov (1997) (S2) and Miller et al. (1992) (S3). Further information about the revised scheme in HIRLAM is given in Nielsen (1998).

4. 3D RESULTS

The revised formulation ($S1$) has been tested in HIRLAM 4.2 for extended periods, including the FAS-TEX period in February 1997 and a summer period in 1998 (1 July to 13 August). The experiments have been run in parallel with a version of HIRLAM 4.2 applying the unmodified surface flux scheme ($S0$). For the data shown in Figure 2 the applied horizontal and vertical resolution was 0.4° and 22 levels, respectively. The 3D parallel experiments confirm the results obtained by the 1D experiments (Figure 1). In strong winds the surface fluxes of sensible and latent heat are considerably reduced in the revised scheme. A typical example for the surface latent heat flux is shown in Figure 2a. On the shown day relatively cold air has been advected over the North sea by near surface winds in the range from 15 to 25 m/s. At the valid time of Figure 2a the latent heat flux forecasted by the unmodified scheme, $S0$, was typically in the range from 100 to 200 W/m^2 over the North Sea (figure not shown). In $S1$ these fluxes have been reduced by 10 to 40 W/m^2.

An example of the enhancement of the surface latent heat flux in $S1$ in weak winds is shown in Figure 2b. In this case the integration domain was centred at 50° N, 30° W over the central North Atlantic. The fluxes are 10 to 20 W/m^2 higher in $S1$ in regions with weak, mainly anticyclonic, flow. In these regions the fluxes in $S1$ were typically between 30 and 70 W/m^2 (figure not shown).

In the long term integrations (period 1 July to 13 August) differences of -2 to +2 hPa in the average mean sea level (msl) pressure patterns for $S1$ and $S0$ were found. These differences are of the same order of magnitude as the typical msl pressure bias found on a monthly basis in verification against observations over Europe.

The long term integrations also showed that the effect of the change in surface flux parameterization was spread to the whole atmosphere. An indication of this process was a clear negative correlation between the thickness fileds of the troposphere (1000-850 hPa, 850-500 hPa, 500-300 hPa) and the stratosphere (300-100 hPa) (figures not shown).

After extensive parallel tests, showing slightly im-

proved verification scores (bias and rms error) in the lower troposphere relative to the operational forecasts at the Danish Meteorological Institute (DMI), the revised surface flux parameterization scheme was implemented in the operational forecasting system at DMI in late February 1999.

5. DISCUSSION

The revised scheme $S1$ can be regarded as a first step in the process of improving the parameterization of turbulent surface fluxes over sea. An accurate parameterization of these fluxes are of primary importance in climate simulations, but due to their significant impact on the evolution of the atmospheric boundary layer and on cyclogenesis over sea, accuracy is also required in short range weather forecasting.

The scheme could probably be further improved by including in z_{0M} a dependence of wave age c_f/u_* (c_f beeing the phase speed at the peak of the ocean wave spectrum and u_* the surface friction velocity). However, such a step requires a coupling of the atmospheric model to an ocean wave model. Furthermore, the scheme does not take into account impacts on the surface fluxes by processes or dependencies such as sea spray (at high wind speeds), precipitation and variation of $q_{sat}(T_s)$ with salinity.

Makin (1998), has demonstrated a significant impact of sea spary on the surface fluxes of sensible and latent heat at wind speeds in excess of 25 m/s in a numerical model of the marine surface layer (including interaction with sea waves).

In numerical models of tropical hurricanes it has been found that the moisture exchange coefficient must be comparable in magnitude to the momentum drag coefficient in order to obtain the observed intensities of tropical hurricanes. This is another indication of an enhancement of the moisture flux by sea spray at very high wind speeds in the marine atmospheric boundary layer.

REFERENCES

[1] Deardorff, J. W., G. E. Willis and D. K. Lilley (1969). Laboratiry investigation of non-steady penetrative convection. *J. Fluid Mech.* **35**, 7–31.

[2] Louis, J. F., Tiedtke, M., and Geleyn, J. F. (1981). A short history of the PBL parameterization at ECMWF. In *ECMWF Workshop on Boundary-Layer Parameterization*, pages 59–79, ECMWF.

[3] Garratt, J. C. (1992). The atmospheric boundary layer. Cambridge University Press, 316 pp.

[4] Källén (1996). HIRLAM Documentation Manual. system 2.5. Technical report, SMHI, Norrköbing, Sweden.

[5] Makin, V. K. (1998). Air-sea exchange of heat in the presence of wind waves and spray. *J. Geophys. Res.* **103**, 1137–1152.

[6] Makin, V. and V. Perov, (1997). On the wind speed dependence of momentum, sensible heat and moisture exchange coefficients over sea in the HIRLAM model - a case study. *Hirlam Newsletter* **29**, 26–31.

[7] Miller, M. J., A. C. M. Beljaars and T. N. Palmer (1992). The sensitivity of the ECMWF Model to the parameterization of evaporation from the tropical ocean. *J. Climate* **5**, 418–434.

[8] Nielsen, N. W. (1998). Inclusion of Free Convection and a Smooth Sea Surface in the Parameterization of surface fluxes over sea. *HIRLAM Newsletter* **32**, 44–51.

Coupling of regional atmosphere and ocean models

Renate Hagedorn

Institute of Marine Research, Kiel, Germany

—

Abstract. The results of a three-dimensional fully coupled regional atmosphere-ocean model for the area of the Baltic Sea Experiment (BALTEX) are compared with simulations of the uncoupled atmospheric model. It is shown that the coupling effects depend not only on the occuring differences in sea surface temperatures (SST) and the considered temporal and spatial scales. There are also other influencing factors, namely the stationarity or non-stationarity of the atmosphere as well as the form of the flow pattern in relation to the location of the differences. Due to these dependencies, it seems that the configuration of the model domain also can have a non negligible influence on the coupling effects.

1 Introduction

In recent years a growing demand for coupled regional atmosphere-ocean models has been realized. They are necessary for determining the impact of climate change on the regional scale as well as for performing consistent simulations of the whole energy and water cycle in a specific region. Therefore the Baltic Sea Experiment (BALTEX), which focusses on the investigation of the energy and water processes in the Baltic Sea catchment area, requires a fully coupled regional atmosphere-ice-ocean model. In order to contribute to an achievement of this scientific objective – the quantification of the energy and water cycle in the BALTEX area – the atmospheric regional model REMO of the Max-Planck-Institute for Meteorology in Hamburg has been coupled to the Baltic Sea model of the Institute of Marine Research in Kiel. Hagedorn et al. (1999) have shown that the coupled model produces reasonable results in the modeled oceanic component as well as in the modeled atmosphere. Therefore no flux correction was necessary, so that a consistent model system has been developed.

The purpose of this paper is on the one hand to describe the differences between uncoupled and coupled simulations on the various spatial and temporal scales. On the other hand it is discussed under which conditions coupling effects pref-

erentially occur. In this context it is investigated whether it is possible to separate situations which tend to prevent or support the development of changes due to the coupling.

2 Model description

The three-dimensional fully coupled high resolution atmosphere-ocean model for the BALTEX region has been developed from two independent models, the atmospheric regional model REMO and the Kiel Baltic Sea model BSMO.

REMO was set up at the Max-Planck-Institute (MPI) for Meteorology in a joint effort by the DKRZ (Deutsches Klimarechenzentrum), DWD (Deutscher Wetterdienst), GKSS (Forschungszentrum Geesthacht) and MPI. It is based on the Europa-Modell (EM), the operational forecast model of the German Weather Service (Majewski, 1991). In addition to the physical parameterizations implemented in the EM, it is possible to use within REMO the physics of ECHAM4, the global climate model of the MPI (Jacob and Podzun, 1997). However, all simulations presented in this paper have been performed with the physical parameterizations of the EM system. The vertical structure is formulated in the terrain-following hybrid coordinate system with 20 model levels. The horizontal grid is a rotated latitude/longitude grid with a resolution of $1/6°$ which corresponds to $\approx 18 \times 18$ km^2 grid boxes.

The oceanic component of the coupled atmosphere-ocean system is a three-dimensional baroclinic model of the Baltic Sea including the Belt Sea and the Skagerrak/Kattegat area. The ocean model has a horizontal resolution of $\approx 5 \times 5$ km^2 with 28 vertical levels specified (Lehmann, 1995). Additional to the atmospheric forcing which is provided by the atmospheric model, river runoff is taken from a monthly mean runoff data base (Bergström and Carlsson, 1994). In case of coupled atmosphere-ocean simulations the surface fluxes of momentum, energy and fresh water (except river runoff) which drive the ocean model are provided directly from the atmospheric model. In case of uncoupled simulations the sur-

face fluxes are calculated from the atmospheric model data by using bulk aerodynamic formulas (Fig. 1).
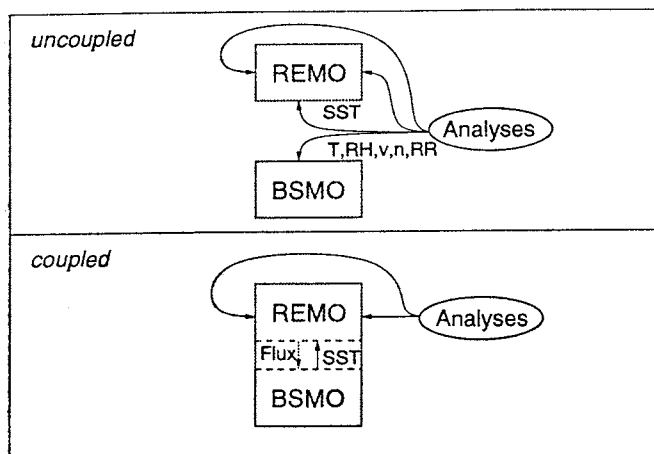

Fig. 1. Schematical depiction of forcing variables in uncoupled simulations and exchanged fields in coupled simulations.

The coupling of both models has been organized in such a way that the ocean model has been implemented into the atmospheric model as an optional subroutine. Although the ocean model is directly incorporated, the atmospheric and oceanographic variables are not directly exchangable, mainly because of the different grids of both models. Therefore a coupling interface has been implemented in which the respective variables are prepared for the respective model. The mutually exchanged variables are on the one hand the SSTs calculated by BSMO, which replace the Baltic Sea SSTs from DWD analyses as lower boundary conditions. On the other hand REMO has to provide the forcing for the ocean model: latent and sensible heat fluxes, net longwave and shortwave radiation fluxes, wind stresses, precipitation and surface pressure. In uncoupled simulations of BSMO the forcing variables are 2 m air temperatures, 2 m humidity, 10 m winds, cloudiness and surface pressure gradient. Based on these variables the fluxes are calculated directly in the ocean model with different parameterizations than in the atmospheric model. However, for the establishment of a consistent model system it is a prerequisite to carry out the coupling via the exchange of the fluxes across the atmosphere-ocean interface.

3 Comparison of uncoupled and coupled simulations

In this section uncoupled and coupled simulations of the time period May to October 1992 are compared. From the atmospheric point of view the only difference between uncoupled and coupled simulations is the lower boundary condition over the Baltic Sea, the SST. In uncoupled simulations SSTs are prescribed from analyses, whereas in coupled simulations SSTs are provided by the Baltic Sea model. (Fig. 1). Therefore the SST differences between uncoupled and coupled runs are the trigger for differences in the simulated atmospheric variables.

The SST differences averaged over the whole simulation period vary at different grid points between -3.1 and +2.1°C (Fig. 2). The greatest differences occur in coastal upwelling regions in the Western Gotland Basin and in the Gulf of Finland, with large areas of negative differences over -2°C. But there are also regions with positive SST differences, e. g. in the Bothnian Bay. However, in most regions, in the temporal mean the coupled SSTs are lower than the uncoupled SSTs.
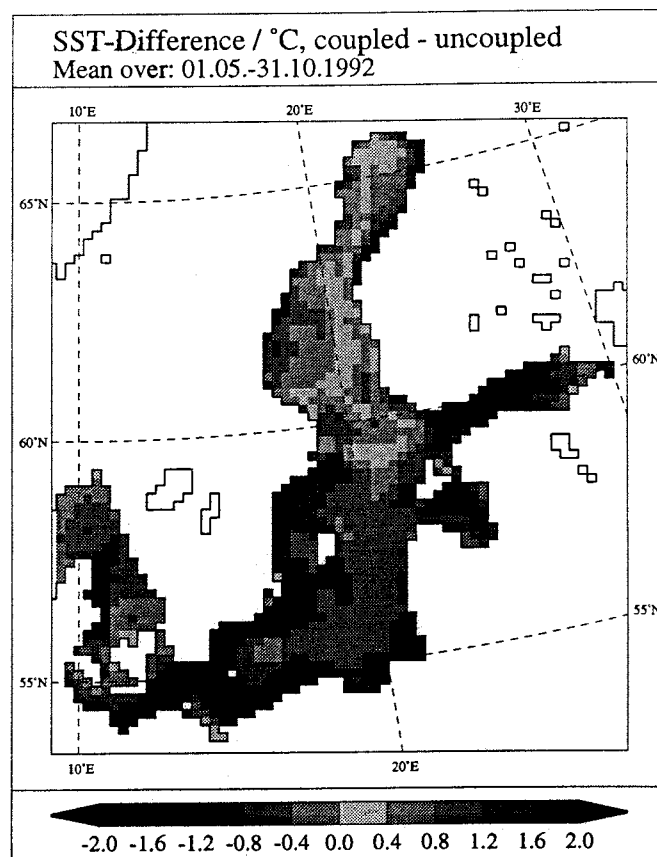

Fig. 2. SST differences between coupled and uncoupled simulations in °Celsius, averaged over the time period from May to October 1992.

3.1 Direct response

As a direct response on these differences in SSTs, changes in sensible and latent heat fluxes occur. Reduced SSTs cause reduced heat and humidity fluxes from ocean to atmosphere. Since the upward heat flux from ocean to atmosphere has a negative sign, this dependency is reflected in highest positive heat flux differences in regions with highest negative SST differences and vice versa. For the values averaged over the whole simulation period, differences of more than 25 Wm^{-2} occur in the simulated latent heat flux (Fig. 3).

The temporal evolution of the differences in SSTs and latent heat fluxes shows that at certain times and regions the differences can be even more pronounced (Fig. 4). The time-series at one extreme grid point, directly in the upwelling region of the western Gotland Basin, reveal that a 6°C cooling in SSTs is related to a reduction of about 100-150 Wm^{-2}
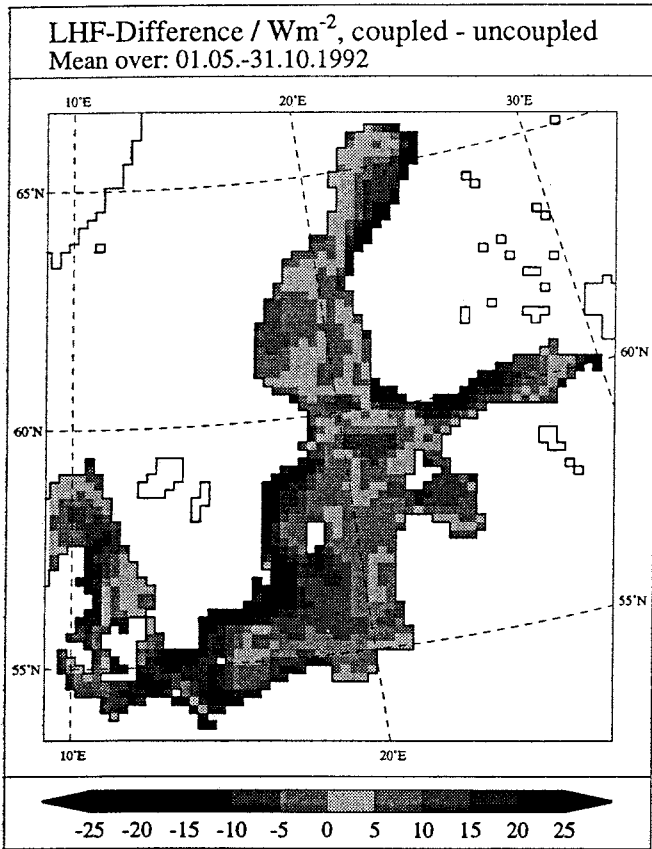
Fig. 3. Latent heat flux differences between coupled and uncoupled simulations in Wm^{-2}, averaged over the time period from May to October 1992.

Fig. 4. Timeseries of differences between coupled and uncoupled simulations. Upper panel: latent heat flux differences in Wm^{-2}, lower panel: SST differences in °C; green lines: values averaged over the whole Baltic Sea, black lines: values at a single coastal grid point in the western Gotland Basin upwelling region.

in latent heat fluxes. In the temporal mean at this gridpoint the SST is 2.1°C lower and the latent heat flux is diminished by 29.5 Wm^{-2} in the coupled simulation. The differences averaged over the whole Baltic Sea are of course lower. But also these timeseries show almost always negative SST differences, and resulting from this, reduced latent heat fluxes. The greatest differences occur in June and July with a 2.5°C lowered SST and about 30 Wm^{-2} reduced latent heat flux. In the temporal and spatial mean over the whole simulation period and the whole Baltic Sea a 0.6°C lower SST and a 7.1 Wm^{-2} reduced latent heat flux occurs in the coupled run.

The different heat fluxes result also in temperature and humidity changes in the atmosphere. This can be seen in Fig. 5, in which SST differences with occuring differences in the 950 hPa temperature are compared. On the one hand the 2.5°C reduced SST in June is directly reflected in an about 0.3°C lowered 950 hPa temperature. These relatively minor changes in the 950 hPa temperature are caused by a vertical and horizontal spreading of the locally restricted SST differences to the surrounding areas in the atmosphere of the larger model domain. On the other hand later in September/October greater differences of up to 0.6°C occur, although the SST differences at that times are only at a lower level. This indicates that also another factor influences the air temperature differences, namely a so-called indirect effect. Indirect effect stands for changes not directly caused by differences
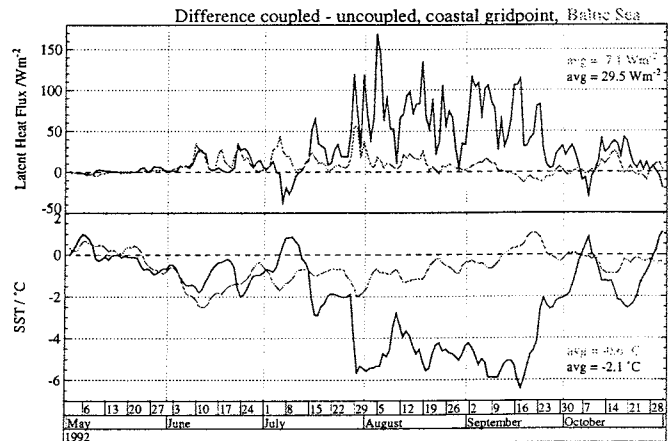
in heat fluxes, but caused by dynamical changes like movements of pressure systems. These changes in the dynamics are of course also triggered by SST differences, but under certain circumstances they can drastically increase. In connection with a displacement of larger air-masses, these enhanced temperature differences occur, despite of the relatively low SST differences at those times.

But the question is why at times with highest SST differences not the highest differences in the dynamics occur. There must be other influencing factors, which prevent or support the development of differences in the dynamics. To find out these features, the concept of composites will be applied.
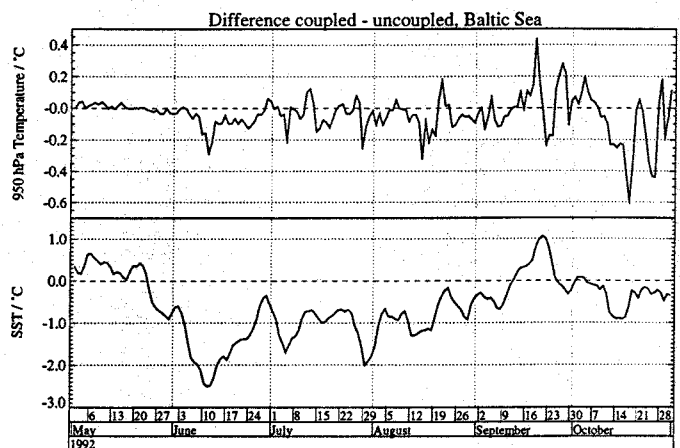

Fig. 5. Timeseries of differences between coupled and uncoupled simulations. upper panel: 950 hPa temperature differences in °C, lower panel: SST differences in °C.

105

High MSLP-RMS Composite
10m Wind / ms⁻¹, MSLP / hPa, coupled

Low MSLP-RMS Composite
10m Wind / ms⁻¹, MSLP / hPa, coupled

0.3 0.6 0.9 1.2 1.5 1.8 2.1 2.4 2.7 3.0 3.6 3.9
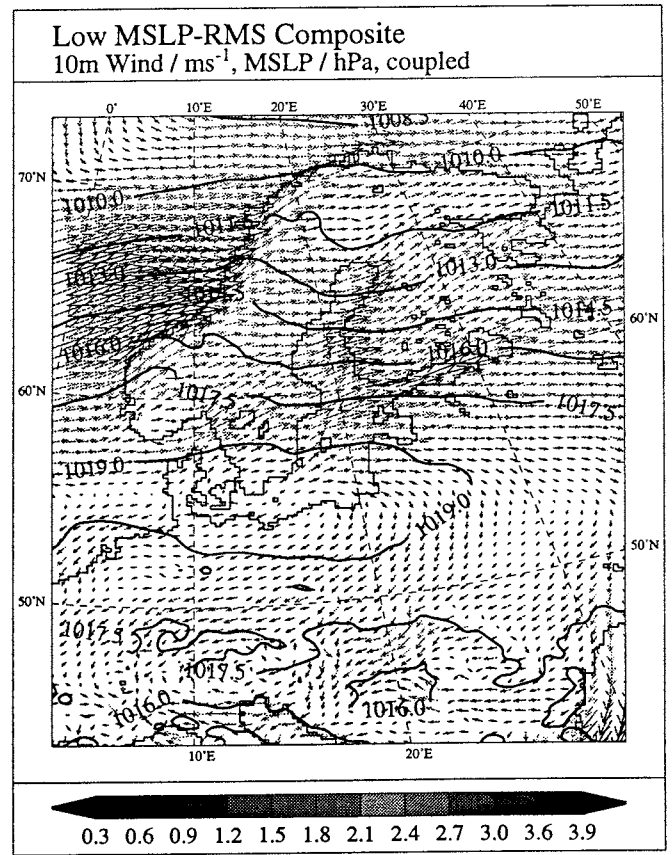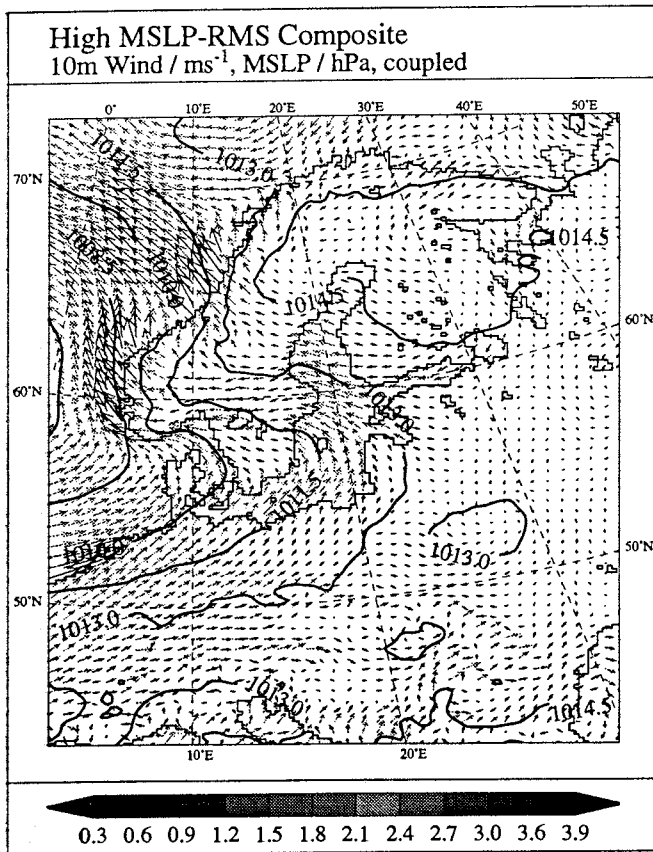
0.3 0.6 0.9 1.2 1.5 1.8 2.1 2.4 2.7 3.0 3.6 3.9

Fig. 7. Composites of the mean sea level pressure and 10m wind field at high index situations (left) and low index situations (right).

3.2 Conditions for changes in dynamics

The principle of this method is to construct an index and consider the mean state of different variables at high or low index times (von Storch and Zwiers, 1999). In this case the root mean square (RMS) difference of the mean sea level pressure (MSLP) of uncoupled and coupled simulations serves as index (Fig. 6). The simulation was extended up to the end of November, because the differences at the end of October seems to be increasing. It was investigated whether this was only a temporal restricted signal or whether possibly a non decreasing error growth occurred. But it turned out that this was only a sequence of some events, with one strong event directly at the end of October and afterwards decreasing differences. The comparison of the MSLP-RMS with the triggering SST-RMS (Fig. 6) once more points out that the changes in the dynamics are not only dependent on the SST differences. On the one hand there are peaks in the MSLP-RMS at times with high SST-RMS, but on the other hand the greatest peaks in MSLP-RMS occur at later times with lower SST-RMS.

To get an idea about the reason for that, the composites of the mean state of the atmosphere at high and low index situations were constructed. It turned out that the pressure and wind fields in these two situations are evidently different (Fig. 7). In high RMS situations the determining pressure system is concentrated just at the western boundary, and an
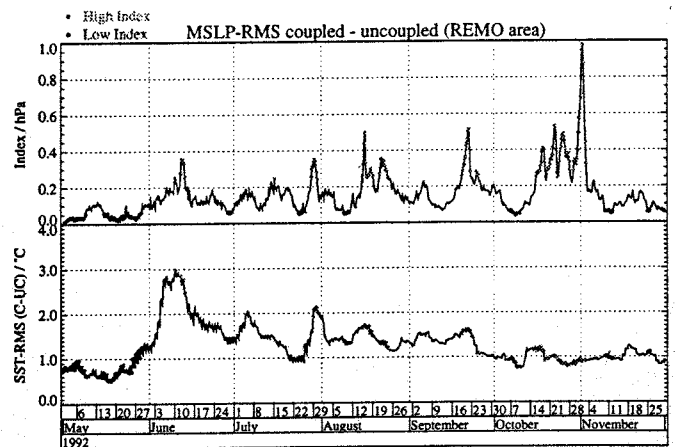

Fig. 6. Timeseries of root mean square differences between coupled and uncoupled simulation. upper panel: Mean sea level pressure RMS in hPa (serves as index for constructing the composites, green/red dots mark high/low index situations); lower panel: sea surface temperature RMS in °Celsius.

overall more meridional circulation prevails. In contrast to that, in the low RMS situation a more zonal flow occurs. But what is the essential difference of these situations, that high or low MSLP differences occur? After investigating various features of these situations, it seems to be that the stationarity of the pressure sytems is an important factor. That means the

106

duration for which a pressure system stays inside the model area, or inversely the renewal time of the air-masses caused by the constraints of the lateral boundary conditions supports or prevents the development of differences. As a representation of the stationarity of the atmosphere, the composites of the temporal pressure gradient were constructed (not shown). In high MSLP-RMS situations an evidently lower temporal pressure gradient occurs, i.e. greater differences in the dynamics are related to more stationary situations and vice versa. This points out that the stationarity of the atmosphere is a factor to seperate between situations which support or prevent the development of coupling effects.

3.3 Spatial and temporal scales

To give an example of the changes in the energy and water cycle, which can occur on the different scales, the total precipitation and evaporation as well as the residual component P-E from May to October 1992 is presented in Tab. 1. An ex-

Table 1. Mean precipitation and evaporation from May to October 1992 in uncoupled (UC) and coupled (C) simulations. Values are given for one coastal grid point in the western Gotland Basin upwelling region, for the whole Baltic Sea and for the whole BALTEX area.

May-Oct 1992		Prec / mm	Evap / mm	P-E / mm
coastal grid point:	UC	279	393	-114
	C	195	206	-11
	C-UC	-84	-187	103
Baltic Sea:	UC	277	352	-74
	C	262	307	-45
	C-UC	-15	-45	29
BALTEX area:	UC	290	234	56
	C	286	224	62
	C-UC	-4	-10	6

treme reduction occurs in the values of the coastal gridpoint, with a 84 mm or 30% reduced precipitation, from 279 mm in the uncoupled simulation to 195 mm in the coupled simulation, and a 48% reduced evaporation. The residuum P-E represents in this case more or less the whole advective component, because for this long term mean the changes in the water storage of the atmosphere are negligible. That means negative values represent humidity divergence, positive values humidity convergence. The reduced humidity input in the coupled run due to the reduced evaporation is therefore balanced by a reduced precpitation as well as by the 90% reduced humidity divergence.

The mean values over the larger areas do not show such extreme differences, but partly also on this scale there are remarkable deviations. In the Baltic Sea region, the 13% reduced evaporation is once more balanced by reduced precipitation and reduced humidity divergence. For the whole BALTEX area positive values for P-E occur, which stand for humidity convergence. The higher value in the coupled simulation mainly does not result from higher humidity conver-

gence through inflow, but from lower humidity divergence at the outflow boundaries. In general, the small resulting differences over the whole BALTEX area are not caused by locally restricted difference signals, but they are mainly due to the compensating character of the spreading differences. Nevertheless, it is remarkable to what extent this in the temporal and spatial mean 0.6°C lower SST can influence the energy and water budget on local as well as on regional scales.

4 Conclusions

The comparison of uncoupled and coupled simulations shows clearly that the coupling effects depend on SST differences, which are the trigger of the changes. It was also demonstrated that the order of the changes is strongly related to the considered temporal and spatial scales. But there are also other influencing factors, namely the stationarity or non-stationarity of the atmosphere as well as the form of the flow pattern in relation to the location of the differences. Depending on these factors, occuring changes are either supported due to a longer stay inside the model area, or in the other case removed due to a renewal of the atmosphere caused by inflow through the lateral boundaries.

Due to these dependencies, it seems to be that the configuration of the model domain also can have a non negligible influence on the coupling effects. Therefore it is worth noting that these findings about the coupling effects are derived only from this specific model configuration with the relatively small Baltic Sea inside the whole model area. Keeping this in mind, it is expected that in other regions, for instance in the North Atlantic region, or under other conditions, maybe under winter conditions with changes in the sea ice distribution, the coupling effects will be even more pronounced. For this reason it would be certainly useful to compare the findings from this coupled BALTEX model with results from other regional coupled models.

References

Bergström, S. and Carlsson, B., River runoff to the Baltic Sea: 1950-1990, Ambio, 23, (nos.4-5), 280–287, 1994.

Hagedorn, R., Lehmann, A., and Jacob, D., A Coupled High Resolution Atmosphere - Ocean Model for the BALTEX Region, Contr. Atmos. Phys., in press, 1999.

Jacob, D. and Podzun R., Sensitivity Studies with the Regional Climate Model REMO, Meteorol. Atmos. Phys., 63, 119–129, 1997.

Lehmann, A., A three-dimensional baroclinic eddy-resolving model of the Baltic Sea, Tellus, 47A, 1013–1031, 1997.

Majewski, D., The Europa-Modell of the Deutscher Wetterdienst, Seminar Proceedings ECMWF, 2, 147–191, 1991.

von Storch, H. and Zwiers, F. W., Statistical Analysis in Climate Research, Cambridge University Press, 503 pp, (in press), 1999.

Choices for parameterization of turbulence in the Baltic Sea

H.E. Markus Meier
(Swedish Meteorological and Hydrological Institute, Rossby Centre, S-60176 Norrköping, Sweden)

1 Introduction

Mixing plays a dominant role for the physics of an estuary like the Baltic Sea. Diffusion controls the vertical salt flux across the halocline and causes a permanent inflow of Kattegat water into the bottom layer of the Baltic Sea.

Wind stirring at the sea surface generates turbulence and a well mixed layer is formed which has in summer a depth of about $20 - 30\,m$ and reaches in winter the permanent halocline. The upper ocean heat content is distributed over the mixed layer so that the sea surface temperature depends very sensitive on mixing and alters the heat fluxes at the sea surface which are functions of the air-water temperature difference.

Due to the outlined importance of mixing processes a regional high resolution model of the western Baltic Sea with open boundary conditions in the Kattegat and Bornholm Basin (Meier, 1996) is used to test different mixing parameterizations. This model has a resolution of 1 nautical mile in horizontal and 3 m in vertical direction, respectively. Simulations with realistic initial and forcing fields are carried out for the BALTEX test year 1992/93 and the results are compared to observations.

Artificial trends as result of inaccuracies of the used mixing scheme show up clearly in multi-year simulations. Within SWE-CLIM (Swedish regional climate modelling programme) a 3D coupled ice-ocean model for the Baltic Sea has been developed for multi-year integrations (RCO - the Rossby Centre Ocean model, c.f. Meier et al., 1999; Meier, 1999). A massively parallel processor architecture makes it possible to overcome computational limits using 3D Baltic Sea models for longterm integrations. Sensitivity and process oriented studies for the period May 1980 until September 1993 are performed to test several mixing schemes and to figure out the role of deepwater mixing within 3D models. Therefor, a horizontal resolution of 6 nautical miles and 41 vertical levels with layer thicknesses between 3 and 12 m have been used. RCO is started from realistic initial conditions and forced with observed atmospheric fields from the SMHI database (Lars Meuller, pers.comm.).

The paper is organized as followed: In Section 2 different mixed layer models are discussed with respect to Baltic Sea application. In Section 3 the embedded $k - \epsilon$ turbulence model is introduced and model results are compared to data. New surface flux boundary conditions for turbulent kinetic energy and dissipation are discussed in Section 4. Deepwater parameterization and results of multi-year simulations using RCO are shown in Section 5. The paper ends with a summary.

2 Comparison of different mixed layer models

In a first step local parameterizations are studied, e.g., the Richardson number dependent friction according to Pacanowski and Philander (1981) or the scheme according to Kochergin (1987), which is based on the reduced turbulent kinetic energy (TKE) equation without diffusion. The mixed layer depth in case of the Richardson number dependent parameterization is underestimated systematically compared to more realistic results of a second-order moment turbulent closure model (Fig.1) or observations (Fig.2), because these local schemes neglect the diffusion of TKE. It is impossible to tune these simple models for all the different physical regimes.

In a second step a reduced Kraus-Turner type

model (Niiler and Kraus, 1977) is embedded into the regional Baltic Sea model. The change of potential energy within the water column which is available for mixing is calculated directly from the supplied wind work at the surface. The simulations lead to surface mixed layers which are too homogeneous, and the turbulent bottom layer is missing completely. In fact, these results are not surprising because of the philosophy of vertical integrated slab models.

In a third step a turbulence model is tested consisting of the prognostic equation for TKE and a diagnostic equation for the turbulent length scale according to Gaspar et al. (1990). Approximately, the length scale is calculated from the square root of TKE divided by the Brunt-Väisälä frequency. Again the mixed layer depth is underestimated so that the vertical diffusion and/or the surface flux of TKE has to be enhanced unphysically to get adequate results (see Blanke and Delecluse, 1993; Meier, 1996). The reason for the underestimation might be that the vertical shear of velocity is not included into the length scale formulation as suggested by Willebrand (pers. comm.).

From these results I conclude that diffusion and viscosity within the 3D Baltic Sea model should be parameterized by an embedded second-order moment turbulence closure model.

3 Embedding a $k - \epsilon$ turbulence model into a 3D Baltic Sea model

As shown by Baumert et al. (1997), the two commonly used second moment turbulence closures, the $k - \epsilon$ (Svensson, 1978; Rodi, 1993) and the $k - l$ model (Mellor and Yamada, 1982), can be written in a canonical presentation. Despite the parameterization of the interaction of turbulence and stratification, the two model types behave rather similar. It is decided to use the $k - \epsilon$ model. Additionally, two prognostic equations for TKE and for dissipation of TKE has to be solved at every grid point of the three-dimensional model:

$$\frac{\partial k}{\partial t} - \frac{\partial}{\partial z}\left(\frac{\nu_t}{\sigma_k}\frac{\partial k}{\partial z}\right) = P + G - \epsilon , \quad (1)$$

$$\frac{\partial \epsilon}{\partial t} - \frac{\partial}{\partial z}\left(\frac{\nu_t}{\sigma_\epsilon}\frac{\partial \epsilon}{\partial z}\right) \quad (2)$$
$$= c_{\epsilon 1}\frac{\epsilon}{k}\,(P + c_{\epsilon 3}\,G) - c_{\epsilon 2}\frac{\epsilon^2}{k} ,$$

with

$$P = \nu_t\left[\left(\frac{\partial u}{\partial z}\right)^2 + \left(\frac{\partial v}{\partial z}\right)^2\right] , \quad (3)$$

$$G = -\frac{\nu_t}{\sigma_t}N^2 , \quad (4)$$

$$\nu_t = c_\mu\frac{k^2}{\epsilon} . \quad (5)$$

Here, k denotes TKE, ϵ dissipation of TKE, ν_t the turbulent friction coefficient, u and v horizontal velocity components and N the Brunt-Väisälä frequency. The constants are given in Table 1 according to Rodi (1993). In case of unstable stratification the constant $c_{\epsilon 3}$ is set equal to 1 to ensure complete mixing between adjacent grid boxes. The turbulence

c_μ	$c_{\epsilon 1}$	$c_{\epsilon 2}$	$c_{\epsilon 3}$	σ_k	σ_ϵ
0.09	1.44	1.92	0	1	1.3

Table 1: *Constants of the $k - \epsilon$ model (Rodi, 1993).*

model gives no information about the turbulent Prandtl number σ_t so that an empirical formula has to be used to complete the mixing scheme. In several experiments we get the best results using a Richardson number dependent Prandtl number (Blanke and Delecluse, 1993).

$$\sigma_t = \begin{cases} 1 & : & Ri \le 0.2 \\ 5\,Ri & : & 0.2 < Ri \le 2 \\ 10 & : & 2 < Ri \end{cases} \quad (6)$$

Here Ri denotes the gradient Richardson number. A constant turbulent Prandtl number results in a too strong erosion of the halocline. It turned out that probably the greatest problems of the $k - \epsilon$ model are related to the unknown turbulent Prandtl number and the unknown constant $c_{\epsilon 3}$ (see also Burchard and Baumert, 1995).

The solar insolation is calculated by using the method of Paulson and Simpson (1977) with two extinction lengths which were determined from climatological data of the Baltic Sea (Tab. 5.3.1 in Dera, 1992) using a least-squares fit.

4 Surface flux boundary conditions for the $k - \epsilon$ model

Commonly, Dirichlet boundary conditions are used for the $k - \epsilon$ turbulence model. At the surface a logarithmic boundary layer is assumed with balance between shear production P and dissipation ϵ (Svensson, 1978):

$$P + G \overset{!}{=} \epsilon, \quad l \overset{!}{=} \kappa \, (z_0 - z) \qquad (7)$$

with von Kármán's constant κ and roughness length z_0. In case of high vertical resolution these boundary conditions are only slightly dependent on the surface roughness length. Within the boundary layer dissipation decays inversely proportional with the distance from the surface. Contrary, measurements show that dissipation decays much faster with the second or third power (see Craig and Banner, 1994; Craig, 1996). Due to breaking surface gravity waves a turbulence enhanced layer is developed which controls the vertical flux of TKE from the wave field to the mixed layer interior. Therefore, flux boundary conditions are included which are calculated from an analytical solution of the TKE equation based on the assumption of a balance of TKE diffusion and dissipation (Craig and Banner, 1994):

$$\frac{\partial}{\partial z} \left(\frac{\nu_t}{\sigma_k} \frac{\partial k}{\partial z} \right) \overset{!}{=} \epsilon, \quad l \overset{!}{=} \kappa \, (z_0 - z) \quad . \quad (8)$$

From the assumed balance (8) the following flux boundary conditions are derived:

$$\left. \frac{\nu_t}{\sigma_k} \frac{\partial k}{\partial z} \right|_{z = -\frac{\Delta z}{2}} = \frac{m \, u_*^3 + \kappa \, z_0 \, B_0}{\left(1 + \frac{\Delta z}{2 z_0}\right)^n} \quad , \qquad (9)$$

$$\left. \frac{\nu_t}{\sigma_\epsilon} \frac{\partial \epsilon}{\partial z} \right|_{z = -\frac{\Delta z}{2}} = a_\epsilon \frac{\left(m \, u_*^3 + \kappa \, z_0 \, B_0\right)^{\frac{4}{3}}}{z_0 \left(1 + \frac{\Delta z}{2 z_0}\right)^{\frac{4n}{3} + 1}} \quad (10)$$

with

$$n = \sqrt{\frac{3}{2} \frac{\sigma_k}{c_\mu} \frac{c_d}{\kappa}} \qquad (11)$$

and $c_d = 0.16$. The value of the constant a_ϵ is given by

$$a_\epsilon = \frac{c_\mu^{\frac{1}{3}}}{\sigma_\epsilon} \left(\frac{3 \sigma_k}{4}\right)^{\frac{2}{3}} \left(\sqrt{\frac{3 \sigma_k}{c_\mu} \frac{c_d}{\kappa}} + 1\right) \quad . \quad (12)$$

Further, u_* is friction velocity, B_0 surface buoyancy flux, $m = 100$ a constant given by Craig and Banner (1994) and $\Delta z = 3 \, m$ is the vertical grid distance. The surface roughness length is calculated from Charnock's formula (Charnock, 1955):

$$z_0 = \alpha \frac{u_*^2}{g} \qquad (13)$$

with $\alpha = 1400$ (Ly, 1990).

It has been shown that the results of the $k - \epsilon$ model converge towards the approximate solution from which the flux boundary conditions are calculated. The depth of the turbulence enhanced surface layer depends only from the roughness length. The approach of the here derived flux boundary conditions makes only sense as long as the depth of the turbulence enhanced surface layer is larger than $\Delta z/2$, i.e., $z_0 > 35 \, cm$ if $\Delta z = 3 \, m$.

It turned out that the main difference between Dirichlet and Neumann (or flux) boundary conditions is the dependence on the surface roughness length in the range between $10 \, cm$ up to $1 \, m$. In case of flux boundary conditions the friction coefficients are much more sensitive against changes of the roughness length than in case of Dirichlet boundary

conditions.

Results of the improved turbulence model are shown in Fig.1a and Fig.2.

5 Deepwater mixing

The Baltic Sea is a stratified estuary with a halocline preventing surface generated wind mixing to influence deeper layers on seasonal time scale. For climate studies deepwater mixing needs to be taken into account. The $k - \epsilon$ model must be extended to include a parameterization for breaking internal waves:

$$\nu = \nu_t + \sigma_t \min\left(\frac{\alpha}{N}, 0.5\, cm^2\, s^{-1}\right) \quad (14)$$

with $\alpha = 0.5 \cdot 10^{-3}\, cm^2\, s^{-2}$.

Results of a multi-year simulation using RCO are shown in Fig.3 compared with observed profiles at the monitoring station Gotland Deep. For the time period May 1980 until July 1993 102 profiles with sufficient quality are available. The model profiles have been extracted at the same dates as the data. The simulated thermocline depths are in correspondence with the observations. In some years they are slightly underestimated indicating an inaccuracy of the used atmospheric forcing. During the 16 year long stagnation period between 1976 and 1992 the salinity in the deeper layer of the Baltic Sea decreases remarkable. The simulated isohaline depths agree well with the observations. Without deepwater mixing the vertical salt flux across the halocline is much too small (not shown). The optimized parameter α is smaller than estimates from budget calculations for the Baltic Sea (Axell, 1998) because in the model coastal mixing in up- and downwelling regions contributes to the basin wide halocline diffusion. Artificial numerical diffusion is unimportant.

6 Summary

Two different 3D Baltic Sea models have been used for testing of different mixing parameterizations. The $k - \epsilon$ model gives the best performance in comparison with available observations. The turbulence model is improved by flux boundary conditions parameterizing the turbulence enhanced layer due to breaking surface gravity waves. The derivation of equations is outlined. For multi-year simulations the $k - \epsilon$ model must be extended to include a parameterization for breaking internal waves. Therefore, deepwater mixing has been added. It is shown that the time development of the halocline in the Baltic proper during the stagnation period between 1980 and 1992 is modeled realistically. The successful simulation of more than 10 years using a 3D Baltic Sea model represent a milestone progress because it was unclear a year ago if artificial numerical diffusion erodes the halocline necessarily.

References

Axell, L.B. (1998): On the variability of Baltic Sea deepwater mixing. *J. Geophys. Res.*, **103**, 21667-21682.

Baumert, H., H. Burchard and E. Kleine (1997): On Second-Moment Closures for Marine Turbulence:

A Review. Manuscript presented at the 29th International Liège Colloquium on Ocean Hydrodynamics: *Marine Turbulence Revisited*, May 5 - 9, 1997.

Blanke, B., and P. Delecluse (1993): Variability of the Tropical Atlantic Ocean simulated by a general circulation model with two different mixed layer physics. *J. Phys. Oceanogr.*, **23**, 1363-1388.

Burchard, H. and H. Baumert (1995): On the performance of a mixed-layer model based on the $k - \epsilon$ turbulence closure. *J. Geophys. Res.*, **100**, 8523-8540.

Charnock (1955): Wind stress on a water surface. *Quart. J. Roy. Meteor. Soc.*, **81**, 639-640.

Craig, P. D., and M. L. Banner (1994): Modelling wave-enhanced turbulence in the ocean surface layer. *J. Phys. Oceanogr.*, **24**, 2546-2559.

Craig, P. D. (1996): Velocity profiles and surface roughness under breaking waves. *J. Geophys. Res.*, **101**, 1265-1277.

Dera, J. (1992): Marine Physics. Elsevier, Amsterdam, 516 pp.

Gaspar, P., Y. Grégoris, and J.-M. Lefevre (1990): A simple eddy kinetic energy model for simulations of the oceanic vertical mixing: Tests at station Papa and long-term upper ocean study site. *J. Geophys. Res.*, **95**, 16179-16193.

Kochergin, V.P. (1987): Three-dimensional prognostic models. In: *Three-Dimensional Coastal Ocean Models, Coastal Estuarine Sci.*, Vol. 4, edited by N.S. Heaps, AGU, Washington D.C., 201-208.

Ly, L.N. (1990): Numerical studies of the surface-wave effects on the upper turbulent layer in the ocean. *Tellus*, **42**, 557-567.

Meier, H.E.M. (1996): A regional model of the western Baltic Sea with open boundary conditions and data assimilation (in German). *Ber. Inst. f. Meeresk., Kiel, Germany*, **284**, 117 pp.

Meier, H.E.M. (1999): First results of multi-year simulations using a 3D Baltic Sea model. *Reports Oceanography, Swedish Meteorological and Hydrological Institute, Norrköping, Sweden*, **27**, 48 pp.

Meier, H.E.M., R. Döscher, A.C. Coward, J. Nycander and K. Döös (1999): RCO - Rossby Centre regional Ocean climate model: model description (version 1.0) and first results from the hindcast period 1992/93. *Reports Oceanography, Swedish Meteorological and Hydrological Institute, Norrköping, Sweden*, **26**, 102 pp.

Mellor, G.L. and T. Yamada (1982): Development of a turbulence closure model for geophysical fluid problems. *Rev. Geophys. Space Phys.*, **20**, 851-875.

Niiler, P.P. and E.B. Kraus (1977): One-dimensional models of the upper ocean. In: *Modeling and prediction of the upper layers of the ocean*, edited by E.B. Kraus, Pergamon, New York, 143-172.

Pacanowski, R.C. and S.G.H. Philander (1981): Parameterization of vertical mixing in numerical models of tropical oceans. *J. Phys. Oceanogr.*, **11**, 1443-1451.

Paulson, C.A. and J.J. Simpson (1977): Irradiance measurements in the upper ocean. *J. Phys. Oceanogr.*, **7**, 952-956.

Rodi, W. (1993): Turbulence models and their application in hydraulics - a state-of-the-art review. *Int. Assoc. for Hydraul. Res.*, A.A. Balkema, Rotterdam, Brookfield, 3rd edition, 104 pp.

Svensson, U. (1978): A mathematical model of the seasonal thermocline. *Rep. 1002*, Dep. of Water Resour. Eng., Univ. of Lund, Lund, Sweden, 187 pp.
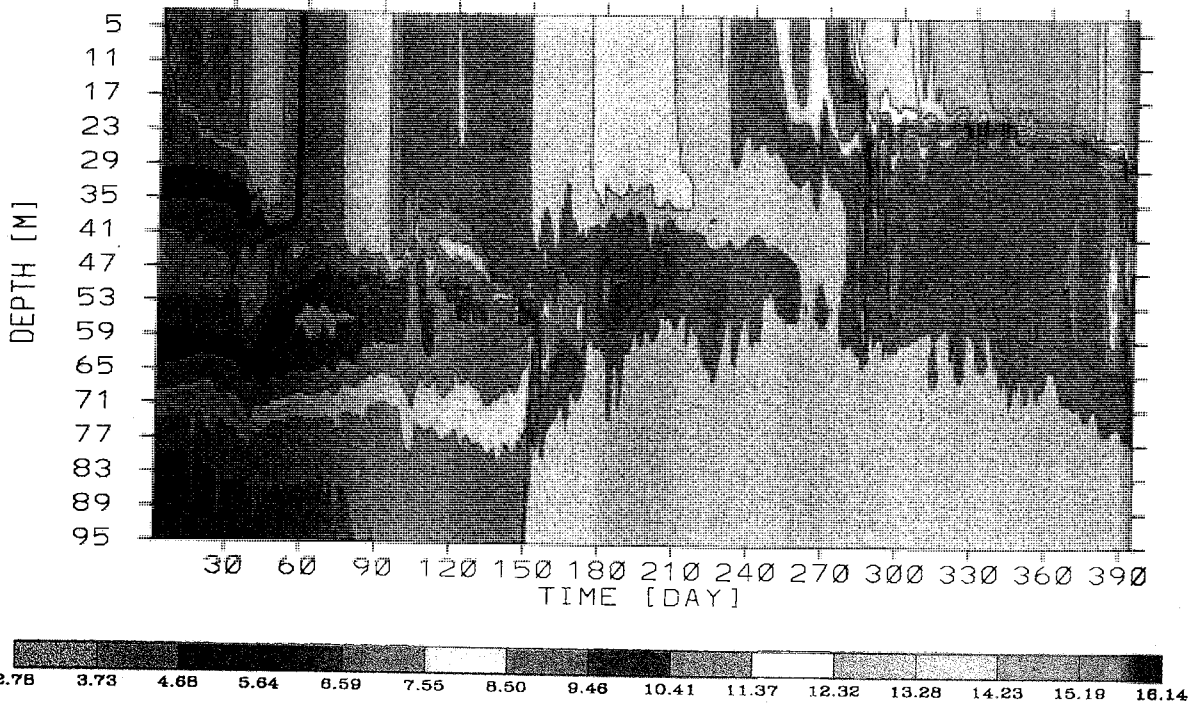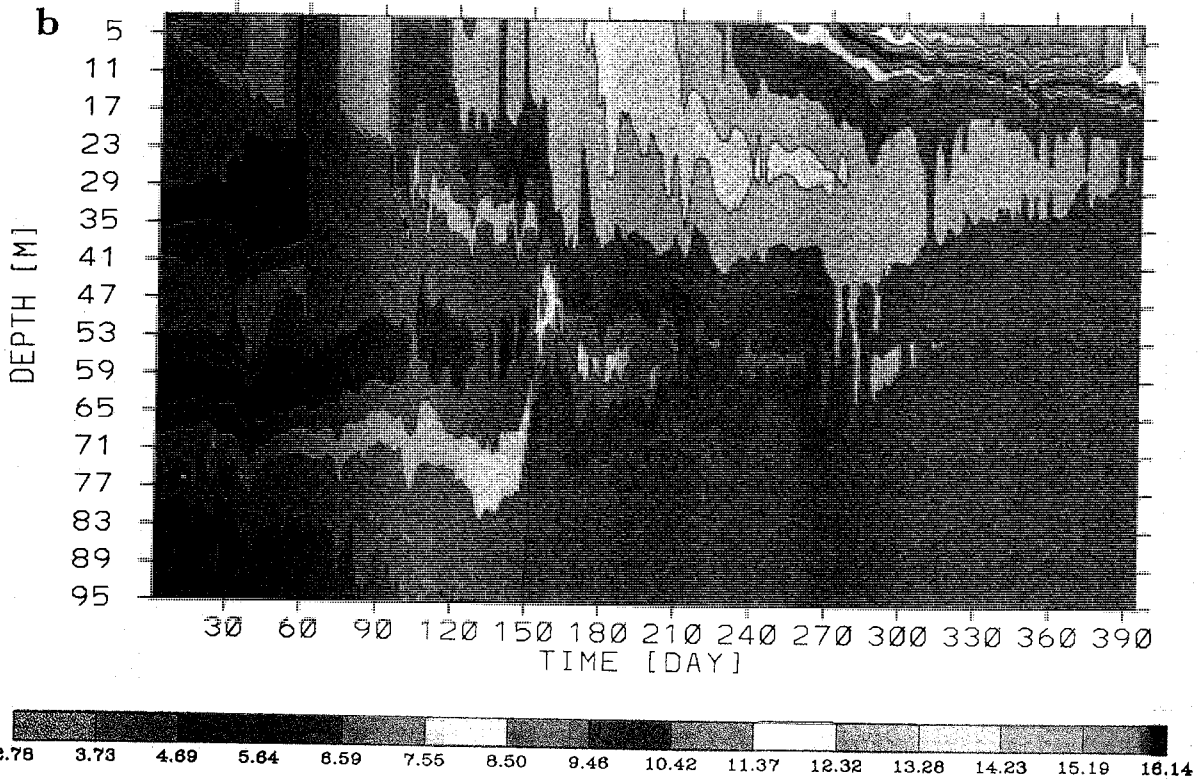
Figure 1: *Isotherm depths (in °C) from September 1992 until September 1993 at Bornholm Deep: k − ϵ turbulence model (a), Richardson number dependent friction (b).*
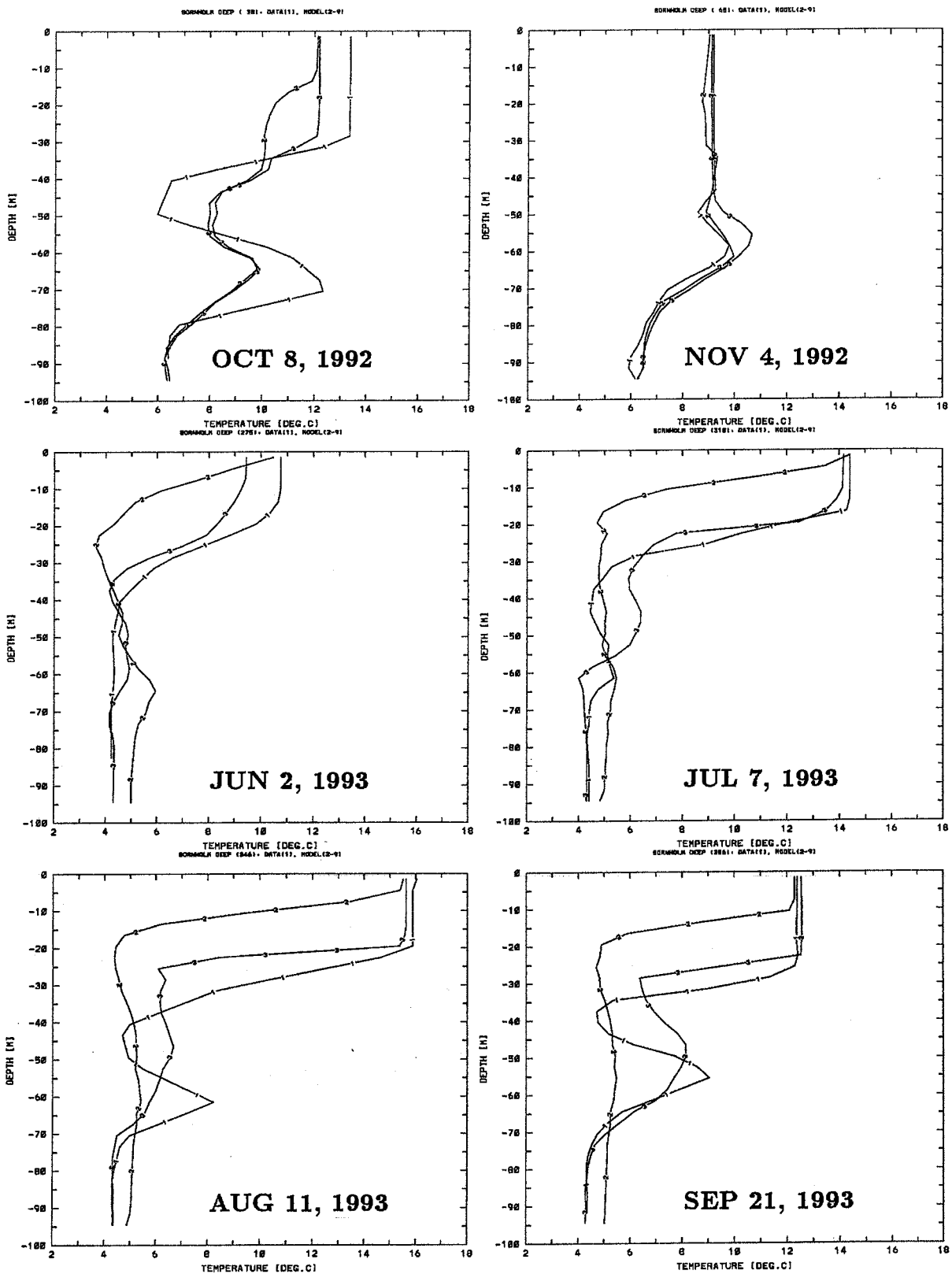
Figure 2: *Selected temperature profiles: (1) observations, (2) Richardson number dependent friction, (3) k − ε turbulence model.*

114
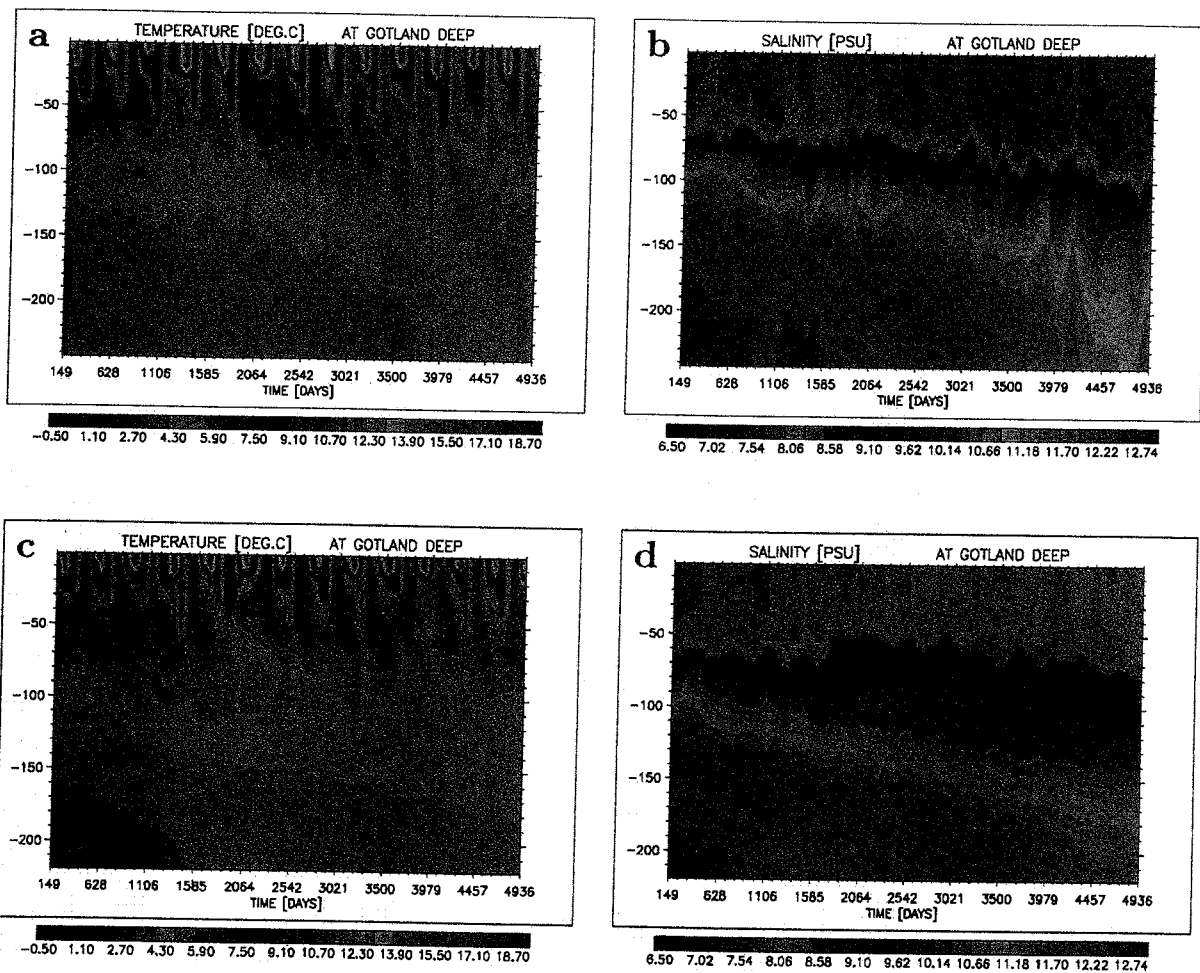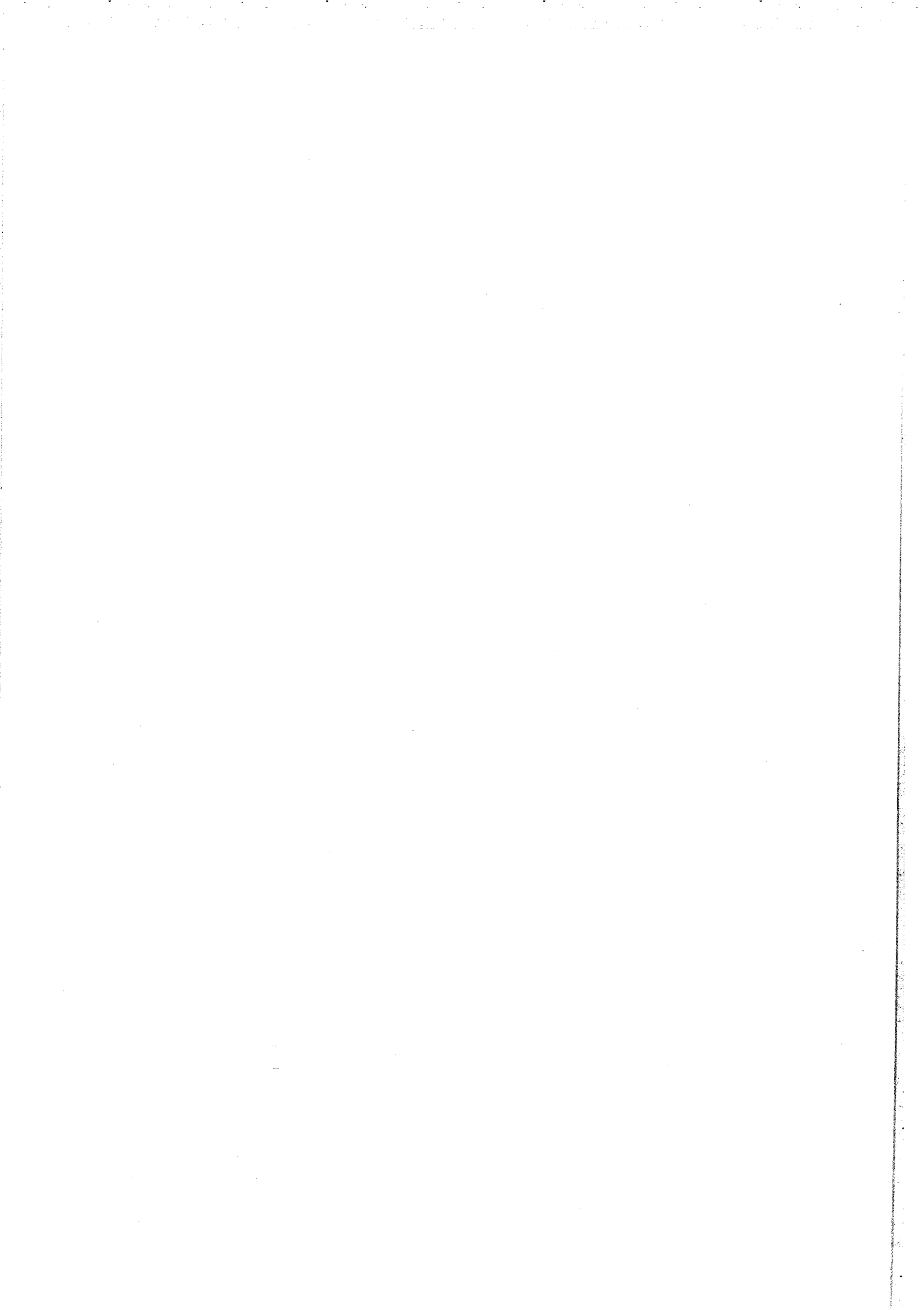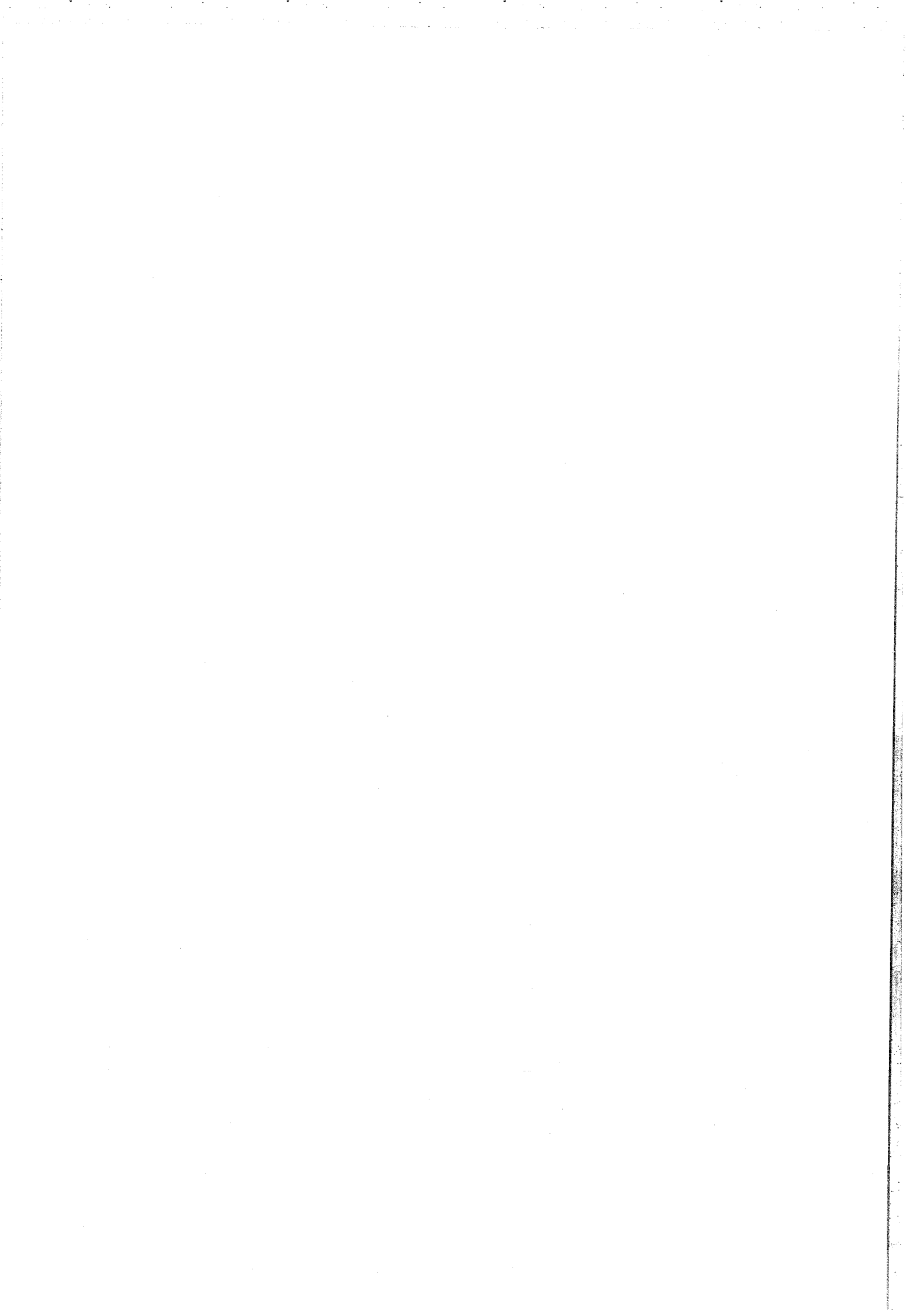
Figure 3: *Isotherm depths (in °C) and isohaline depths (in PSU) from May 1980 until July 1993 at Gotland Deep. Observations are depicted in (a) and (b) and model results in (c) and (d). The counting of days start at January 1, 1980.*

International BALTEX Secretariat Publication Series

No. 1 : Minutes of First Meeting of the BALTEX Science Steering Group
at GKSS Research Center in Geesthacht, Germany, May 16-17, 1994.
August 1994.

No. 2 : Baltic Sea Experiment BALTEX – Initial Implementation Plan.
March 1995, 84 pages.

No. 3 : First Study Conference on BALTEX, Visby, Sweden,
August 28 – September 1, 1995. Conference Proceedings.
Editor: A. Omstedt, SMHI Norrköping, Sweden. August 1995, 190 pages.

No. 4 : Minutes of Second Meeting of the BALTEX Science Steering Group
at Finnish Institute of Marine Research in Helsinki, Finland, January 25-27, 1995.
October 1995.

No. 5 : Minutes of Third Meeting of the BALTEX Science Steering Group
at Strand Hotel in Visby, Sweden, September 2, 1995.
March 1996.

No. 6 : BALTEX Radar Research – A Plan for Future Action.
October 1996, 46 pages.

No. 7 : Minutes of Fourth Meeting of the BALTEX Science Steering Group
at Institute of Oceanology PAS in Sopot, Poland, June 3-5, 1996.
February 1997.

No. 8 : *Hydrological, Oceanic and Atmospheric Experience from BALTEX.*
Extended Abstracts of the XXII EGS Assembly, Vienna, Austria, April 21-25, 1997.
Editors: M. Alestalo and H.-J. Isemer.
August 1997, 172 pages.

International BALTEX Secretariat Publication Series (continued)

No. 9 : The Main BALTEX Experiment 1999-2001 – *BRIDGE.* Strategic Plan.
October 1997, 78 pages.

No. 10: Minutes of Fifth Meeting of the BALTEX Science Steering Group
at Latvian Hydrometeorological Agency in Riga, Latvia, April 14-16, 1997.
January 1998.

No. 11: Second Study Conference on BALTEX, Juliusruh, Island of Rügen, Germany,
25-29 May 1998. Conference Proceedings. Editors: E. Raschke and H.-J. Isemer.
May 1998, 251 pages.

No. 12: Minutes of 7th Meeting of the BALTEX Science Steering Group
at Hotel Aquamaris in Juliusruh, Island of RÜGEN, Germany, 26 May 1998.
November 1998.

No. 13: Minutes of 6th Meeting of the BALTEX Science Steering Group at
Danish Meteorological Institute in Copenhagen, Denmark, 2 to 4 March 1998.
January 1999.

No. 14: BALTEX – BASIS Data Report 1998. Editor: Jouko Launiainen
March 1999, 96 pages.

No. 15: Minutes of 8th Meeting of the Science Steering Group at Stockholm University
in Stockholm, Sweden, 8 to 10 December 1998.
May 1999.

No. 16: Minutes of 9th Meeting of the BALTEX Science Steering Group at Finnish
Meteorological Institute in Helsinki, Finland. 19 to 20 May 1999.
July 1999

No. 17: Parameterization of surface fluxes, atmospheric planetary boundary layer and ocean
mixed layer turbulence for BRIDGE – What can we learn from field experiments?
Editor: Nils Gustafsson.
April 2000

Copies are available upon request at the International BALTEX Secretariat.